INFORMATION TO USERS

This manuscript has been reproduced from the microfilm master. UMI films the text directly from the original or copy submitted. Thus, some thesis and dissertation copies are in typewriter face, while others may be from any type of computer printer.

The quality of this reproduction is dependent upon the quality of the copy submitted. Broken or indistinct print, colored or poor quality illustrations and photographs, print bleedthrough, substandard margins, and improper alignment can adversely affect reproduction.

In the unlikely event that the author did not send UMI a complete manuscript and there are missing pages, these will be noted. Also, if unauthorized copyright material had to be removed, a note will indicate the deletion.

Oversize materials (e.g., maps, drawings, charts) are reproduced by sectioning the original, beginning at the upper left-hand corner and continuing from left to right in equal sections with small overlaps.

ProQuest Information and Learning
300 North Zeeb Road, Ann Arbor, MI 48106-1346 USA
800-521-0600

Surface Characterization of Metal-Metal Hip Implants Tested in a Hip Simulator

Adi Wang

Metallurgical Engineering Department
McGill University, Montreal

June, 2000

A thesis submitted to the Faculty of Graduate Studies and Research in partial fulfillment of the requirements of the degree of Masters of Engineering

ABSTRACT

The purpose of this study was to characterize metallurgical and tribological events occurring at the articulating surfaces of all metal implants in order to gain understanding of the wear characteristics of Co-Cr-Mo alloys. The surfaces of fifteen implant heads (or balls), made of either cast, low carbon wrought or high carbon wrought Co-Cr-Mo material, were examined using scanning electron and atomic force microscopes. In the first part of the study, six of the implants were examined prior to simulator testing, three after 3 million cycles of testing at 3 times body weight, and six after 6 million cycles of testing, also at 3 times body weight. In the second part of the study, the six implants that were examined prior to testing in the first part, were progressively wear tested at 5 times body weight and were periodically examined until 2 million cycles of testing.

Second- and third-body abrasive scratches of varying amounts were observed on all 15 heads. Residual grinding stones from the manufacturing process were also found in varying amounts on the surfaces of all fifteen heads. There was a strong correlation between the extent of this residual material and the extent to which the surfaces were scratched. Grinding during manufacturing also appeared to increase the hardness of the implant surfaces, rendering the material more resistant to abrasive scratching. Initially, the carbides in the cast and high carbon wrought components were proud of the surface. With testing, in the high carbon wrought components, the carbides were worn below the matrix surface and were also a source for fatigue pitting. In the cast components, some of the carbides remained proud of the surface,

while others were worn below the matrix surface with increased test cycles. Some of the carbides in the cast alloy also experienced fatigue pitting, resulting in partial or full pull-out of the carbides. At 3 times body weight, the fatigue pitting did not appear until 6 million cycles of testing and was not significant. At 5 times body weight, fatigue pitting was extensive and appeared after only 0.25 million cycles of testing. All 3 alloys showed evidence of matrix wear through a process known as delamination. The matrix also wore by continuous oxide formation and removal.

This study has shown that the metallurgical and tribological events taking place at the articulating surfaces of metal-metal hip implants are numerous and complex. It appeared that the low carbon wrought was an inferior choice of material for the application at had when compared to the cast and high carbon wrought. The wear behavior of the cast and high carbon wrought were shown to be similar and more studies are necessary to determine which is better for the all metal hip arthroplasty.

ABSTRAIT

Le but de cette étude était de décrire les effets métallurgiques et tribologiques sur les surfaces d'articulation des implants métalliques afin de mieux comprendre les caractéristiques de l'usure des alliages Co-Cr-Mo. Les surfaces de 15 articulations d'implants mouler d'alliage à haute teneur en carbone et forger en alliage de basse ou haute teneur en carbonne Co-Cr-Mo ont été scrutés avec des microscopes à balayage d'électron et de force atomique. Dans la première partie de l'étude, six de ces implants furent examinés avant la simulation, trois après 3 millions de cycles sous 3 fois le poids d'un homme et six après 6 millions de cycles sous la même charge. Dans la seconde partie de l'étude, les six premiers implants furent de nouveau examinés progressivement et périodiquement après un test d'usure à 5 fois le poids d'un homme juqu'à 2 millions de cycles.

Des éraflures abrasives en nombres variables de type deux ou trois corps furent observées sur les 15 têtes. Un résidu de pierres originant du procédé manufacturier de sablage ont également été découvert sur la surface de toutes les têtes. On note une forte corrélation entre l'étendue de ces résidus manufacturiers et l'étendue des surfaces usées lors des simulations. Le processus de sablage en manufacture semble augmenter la dûreté de la surface des implants transformant le matériel plus résistant aux éraflures abrasives. Initialement, les carbures de l'alliage forgé à haute teneur de carbone apparaissent rond et sortant de la surface. Pendant les tests, les carbures dans les composantes forgées en haute teneur de carbones furent usées jusqu'en dessous de la matrice de surface et on dénote le retrait partiel ou

complet des carbures de surface. En ce qui concerne les composantes moulées, une partie des carbures restèrent rond et sortant de la surface, et on nota ces mêmes dépressions résultant du retrait partiel ou total des carbures en augmentant les cycles de test. A 3 fois le poids du corps, le retrait des carbures n'apparait pas avant 6 millions de cycles et l'usure n'est pas significative. A 5 fois le poids du corps, le retrait des carbures s'amplifient beaucoup et commence à apparaître après 0.25 millions de cycles de test. Les trois types d'implants testés mettent en évidence l'usure de la matrice à travers un processus nommé délamination. La matrice s'use également par l'apparition et la disparition continuelle d'oxydation.

Cette étude a démontré que les événements métallurgicals et tribologicals qui surviennent sur les surfaces articulées métal-métal des implants de hanche sont nombreux et complex. Il apparait à première vue que les implants forgés à basse teneur de carbure soit un choix inférieur comparativement aux implants moulés et forgés à haute teneur de carbure; mais le comportement de l'usure sur les alliages moulés et forgés à haute teneur de carbure s'est montré similaire à celle de basse teneur. D'autres études sont nécessaires pour déterminer le meilleur candidat pour les implants tous métalliques arthroplastiques.

ACKNOWLEDGEMENTS

The author would like to thank all those whose generous help and encouragement expedited the completion of this study.

First and foremost, she would like to thank her supervisors, Dr. Steve Yue and Dr. Dennis Bobyn, for their suggestion of topic and for their support and guidance. Gratitude is expressed for their contribution to the two papers published during this study.

She would also like to thank Dr. John Medley for his support, suggestions, encouragement and his contribution to the two papers published during this study.

The author would like to thank Dr. Frank Chan for contributing specimens for this study, as well as for his encouragement, support and contribution to the two papers published during this study.

Gratitude is expressed to Medical Research Council of Canada and National Science and Engineering Research Council of Canada for their financial support, as well as to Wright Medical Technology for providing implants for this study.

TABLE OF CONTENTS

1.0 INTRODUCTION

1.1 THE HUMAN HIP

The human synovial joint consists of two articulating bones, each of which is covered by an elastic layer of cartilage. Between them is a lubricating viscous fluid, called synovial fluid. The synovial fluid is a dialysate of blood plasma consisting of water with proteins and salts, including a high molecular protein called hyaluronic acid, which together aid in fluid film lubrication. This tribosystem is sealed by an impermeable membrane called a capsule that ensures the fluid is contained within the joint space. In order to achieve minimum friction and, under normal conditions, minimum wear, the joint is lubricated by various hydrodynamic and elastohydrodynamic mechanisms. These mechanisms include the squeeze effect, the wedge effect, weeping lubrication and boosted lubrication, all of which lead to a very low friction coefficient of 0.005 to 0.025, as is observed in a healthy joint.[73]

This complex tribosystem is found in all of the joints of the human body, including the hip joint (Fig. 1.1). The human hip has a ball and socket configuration which allows abduction/adduction, extension/flexion and internal-rotation/external-rotation motion of the leg (Fig. 1.2).[23] The socket, known as the acetabulum, is located on the pelvic bone, while the ball, known as the femoral head, is located on the femur, which is the upper bone of the leg. The articulation of the hip joint takes place between the acetabulum and the femoral head. As for any other joint, these two com-

ponents are lined with cartilage and are covered by the capsule membrane containing the synovial fluid.

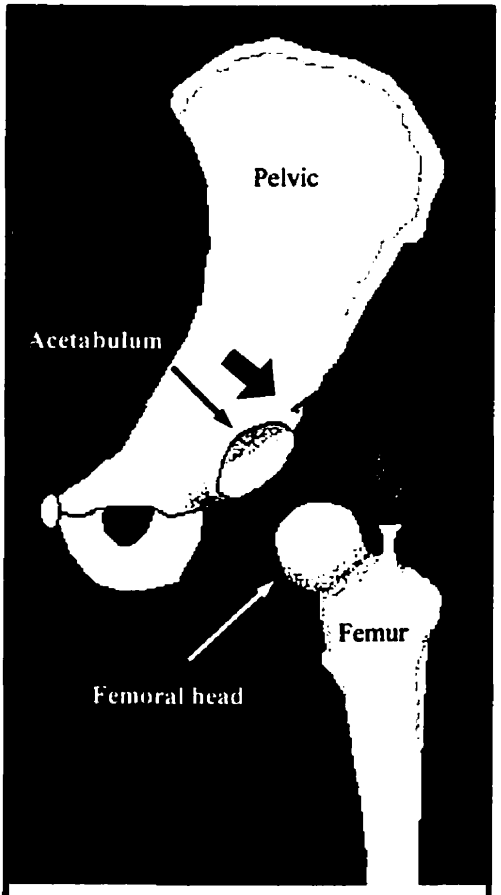

Figure 1.1 – Schematic of the human hip.

1.2 Reasons for a Hip Implant

There are several conditions of the human joints where function is severely impaired. The reasons for the disability depend upon the disease, but usually the bearing surfaces are involved. For example, in osteoarthrosis, the normally smooth layers of articular cartilage become worn and the shape of the joint becomes distorted. Pain usually results from the sliding together of the two roughened bony surfaces.[79] In rheumatic joint disease, an unfavorable tribological situation develops due to the reduced lubricating capacity of the synovial fluid. The

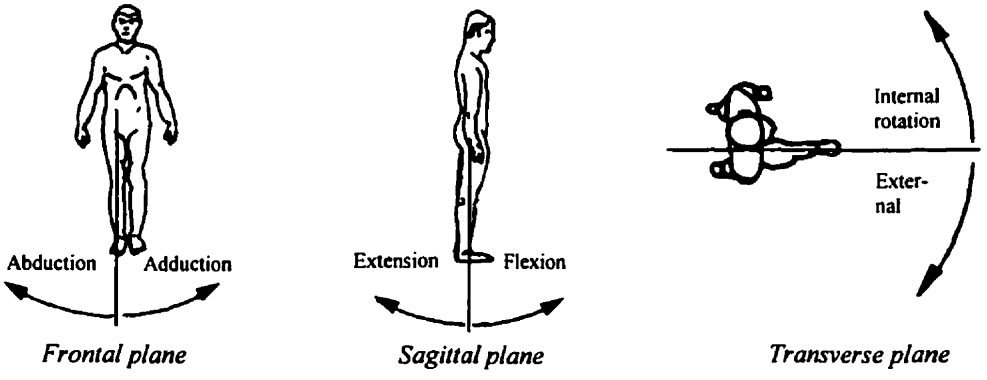

Figure 1.2 – Movement allowed as a result of hip joint geometry (taken from Ref. 23).

fluid lubrication ceases, once again leading to extreme wear of the joint surfaces, which in turn leads to increased friction values and pain.[73]

The joint most commonly affected by disease or injury, and where loss of function causes the severest handicap, is the hip joint. The loads which these ball-and-socket joints may be required to sustain can reach five times body weight.[60] In order to rehabilitate patients with defective hip joint function caused by injury or disease, as the last resort, joint replacement with artificial materials is used.[73] The idea of hip arthroplasty is to replace the articulating surfaces with artificial materials in order to eliminate the painful bone-on-bone articulation. This is done by replacing the femoral head with a ball on a stem, and the acetabulum with a hemispherical lining called a cup (Figs. 1.3 & 1.4).[32] When both components of the hip joint are replaced, this is known as a total hip arthroplasty. The most commonly used modern hip implants, the Charnley total hip arthroplasty and the like, are comprised of a polyethylene cup, coupled with a metal ball. Other combinations include metal cups with metal balls, ceramic cups with ceramic balls and polyethylene cups with ceramic balls.

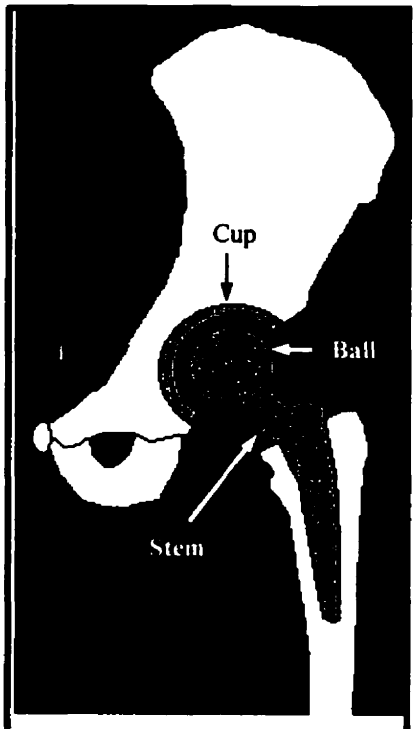

Figure 1.3 – Schematic of the hip with a total hip implant.

Only in recent years has degenerative arthritis of the hip become a major problem in orthopaedic surgery. This change in orthopaedic practice stems from many factors. The population of today has a greater number of old people who are not prepared to cope with pain and disability as were previous generations. Modern standards demand a higher level of physical comfort and function. Fortunately, today the orthopaedic surgeons have much improved methods of treatment at their disposal.[34] For these reasons, as we progress into the fourth decade of modern total hip arthroplasty, more than 500 000 hip joint replacements are performed worldwide annually.[3]

Figure 1.4 – Examples of total hip prostheses (taken from ref. 65).

1.3 Problems With The Hip Implant

Even after four decades of modern hip arthroplasty research, lab experimentation and clinical experience, the most commonly used modern hip implant is not without its perils. What is regarded as the leading long term problem faced by these implants is aseptic loosening, which is the partial or total detachment of the implant from the bone.[3,12,27,32,62,65,77] Usually, loosening is accompanied by pain, and often revision surgery is necessary to correct the problem.

Loosening of the implant is most often caused by wear particle induced osteolysis.[3,12,27,32,62,65,77] The shear stresses imposed on the artificial hip joint cause wear particles to be released from the articulating surfaces of the ball, and especially the polyethylene socket. These wear particles migrate through the synovial fluid and eventually come to rest against a non-articulating part of the implant, surrounding bone or surrounding tissue. These particles are released in a variety of shapes and sizes, most of which are small enough for the body to perceive as foreign bodies. Once the body detects foreign bodies, the immune system attempts to eliminate them. It does this by dispatching cells called macrophages to the site of the foreign particles. The macrophages engulf the wear particles and release chemicals and enzymes with the intention of dissolving the particles. This is largely unsuccessful and some of the released substances serve as mediators or catalysts for progressive tissue inflammation that , with time, can cause bone destruction or dissolution. This process, known as osteolysis, can result in joint pain, implant loosening, and the need for a revision procedure.[29, 31] Because this process is directly related to the volume of wear debris

(or number of wear particles), it is important to develop bearing materials for the hip that are as wear resistant as possible.[65]

In recent years, histologic analyses of the tissues surrounding the Charnley prosthesis and similar implants using polyethylene cups, have implicated particulate polyethylene as the most prevalent material inducing osteolysis.[3,12,62,65,77] As a result, these implants are likely to experience high rates of aseptic loosening. The common occurrence of osteolysis with these implants suggests a high wear rate of polyethylene. In fact, studies have shown polyethylene to have wear rates 10 to 100 times greater than that of metal-on-metal implants, the Charnley predecessors.[3,12,23,33,63,65,73] Therefore, one must question the candidacy of polyethylene for long term use of an implant. It is for this reason that in recent years the orthopaedic surgeon has been actively searching for alternative bearings. The best place to start the search is in the examination of the history of the implant.

As will be shown in more detail in later chapters, history suggests that metal-on-metal implants have the potential to be more suitable for long term implant function. In recent years, it has been shown that metal-on-metal implants wear significantly less than metal-on-polyethylene. Both clinical studies, as well as laboratory investigations continually show metal-metal couples to wear 10 to 100 times less than polyethylene.[3,12,23,33,63,65,73] For this reason, in the past decade or so, there has been a revival of the all-metal hip arthroplasty. As in the past, the metal most successfully used for these implants is a Co-Cr-Mo alloy. However, unlike in the past when the alloy was used only in the cast form, modern metal-on-metal implants are made of either cast, high carbon wrought or low carbon wrought Co-Cr-Mo alloy. Each form of this alloy possesses a different microstructure and thus might experience different wear mechanisms and a different wear resistance. At the time the present study was formulated, the mechanisms of wear and the factors governing wear resistance of each alloy were not well understood.

2.0 LITERATURE SURVEY

When searching for ways to improve a certain technology, it can be beneficial to examine the history leading to the advancements achieved thus far. This chapter will attempt to examine clinical experiences and laboratory experiments documented from the first attempts at hip arthroplasty to current studies.

2.1 HISTORY OF THE HIP IMPLANT

2.1.1 HISTORIC ACHIEVEMENTS

The first recorded successful hip arthroplasty was performed at the Westminster Hospital in London in 1822 by Anthony White.[34,60] The procedure was performed on a nine year old boy who fell down the stairs causing the head of the femur to be displaced, rendering the boy bedridden. During the arthroplasty, White excised the femoral head, giving the boy full range of motion only 12 months after the operation.[34] When the boy died at the age of 40, an autopsy revealed that a fibrous union between the pelvis and the femur had developed, demonstrating the healing ability of the skeleton.[60]

The idea of interposing a foreign material between bone ends is credited to J. M. Carnochan who, in 1840, placed a piece of wood between two jaw bones. Later, Verneuil in France interposed muscle, fat and connective tissue between articulating

bones in order to prevent bony union.[60] Preventing articulation between bare bones is the idea behind the modern total hip arthroplasty.

2.1.2 Early Attempts At Hip Replacement

Thomas Gluck, in 1891 in Germany, was experimenting with a variety of materials for the repair and replacement of bone and joints. He constructed an ivory ball and socket joint which was fixed to the bone with nickel plated steel screws. He even attempted to achieve fixation with glue, making him a pioneer in total hip replacement using glue or cement fixation.[34,60] The first resurfacing hip arthroplasty is credited to Robert Jones, who in 1902, performed an arthroplasty operation by removing the head of a femur and covering the neck with gold foil.[34,60] In 1923, Hey Groves performed the first recorded replacement of the femoral head, by using Gluck's idea of the ivory joint. Groves replaced the femoral head in a patient who suffered from severe pain due to a fracture in the neck of the femur, which connects the head to the lower bone. This procedure allowed the patient to lead an active life, both legs being of the same length.[34,60]

Smith-Petersen of Boston recognized the need for proper material selection in order for a hip arthroplasty to be successful. In 1923, he attempted to use Viscaloid for the procedure, which produced a marked foreign body reaction, in 1933 Pyrex glass, in 1937 Bakelite and finally in 1938 a Vitallium (cobalt-chromium alloy) mould or cup,[34,60] which proved to be the most successful of his attempts. In 1962, it was reported by Alexander Law of London that follow-ups of 1110 patients with Smith-Petersen cup arthroplasties 2 to 4 years after operation showed that 55% of the patients conditions were excellent or good and 45% were fair or poor. Later, at more than 10 years after the procedure, the corresponding figures were 69% and 31% respectively, indicating that the short term results were not outstanding but that the operation stood the test of time and indeed improvement tended to occur for many years postoperatively.[34,60]

In 1938 while Smith-Petersen was developing the Vitallium mould arthro-

plasty in Boston, Philip Wiles, at the Middlesex Hospital in London, was attempting to replace an entire hip joint with stainless steel components that were ground to fit together accurately. The acetabular cup gained fixation by 2 screws and the femoral component was secured by a bolt passing through the neck of the femur. Six operations were performed on patients suffering from Still's disease. Unfortunately, all the radiographs were lost during World War II and only 1 patient with a disintegrated prosthesis was still alive in 1951. In 1957, Wiles developed another total hip design with improved engineering and a stronger method of fixation. Eight operations were performed but the results were not encouraging because of bone resorption and loosening.[3,34,38,60] A similar stainless steel implant was used by Denneth Coutts in Boston. One prosthesis, implanted in a postman who was light weight, remained *in situ* for 6 years before it had to be removed for pain,[3] indicating that the implant was likely loose.

While Wiles was experimenting with stainless steel total hip arthroplasty, Edward Haboush thought it might be preferable to convert the cobalt-chrome cup of Smith-Petersen into a hollow ball with a skirt that would fit onto and about the reshaped head and neck of the femur,[60] giving rise to another design of a total hip replacement, using the metal which today proves to be the most successful of the metal-on-metal arthroplasties. His early attempts at implantation were not successful due to the poor design of the fixation components. In 1951, he attempted the procedure with a new design at the Hospital for Joint Diseases in New York. Unfortunately, the joint dislocated in the postoperative period because of a vertically positioned acetabular component and never actually functioned.[3,60]

2.1.3 Later Attempts

The next phase in the development of metal-on-metal total hip arthroplasties largely took place in England and is associated with Kenneth McKee, Peter Ring and John Scales.[3] While the metal-on-metal implant was being developed by many, such as the individuals mentioned above, John Charnley, who initially was pessimistic

about total hip arthroplasties,[3] was developing the metal-on-polyethylene hip replacement, which later proved to render the metal-on-metal implant near obsolete.[3,33,65]

2.1.3.1 McKee-Farrar Total Hip Arthroplasty

Kenneth McKee, who had initially worked with Wiles, designed a model similar to that of Wiles and used it in three cases in 1950. Two of the prostheses were made of stainless steel and became loose within 1 year. The third prosthesis was also one of stainless steel but was fixed with cobalt-chromium alloy screws and survived for 3 years.[3,34,60] In 1953, McKee visited the United States and was impressed by the Thompson prosthesis,[3,34,60] whose stem passed down the shaft of the femur,[60] as opposed to being attached to its exterior wall. This stem was made of the cobalt-chromium alloy Vitallium. After his return back to Norwich, McKee matched to his clover leaf socket a modified Thompson stem with a 1¼ inch diameter head. Both components were made of Vitallium.[3] McKee believed that both components should be made of a cobalt-chromium alloy, because it was the metal combination which gave the least friction, least wear and was apparently tolerated by the body tissues.[34] Between 1956 and 1960, McKee and Chen performed 26 replacements using McKee's latest design. Fifteen were satisfactory for more than 7 years, ten failed and were revised and one patient died postoperatively.[3] Some of the failed prostheses had been functioning for several years,[3] proving to be more successful than the design utilizing stainless steel.

McKee found that success depended on the components remaining tight within the bone. If one of the components became loose, the patient developed pain upon weight bearing.[60] For this reason, the introduction of bone cement by John Charnley in 1960 prompted McKee to modify the acetabular component so that acrylic fixation could be used.[3,60] Along with the redesign of the acetabular component, he changed several parameters of the femoral component and between 1961 and 1964, 100 of these joints were implanted, thirty of which had to be revised, partly due to impingement, and partly due to the poor surface finish and mismatch of the articu-

lating components. In 1965, Watson-Farrar contributed by modifying the neck of the femoral component in order to minimize impingement (hence McKee-Farrar). In addition, an attempt was made to better match the articulating components, and the size of the implant was reduced in order to achieve better bony growth on the acetabular component (the smaller the component, less is the needed amount of bony growth). By 1968, it was thought that some of the perfect fit matched pairs resulted in equatorial bearing (as opposed to the desired polar) and excessive wear. Polar bearing was then achieved by reducing the size of the head with respect to the socket, providing a certain clearance. Some of the implants that were produced and implanted after 1968 had been in use for as long as 20 to 22 years. However, McKee stopped using the all metal system in 1972,[3] perhaps because of the decline in metal-on-metal popularity due to the increased popularity of the metal-on-polyethylene prosthesis.

2.1.3.2 Ring Total Hip Arthroplasty

In 1964, at Redhill, Surrey, Peter Ring, who believed proper fixation should be achieved in the absence of cement, designed a cup with a long threaded stem that was inserted into the pelvis. He designed such a stem with the assumption that its length would be sufficient for fixation with bone growth and no cement. The cup and threaded stem were made of cobalt-chromium alloy and were coupled with an Austin Moore femoral component, which had a self locking stem (big enough in cross-section in order to fully fit in the femoral cavity and stay jammed in). The stem therefore required no cement for fixation, and it too was made of cobalt-chromium alloy.[3,60] Ring modified the femoral component by elongating the neck intended to increase the range of motion. The articulating surfaces were lapped together (creating a perfect fit) giving an equatorial bearing. In total, 185 of these implants were inserted. After 11 to 14 years follow-up, there were 38% poor results including revision. In 1967, several design adjustments were performed, including the creation of a 0.5mm clearance between the head and socket in order to establish a polar bearing instead of the previous equatorial one. With these changes, the survivorship in-

creased to 80% at 17 years. The design of the stem, however, resulted in poor gait, secondary valgus deformity of the knee, and component loosening. In 1971, several changes were made to the stem in order to correct these side effects and the metal cups, despite their success, were relinquished in favor of polyethylene ones. These new components proved to be inferior because of what is now described as polyethylene wear debris induced osteolysis.[3]

2.1.3.3 Stanmore Metal-on-Metal Total Hip Replacement

In 1956, laboratory work on a cobalt-chromium metal-on-metal total hip replacement was started by John Scales and J. N. Wilson at the Royal National Hospital, Stanmore. The first implant designed at Stanmore included an acetabulum component made of two parts, the first of its kind. The outer baseplate was attached to the bone with multiple pins, which were eventually changed to 3 nails at 120° to each other. The inner part was attached to the outer shell with a screw thread lock and later with a 3-clip retention mechanism. The cup was in the shape of a horseshoe, a shape which was adapted in order to provide a relieved portion that would permit ingress of fluid to the inner bearing edges and provide an exit for wear particles. The apex of the femoral head was also relieved. With these implants, there was a high incidence of early prosthetic loosening that was attributed to a high initial frictional torque as a result of equatorial bearing, irregular geometry of the articulating surfaces, and poor surface finish. Seizure of components, some of which had to be hammered apart at revision, was also observed.[3]

In 1968, the cup was modified from the horseshoe shape to an annular one, and sufficient clearance was provided between the head and cup in order to provide a polar bearing instead of the previous equatorial one. The channel to permit lubrication and egress of wear debris was maintained and the engineering practice of finishing the bearing surfaces was also dramatically improved. Follow-ups of about 10 years of the Stanmore implants showed the overall incidence of component removal using the first designs to be 58% versus 15% using the 1968 polar bearing.[3]

2.1.3.4 Other Notable Total Hip Arthroplasties

Muller and Hugger designed an all metal hip implant using cast cobalt-chromium alloy with highly mirror polished articulating surfaces and 3 plastic sliding bearings in the inner side of the cup to enhance lubrication. These implants provided a clearance of 0.12 to 0.5mm resulting in a polar bearing. Despite excellent early results, the metal-on-metal implant was abandoned in favor of polyethylene cups. Six of the articulations were revised after function of as many as 25 years. Retrieved components showed no macroscopically detectable wear of the bearing surfaces.[3]

There were many other attempts at creating the perfect metal-on-metal design for total hip arthroplasty. Some were more successful than others, but most eventually gave way to the metal-on-polyethylene design, which proved to have very good initial, short term results.[3,65]

2.1.3.5 The Charnley Total Hip Arthroplasty

John Charnley has regarded the coefficient of friction as the primary factor affecting the design of a hip joint. Low friction not only makes movement easier and causes less muscle fatigue, but has the important effect of transferring less strain to the components and to their fixation within the bone. Thus, to minimize friction, Charnley adapted a small metal head rotating in a plastic cup. Stainless steel was used for the head, and at first, polytetrafluorethylene for the socket. This gave a very low coefficient of friction, but the high density loading on the plastic material caused wear at a rate too fast to be acceptable. In order to reduce the wear, the plastic was replaced by an ultra-high-molecular-weight polyethylene, which proved to have a very low coefficient of friction, and initially appeared to have acceptable wear resistance.[34]

2.2 Revival Of The Metal-On-Metal Hip Implant

2.2.1 Why Were They Abandoned?

There are several factors that can explain why metal-on-metal implants, such as those of McKee-Farrar, were abandoned, even though some of their designs were exceptionally successful:

2.2.1.1 Early Success of the Charnley Prosthesis

The early results achieved by Charnley using a metal-on-polyethylene bearing with a 22mm head were excellent. With current knowledge, these results can be explained by the use of a well designed stem and cup, sound and consistent implantation technique and sepsis (infection) control. The excellent results achieved by a scientist of international repute justifiably led to the rapid widespread use of his prosthesis.[3]

At the time when the Charnley principles were gaining in popularity, early outcomes of the contemporary metal-on-metal total hip replacements were clearly inferior. It is apparent that the higher early failure rates of the McKee-Farrar arthroplasties were due to bearing flaws of the initial generations of components, poor stem design and suboptimal implantation technique. Before the need for a certain clearance was appreciated, many components had an equatorial bearing leading to excessive wear and loosening. Poor surface finish and irregular geometry was also not uncommon in the early stages. McKee-Farrar stem was curved and had sharp corners which are now known to be undesirable.[3,12,73] At the time, appreciation of the mechanical design was not as well understood, and as a result, the early failures of the metal-on-metal implants were wrongly blamed on poor material selection.[12]

2.2.1.2 Frictional Torque Issue

Frictional torque and its clinical significance on the bone-cement interface have long been important issues in total hip replacement. The frictional torque of

McKee-Farrar implants was greater than that of Charnley prostheses because of a higher coefficient of friction and larger head diameter.[3,12,73] Pendulum friction tests, performed by Charnley, which compared metal-on-metal to metal-on-polyethylene demonstrated the seizure characteristic of metal-on-metal. However, some of these tests were run without lubrication, now known to adversely affect metal-on-metal bearings. Wilson and Scales, in 1970, and Swanson et al, in 1973, also reported higher frictional torque of all metal bearings *in vitro*.[3] Both studies postulated that the high frictional torque was a contributing factor in aseptic loosening. However, in another study, Crowninshield & Anderson[18] reported that these torques were 4 to more than 20 times lower than the torque needed to loosen acetabular cups fixed by cement. It has also been shown that higher friction at the bearing surface and higher frictional torque can be tolerated if the release of wear particles into the periprosthetic tissues is sufficiently limited.[40] In 1971, Walker and Gold reported that equatorial bearing (found in the early McKee-Farrar designs) generated frictional torque many times higher than that of polar bearing and that surface irregularities as small as 1μm (often seen in the contemporary implant) could radically alter the location of the contact between ball and socket and hence the frictional torque.[34] It is speculated that although some early failures of the McKee-Farrar prostheses were related to high frictional torque due to equatorial bearing, many other failures were wrongly attributed to high frictional torque, which at the time was widely considered an important factor in prosthetic bone interface destruction and component loosening.[3]

2.2.1.3 Health Concerns

Several health issues were of concern with the introduction of total hip replacement, especially those made solely of metal. The carcinogenic and toxic effect of metal particles and ions was unclear and thus feared. Wear particles obtained from prostheses composed of cobalt-chrome alloy were injected into laboratory rats and caused tumors. The tissue discoloration observed at revision of metal-on-metal implants intensified fears for a similar effect on humans. This staining was attributed

by many surgeons to debris generated in the articulation, although in many instances it could have been the result of impingement of the tissue by the implant and/or motion at the implant cement interface. The issue of local and remote carcinogenesis caused by implant remains controversial, even today. When the Charnley prosthesis was introduced, carcinogenesis was not of great concern because there was no detectable polyethylene debris around the implant nor in remote sites. It is now known that such debris was not present because at the time, techniques for the identification of submicron polyethylene particles had not been developed.[3]

Another health concern, and one of great controversy, is that of metal sensitivity. Many studies by scholars have been conducted in order to solve the issue of metal sensitivity. Findings of these studies showed at times in favor of the all metal implants, and at others against. There were those who concluded that patients who were initially not sensitive to metal became sensitive postoperatively. Other studies found that patients with all metal implants who were not sensitive to the metal before, were not sensitive after the arthroplasty. One study found that aseptic loosening was not caused by metal sensitivity, but sensitivity could develop because of the release of wear debris from a loose implant. Even today, the issue of metal sensitivity from all metal implants as well as the metal used in that of the Charnley metal-polyethylene implants, is of great controversy.[3]

It was noted that the acetabular cup failure rate was much greater for the McKee-Farrar implant than for that of the Charnley. It was thought that the increased strain rates experienced by the bone-implant interface of the McKee-Farrar cup was due to the poor shock absorbing property of the metal in comparison to that of the polyethylene. It is now known that it is not so much the shock absorbing property as much as the thickness of the cup which causes an increase in strain on the bone. The Charnley cups were of considerable greater thickness. Also, impingement of the neck against the cup would also cause greater strain rates on the bone, a problem often experienced by the McKee-Farrar implant due to its poor design. It is now known that acetabular cup failure is multifactorial and relates to initial bone quality, effects

of bone preparation, amount of wear debris and osteolysis.[3]

2.2.2 Renewed Interest In The Metal-On-Metal Implants

As was mentioned earlier, what is regarded as the leading long term problem with the Charnley prosthesis, which today is the most commonly used total hip implant, is aseptic loosening. It is now known that aseptic loosening is most often caused by wear particle induced osteolysis.[3,12,27,32,62,65,77] The greater the amount of wear, the greater is the chance for aseptic loosening. In recent years, histologic analyses of the tissues surrounding the Charnley prosthesis and similar implants using polyethylene cups, have implicated particulate polyethylene as the most prevalent material inducing osteolysis,[3,12,62,65,77] and thus loosening. Improvements and alternatives to the current technology of articulating metal femoral heads with polyethylene acetabular cups are therefore being sought in an attempt to mitigate the osteolysis problem by reducing the amount of wear debris generated at the head cup interface.[12]

A peek into the history of the total hip arthroplasty suggests that metal-on-metal bearings are a potential alternative to the polyethylene cup.[12,43,65] Although the early success of the all metal hip arthroplasty was limited by what is now understood as poor implant design,[12] a great number of them have survived in service for more than 20 years.[3,12,63,73] The wear of metal-on-metal hip implants has been documented in the literature in retrieval studies and in those involving the use of mechanical devices (simplified models of metal-on-metal bearings and complex models simulating hip joint kinematics). Compared with the wear rates of conventional metal-on-polyethylene articulations, those experienced by metal implant pairings have been shown to be 10 to 100 times lower.[3,12,23,33,63,65,73] These statistics warrant further investigation into the factors determining the success or failure of all metal hip implants, as they show great promise in significantly reducing the wear inducing osteolysis problem being experienced by the implant using the polyethylene cup.[3]

It is now recognized that the early failures of all metal hip implants made of cobalt-chrome were not due to poor material selection, but rather poor implant de-

sign. Very often, the ball and socket were too well matched with little or no clearance, resulting in an equatorial bearing which caused high frictional torques,[3,12,73] and thus early loosening due to the high torque as well as increased wear rates leading to osteolysis. Also, poor manufacturing techniques, which have since been greatly improved, provided for an irregular geometry of the articulating surfaces as well as poor surface finish.[3,12,73] such factors are known to severely degrade the wear and friction properties of an implant.[23] With today's manufacturing technology, near perfect spheres are achievable with a much improved surface finish.

Aside from inadequate bearing surfaces, the rest of the implant design was suboptimal. For example, the Charnley implant has an excellent stem design: the stem is straight with broad medial and lateral surfaces and a gentle dual wedge taper. There are smooth contours and no sharp edges. In contrast, by today's standards, the McKee-Farrar femoral design is inferior: there is a curve in the stem, the medial and lateral borders are narrow and there are multiple sharp corners. These features can result in high localized stresses within the cement mantle and early loosening. Further, the broad neck of the McKee-Farrar femoral component was prone to impingement against the metal rim of the acetabular component that could initiate loosening.[63] It is hoped that once these design parameters are corrected, the metal-on-metal implant would function successfully for many years with little wear and low frictional torque leading to no aseptic loosening.

2.2.3 Challenges Faced In Their Return

The reintroduction of all metal hip implants meant that several challenges would have to be overcome. It was questioned whether the traditional carbide containing cobalt-chromium cast alloys are still the best materials of choice,[65] especially with the introduction of so many new superalloys, including wrought Co-Cr-Mo alloys. Another concern was the desire for a bone sparing implantation, which means a smaller acetabular component and a larger range of motion with an acceptably low risk of dislocation. This desire led to a reduced ball head diameter (28-32mm instead

of 37-42mm), which changed the contact area and surface pressure and thus the tribologic conditions at the sliding surfaces. The most important question arising from this change was the appropriate clearance between the ball head and acetabular component to minimize friction and wear.[65] A third challenge was to take the metal combination and adapt it to existing anchoring components. It would be neither scientifically or economically efficient to change clinically successful fixation designs simply to accommodate a change in the tribologic concept of the articulating surfaces.[65] Finally, the renewed enthusiasm for this concept could possibly be marred by certain biologic and practical issues. The effect of increased metallic burden, ionic and particulate, on local and systemic biology has yet to be fully appreciated. The small nature of the metal particulate debris as well as the higher reactivity of metal in comparison to polyethylene, raises important questions about long term toxicity and carcinogenicity.[12]

2.2.4 Recent Developments In Metal-On-Metal Hip Implants

There were many problems faced by the first generation metal-on-metal hip arthroplasties, many of which have been mentioned in previous sections of this chapter. The first problem that needed to be solved with the reintroduction of the all metal hip implant was the ability to consistently produce mirror finish, perfectly spherical articulating surfaces. With today's technology, a mirror finish is easily attained and near perfect spheres are produced using computer controlled manufacturing.

The desire to spare the bone led to the reduction of the femoral head from 37-42mm in diameter to 28-32mm.[65] Tribologically, such a reduction is favorable in terms of friction and wear. The smaller the implant head, the lower the frictional torque and less is the amount of wear.[40] Such a statement should be taken with caution, however, as the friction and wear also greatly depend on the clearance between the head and cup. If the clearance is too small, an equatorial bearing is established, leading to high frictional torques.[40] In order to favor friction, the clearance should

therefore be large. However, with a large clearance, the wear is compromised. If the clearance is too large, excessive amounts of wear are produced.[3,12,40] Therefore, aside from reducing the diameter of the head and cup, an optimal clearance for each head/ cup size has to be determined in order to both minimize wear as well as friction. The optimal clearance is still being determined with such studies conducted by Chan et al,[12] Medley et al[43] and Amstutz et al[3] using hip simulators.

Because of the current understanding behind what is a superior stem design, the stem of all metal hip implants is no longer a major concern. This is especially true when considering modular prostheses, where a surgeon can mix and match components according to his/her preference and manufacturer recommendations. With the flexibility of modular prostheses, a well designed stem can be coupled with the desired articulating ball. The same is true for the socket. A well designed acetabular fixation component can be coupled with a polyethylene or a metal inner liner.

In 1984, when Muller and Webber attempted to reintroduce the concept of metal-on-metal bearings, they developed a cobalt-chromium alloy head coated with TiC and a socket liner of the same alloy coated with a thin layer of TiN, which gave rise to the TiC-TiN low friction prosthesis. Although this design showed early promise, it was abandoned because of concerns about the durability of the coatings and also because by that time, the Co-Cr-Mo forged alloy Protasul®-21 WF had been developed by Sulzer.[3] The new alloy's high carbon content and the forging process made the structure more homogeneous because the grains were refined and the carbides were reduced to a diameter of 2 to 3μm,[3,73] which is considerably smaller than those observed in the cast structure with approximate diameter of 20μm.[73] As a result, the surface can be more highly polished, thereby reducing the frictional resistance and also wear.[3,12]

2.3 WEAR AND MATERIAL OF CHOICE

As previously discussed in this chapter, the two early concerns regarding bearing surfaces in joint replacement were friction and wear. With improved implant fixation techniques, it is now apparent that the principal problem is the quantity of wear debris produced from the bearing surfaces during articulation and not so much the friction. Wear debris can be produced through several mechanisms, such as adhesion, abrasion, fatigue and delamination, all of which may take place during running-in as well as during steady state wear conditions. When choosing a material suitable for the application of hip implants, it is therefore important to choose a material that will experience low rates of the above wear mechanisms. Even though there are many wear resistant materials available for bearing surfaces, only a few are biocompatible.

2.3.1 WEAR MECHANISMS

Running-in is known as the period during which two mating surfaces improve in conformity, topography and frictional compatibility. During this period, the wear rate is often initially quite high, but, as the surfaces become smoother and the more prominent asperities are lost or flattened, the wear rate falls. During running-in, a number of mechanical wear processes, especially those that depend on adhesion or abrasion, are likely to be operating simultaneously. Once running-in is complete, a steady low wear rate regime is maintained for the operational life of the component. The wear rate may rise again once the operating time becomes sufficiently long for fatigue processes in the upper layers of the loaded surface, driven by the cyclic nature of the component loading, to start making a significant contribution to material loss.[85]

2.3.1.1 Adhesive Wear

When two surfaces are loaded together, strong cold welds can be formed at some asperity junctions, and these junctions must then be broken if relative sliding is

to take place. The amount of wear then depends on where the junction is sheared. If the shear takes place at the original interface, then wear is zero. If shear takes place away from the interface, a fragment of material is then transferred from one surface to the other. In practice, this transfer of material is observed normally from the softer material to the harder, but occasionally from the harder to the softer. Subsequently, the transferred material may become detached, giving rise to wear particles (Fig. 2.1).[5,59,85] The liquid contact angle of the bearing surfaces can be important for the reduction of adhesive wear as well as for good lubrication of the surfaces. A high contact angle of a fluid on a hard surface results in that liquid beading up on the surface, while a low contact angle results in the formation of a tribologicaly favored liquid film on the surface.[27] Therefore, in order to minimize wear and increase lubrication, a material should have a low liquid contact angle.

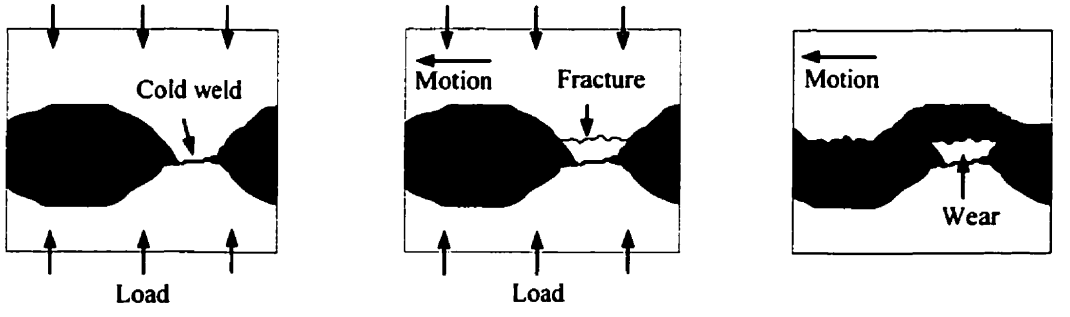

Cold weld at asperity junction.

Shearing of asperity due to relative motion of mating surfaces.

Transfer of material from top surface to bottom. Wear particle produced.

Figure 2.1 – Schematic of adhesive wear.

2.3.1.2 Abrasive Wear

The term abrasive wear covers two types of situations, known as two-body abrasion and three-body abrasion, in each of which a soft surface is ploughed by a relatively hard material. In two-body abrasion, a rough, hard surface slides against a

relatively soft opposing surface. In three-body abrasion, hard particles trapped between the two sliding surfaces cause one or both of the surfaces to be abraded. Abrasive wear gives a characteristic surface topography consisting of long parallel grooves running in the sliding direction.[5,59,85]

Abrasion, however, does not always lead to the production of wear particles. When a hard material ploughs through a soft one, the material may simply pile up at the edges of the groove. Studies of metals scratched by model hard asperities generally show that the surface damage is of three types, as illustrated in Fig. 2.2. The blunter asperities allow the softer metal to flow around them as a wave (Fig. 2.2a). This does not cause any removal of metal on the first pass, although metal may be removed on subsequent passes. Sharper asperities cause chips to be machined from the softer surface (Fig. 2.2b). Asperities of intermediate shapes cause a wedge or prow of deformed metal to form ahead of them at the start of sliding (Fig. 2.2c). This wedge effectively blunts the asperity, so that further metal may flow around the wedge without removal, or it may intermittently displace the wedge to form a new one.[5]

a) Abrasion by a blunt particle *b) Abrasion by a sharp particle* *c) Abrasion by an intermediate particle*

Figure 2.2 – Types of abrasive action (taken from ref. 5).

2.3.1.3 Wear by Fatigue

Fatigue wear is seen as both a macroscopic phenomenon as well as a microscopic one. Macroscopic fatigue wear occurs most often in rolling-contact, while microscopic fatigue occurs at the contacts between sliding asperities. As the articulation of hip implants involves mainly sliding contact, the discussion in this section will be limited to microscopic fatigue wear. When any two solid surfaces are placed in contact under a normal load, the surfaces approach each other and strain until the load is supported. In sliding, the material must also support the tangential forces. Because of their height distribution, the contacting asperities are strained to different extents, so that the contact stresses will vary from a very low level of elastic stress up to perhaps the fracture stress. Truly elastic stresses will cause no damage, while the fracture stress will cause the formation of a wear particle during a single interaction. However, at intermediate stresses, defined as any stress above the fatigue limit but below the fracture stress, the asperity will be subjected to a single fatigue cycle, and the accumulation of such cycles with continued sliding will eventually cause a surface fatigue fracture and the generation of a wear particle. This type of wear often results in the formation a pit.[5,59,85]

2.3.1.4 Wear by Delamination

During the initial contact or running-in period of a typical tribological pair, the surfaces in contact will be losing material in such a way that they become smoother. Once this happens, the surfaces in contact with one another exert repeated subsurface cyclic shear loading, similar to that experienced during fatigue wear. As this cyclic loading continues, voids and cracks are nucleated below the surface, usually at the plane of maximum shear. Crack nucleation at the surface is prevented by the triaxial compressive stress which exists immediately below the surface. Further cycling causes the voids and cracks at the plane of maximum shear to link up and form long cracks at an approximately constant distance below the surface. When the cracks reach some critical length, the stress situation at the crack tip causes the crack

to break through the free surface, resulting in the formation of thin plate-like wear particles. The surface thus appears to be missing plates from its top layer once delamination takes place.[5,85]

As described above, fatigue and delamination appear to somewhat contradict one another. Fatigue wear describes the formation of fractures at the surface, while delamination takes place because fracture occurs at the subsurface and at the same time, fracture is prevented at the surface level. It would seem that for fatigue wear to take place, the surface must have asperities, while for delamination to occur, the surface would have to have been flattened. With this in mind, it is possible that fatigue would occur if running-in does not polish the surface well or after other wear mechanisms, such as delamination, deteriorate the polish.

2.3.2 Material Selection

As previously discussed in this chapter, numerous materials have been considered for the use of hip implant applications. What follows is a discussion of the potential of some of these materials for this application.

2.3.2.1 Stainless Steel and Titanium Alloys

When McKee was challenged to find an appropriate material for articulation, he quickly realized that stainless steel lacked the required bioinertness and wear properties for a successful combination with itself.[65] His first metal-on-metal implants, which were made of stainless steel, would loosen after only 1 year in service.[3] Despite their very good surface corrosion resistance, stainless steels are subject to several other types of corrosion processes, including crevice, pitting, intergranular and stress corrosion. These processes can lead to the release of metallic ions into the surrounding tissue with undesirable biological consequences and, in addition, can profoundly degrade the mechanical strength of the alloy. Duff-Barclay et al[23] have shown that under lubricated conditions, stainless steel had a very high wear rate as well as high frictional torques. Under dry conditions, which is not that uncommon in

hip joints, especially during the first motions after a static situation, the steel seized after only a short time due to adhesive wear.

The titanium alloy used in surgical implants is most often Ti-6Al-4V, which possesses a surface hardness of 330, and a very low contact angle of 20 degrees with distilled water,[27] which implies that it should form a good lubricating film. It has been shown by Duff-Barclay et al[23] that under dry conditions it performed very poorly compared with the cobalt-chrome, and seized only a short time after the stainless steel. They have also shown that despite the low contact angle water forms on Ti, under wet conditions, it performed especially poorly in terms of wear and friction. This poor tribological performance may be due to the oxide layer present on the titanium. Although highly passive, the oxide is mechanically weak, and would therefore readily experience several mechanisms of wear, resulting in surface finish degradation causing the friction to be high.

2.3.2.2 Polyethylene

The low elastic modulus of polyethylene is the main reason behind its low friction in the joint. During articulation, the deformation of the plastic, made possible by its low elastic modulus, allows the ingress and egress of the lubricating fluid. Its low elastic modulus, however, causes a problem in terms of wear. Abrasive wear was described as a result of a soft surface (with a low elastic modulus) being abraded by a harder, rougher surface, which is exactly the scenario seen in the articulation of a metal head in the polyethylene cup. Also, adhesive wear has been reported to greatly affect the performance of polyethylene. The polyethylene is transferred to the harder metallic surface with several subsequent results. The bond between the transferred polyethylene and metal component is weak and therefore the polyethylene sheds off the ball into the joint space.[27] Polyethylene also forms a very high contact angle of 100 degrees with distilled water,[27] which means that it is not wet well by the lubricant. Once the metal head is covered by the polyethylene (due to adhesive wear), the result is the articulation of two poor-wetting, soft materials. This dry articulation re-

sults in excessive amounts of wear, which is often observed with the metal-on-polyethylene implants. Another aspect of adhesive wear is the adhesion of the passivated layer of oxide on the opposing implant surface (metal head component) to the polyethylene, resulting in transfer of the passivated layer to the polymer. This material is then essentially a free oxide polishing powder that can accentuate the roughening process of the hard bearing surface.[27] Polyethylene also suffers from fatigue wear. The high stress on the polyethylene, resulting from low conformation of the articulating surfaces, high loads, or both, can cause surface stress that exceeds the fatigue strength of the polyethylene. Multiple stress cycles can progress to crack formation and production of polyethylene wear debris.[27]

2.3.2.3 Cobalt-Chrome

Cobalt as a Base

Cobalt alloy systems consist primarily of an austenite matrix, γ, which is of a face centered cubic (FCC) structure. Although the FCC structure is the high temperature phase, it usually exists as a metastable room temperature phase. The stable room temperature phase is hexagonal close packed (HCP), which has a transformation temperature of 417°C. Upon cooling of cobalt, the kinetics of transformation from FCC to HCP are very slow, and therefore the FCC is most often the phase found at room temperature.[68]

The cobalt FCC matrix has a low stacking fault energy and thus has the tendency to from stacking faults. Stacking faults are layers of atoms arranged in one crystal structure within a lattice matrix of another. Therefore, in cobalt, which is mainly FCC, small layers or volumes of HCP structure can be created by stacking faults. It is considered that for cobalt alloys, stacking faults can be regarded as a precursor to more massive HCP formation.[68] The transformation from FCC to HCP is a diffusionless transformation and can be induced thermally or through applied strain.[12,65,78] Stacking faults and the HCP phase inhibit dislocation motion, and therefore, with such a transformation, the cobalt increases in hardness while loosing duc-

tility. Because of the increase in hardness, such a transformation may be desirable in the cobalt alloy used for the articulating surfaces of the hip implant, as an increase in hardness may mean an increase in wear resistance.

Effects of Alloying Additions

Surgical grade cobalt-chromium alloys include the addition of 27-30 wt% Cr, 5-7 wt% Mo, 0.35 wt% C (maximum) and Co for the balance. The addition of chromium is necessary in order to create a highly resistive passive film, which contributes substantially to corrosion resistance.[65] Molybdenum is added for solid solution strengthening.[6] Cr and Mo also have the effect of lowering the stacking fault energy and therefore contribute to the formation of HCP.[68] Carbon, on the other hand, increases the stacking fault energy and therefore stabilizes the FCC structure.[12,68]

Although carbon stabilizes the FCC phase, its presence appears to be essential for wear resistance. Carbon plays two roles in cobalt alloys. By forming an interstitial solid solution with cobalt it strengthens and hardens the material.[68] Carbon also forms very hard carbides, which are highly cohesive with the FCC matrix.[65] It is possible, that in the presence of HCP, the cohesiveness of the carbides would differ.

The main carbides formed with the composition of the surgical grade alloy, are of the forms M_7C_3 and $M_{23}C_6$, where M is some combination of Co, Cr and Mo. These carbides are very hard and increase the strength and hardness of the alloy, which is a desired effect for wear resistance. Very often, only $M_{23}C_6$ carbides are found in these alloys. They form directly from the alloy matrix as residual carbon is precipitated during solidification or aging, and combines with the metal (often chromium) in the following reaction:

$$6C + 23Cr \rightarrow Cr_{23}C_6$$

If M_7C_3 is formed, it too often transforms to $M_{23}C_6$ by the following reaction:

$$23Cr_7C_3 \rightarrow 7Cr_{23}C_6 + 27C$$

Subsequently, the carbon released by this reaction diffuses locally in the alloy matrix, reacting with more chromium to form fine precipitates of $M_{23}C_6$. The fine precipitate occurs as a background dispersion generally surrounding the larger blocky primary carbides. These secondary carbides tend to further strengthen the alloy, as they too are hard and are finely dispersed.[68]

Effects of Carbon Levels

As discussed above, during the manufacturing process of the surgical grade cobalt-chrome alloy, carbides are formed. These carbides, which adhere firmly to the surrounding metal matrix, have ceramic-like properties. They are approximately 5 times harder than the Austenitic metallic phase and are relatively brittle.[65]

With the above statement in mind, the excellent wear properties of the alloy can be examined. In the application of joints, metal couples must be of the same metal, as the risk of galvanic corrosion is present when two dissimilar metals are placed in contact. It is an argument heard often that similar or identical materials, especially metals, perform poorly as sliding partners. But the diagram in Fig. 2.3 indicates that metal combinations not only exist, but are even regarded as tribologically more favorable than metal/polymer or ceramic/polymer combinations in some applications. However, sliding partners made from similar or identical metals have the tendency to perform poorly compared with dissimilar metals. This is an argument against metal combinations. However, if the alloy contains carbides, the contact between sliding surfaces with slightly protruding carbide asperities may be dominated by carbide-on-metal microcontact. In Fig. 2.3, this corresponds to the metal-on-ceramic or dissimilar metals region with favorable wear and friction properties. Further, in terms of wear mechanisms, to provide sufficient resistance against adhesive wear, sliding partners with a high interfacial energy may be chosen. In general, these are materials that are insoluble in each other and have different types of chemical bonds. This condition is formally met for two-phase cobalt-chrome alloys with predominantly metal-carbide (metal-ceramic) microcontact. A high resistance against

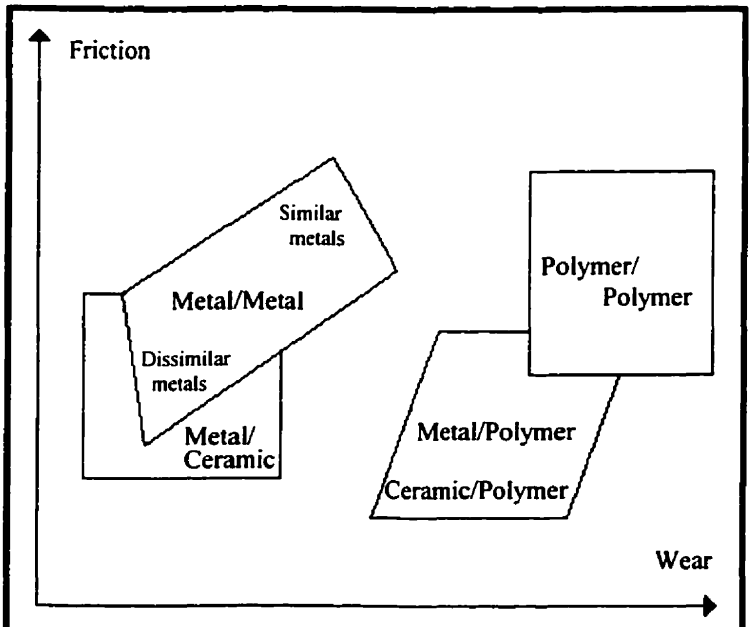

Figure 2.3 – Schematic representation of the wear and friction properties of different material combinations (taken from ref. 65).

adhesive and abrasive wear is usually provided by materials with high hardness and high fracture toughness, respectively. Hardness is a typical property of ceramics, whereas fracture toughness is characteristic for metals. Appropriate metal alloys with dispersed hard, ceramic-like particles combine these favorable properties. The hard particles increase both the surface hardness and the resistance against plastic deformation. This has a positive effect on the wear resistance, and therefore, the presence of carbon can be argued to be essential for the successful articulation of metal-on-metal combinations made of cobalt-chrome.[65]

It is essential to note, however, that a prerequisite for the metal/ceramic system to be effective, is a good adherence of the hard, ceramic-like particles in the metallic phase.[65] Although it is thought that the carbides adhere firmly in the matrix, there have been reports of worn surfaces which have shown evidence that the carbides have been removed from the surface.[12] This suggests that even though it would appear that a high carbon content would improve the wear properties as a result of the presence of carbides, these carbides may be present on the articulating surfaces only initially. What may be left after a certain period of articulation is only metal, which is mainly FCC because of the presence of high levels of carbon to stabilize it. If in fact the carbides do not remain imbedded during the service of the implant, it may be

best to have a low carbon alloy in order to facilitate the transformation from FCC to the harder HCP phase. Other reports, however, maintain the argument that the integrity of the carbides is good, and that they are not gouged out in single pieces, but rather in fragments. This does imply that they certainly adhere well to the matrix.[65]

Effects of Material Processing

In the as-cast condition, the carbides formed in the cobalt-chrome alloy are mainly found in the grain boundaries and the interdendritic regions.[68] They tend to be of approximately 20μm in diameter[73] and the grains tend to be very large, in the millimeter range. When wrought, the carbides are reduced in size to 2-3μm,[3,73] and the grains are reduced in size to approximately 10μm in diameter. As such, the wrought alloy is more homogeneous and thus a better surface finish is obtained with this structure.[3,12] The better surface finish of this wrought alloy has been shown to result in lower friction and wear when compared to the cast alloy.[3,12,43,73] The wrought alloy also possesses better mechanical and fatigue properties, making it a better candidate for the application of hip prostheses. It cannot be ignored, however, that the cobalt-chrome cast alloy has historically performed well as a self-bearing material in first generation metal-on-metal implants.[12] Further testing is therefore necessary in order to determine which alloy is the better candidate for articulation in the hip joint.

3.0 OBJECTIVES

As was pointed out in the previous chapters, it is essential to minimize the wear rate of hip implants in order to ensure their long term success. Although the re-introduction of metal-metal hip implants has reduced the volume of wear debris released into the body when compared with polyethylene, wear debris is nonetheless still produced. It is therefore desirable to entertain any feasible idea that would potentially minimize the wear of metal-metal implants.

Studying and optimizing the geometry of the ball and socket configuration is one approach that was, and still is, being studied in great detail by workers such as Medley et al[43] and Chan et al.[10,12] In this project, a more materials oriented approach was chosen as a potential for reducing the metal-metal implant wear. This study was based on the assumption that knowledge of the wear mechanisms in metal-metal joints will lead to potential improvements in the metal with respect to wear.

Therefore, the main objectives of this study are:

1) To qualitatively characterize the morphology of the wear surfaces of femoral heads of metal-metal implants.
2) To describe the probable wear mechanisms as suggested by the morphology characterization. This objective relies on the fact that different wear mechanisms have different characteristic features, which may therefore be determined by the wear surface characteristics.
3) To compare and contrast the wear mechanisms in the three different Co-Cr-Mo alloy types, both qualitatively and if possible, quantitatively.

4) To determine if examination of the wear surfaces may quantitatively reveal the volumetric wear.

5) To make recommendations for ways to reduce the wear and/or suggest further studies based on the findings from the above objectives.

4.0 MATERIALS & METHODS

In order to achieve the goals of this project, it was necessary to decide what samples would be wear tested and characterized. Ideally, the most accurate characterization would be achieved by examining implants that were retrieved from patients. However, choosing retrievals for this study had several drawbacks. Most limiting was the availability of such samples, as they are difficult to come by. Also, even if a sufficient number of them could be collected in a timely manner, they would almost certainly have large variability. For example, if the wear characteristics of the three Co-Cr-Mo alloys are to be compared, it would be best to articulate them under the same conditions. However, different patients have different body weights, activity levels and synovial fluid lubricating characteristics, just three factors of many. The different patient properties vary the articulating conditions, and therefore, examining retrievals was considered only if they became available, and for the sole purpose of comparing them to the samples actually chosen for this study.

A more appropriate set of samples, the ones actually characterized in this study, were implants that were tested or articulated in a hip simulator. This sample set was more readily available than retrievals, and the simulator made it possible to minimize the variability between samples, namely body weight, activity level and lubricating fluid properties. The disadvantage to using hip simulator samples is that the tribology system in question is not perfectly simulated. Of greatest concern is the difference in lubricating characteristics. The simulator did not articulate the implants in the physiological position, arguably making it easier for the fluid to ingress into the

joint. Also, the human body uses synovial fluid for lubrication, while the lubricant used in the simulator was bovine serum. There is controversy over the concentration of bovine serum that would best simulate physiological conditions. Nevertheless, the simulator is better at reproducing the tribology of the joint when compared to pin-on-disk wear studies, and therefore, it was decided that implants tested in a hip simulator would serve this study best.

4.1 STUDY OVERVIEW

There were two main components to this study. The first entailed characterizing 15 implants that were wear tested in the simulator to different test cycles, all at three times body weight. Six of the implants were characterized before wear testing, three others were characterized after 3 million cycles of testing, which is equivalent to 3 years in the body, and six more implants were characterized after 6 million cycles of testing (6 years in the body). In the second part of the study, the six implants from the first part that were not wear tested, were now wear tested at five times body weight, and they were progressively followed and characterized. They were characterized once again before wear testing and after 0.25, 0.45, 0.75, 1.0, 1.5 and 2.0 million test cycles. To better put the overview into perspective, a flowchart of the study can be seen in Fig. 4.1, which shows all the heads examined. Please note that only the heads, and not the cups, were characterized, for the reason that the cups were either too large or of an unsuitable geometry for the microscopy equipment that was used.

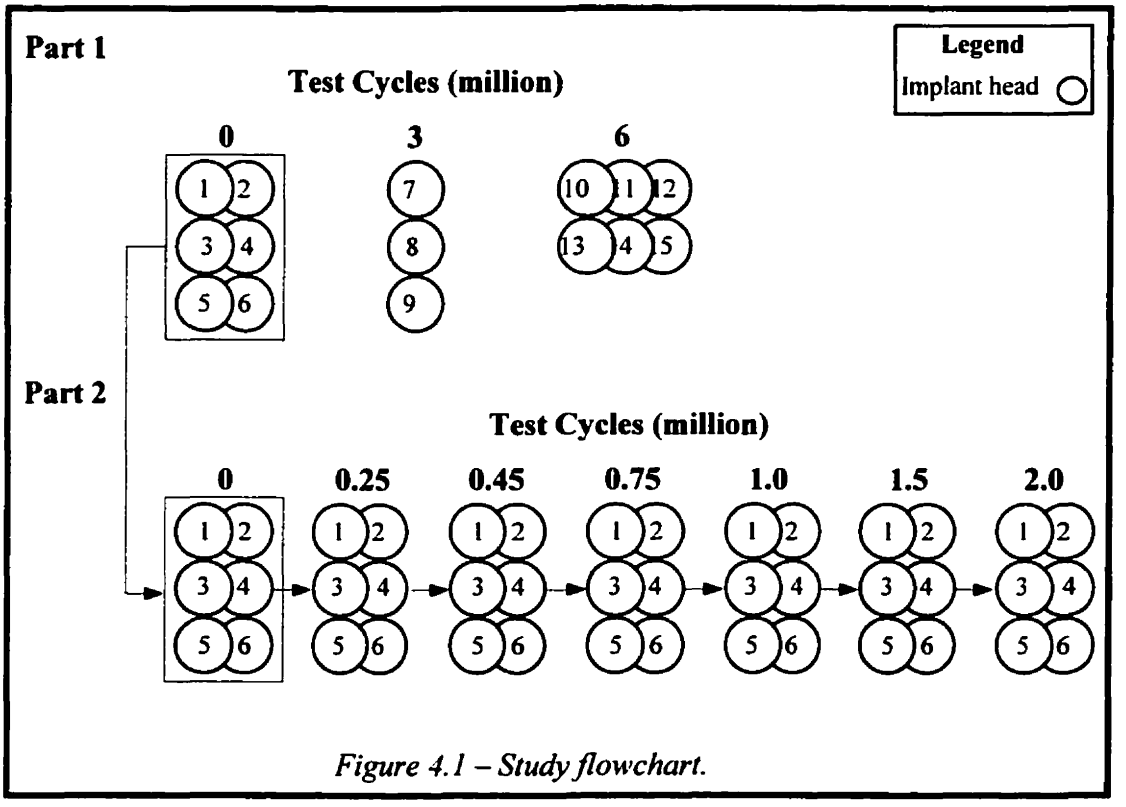

Figure 4.1 – Study flowchart.

4.2 THE SIMULATOR

The simulator used for this study was a model EW08 MMED hip simulator (MATCO, La Canada, CA), which had 8 test stations available for use at one time (Fig. 4.2). The simulator subjected the articulating surfaces to a biaxial rocking motion with a peak load of 2.1kN (three times body weight) or 3.5kN (five times body weight) applied in a Paul loading cycle at 1.13Hz, approximating the resultant normal force during walking and jogging respectively.[51] All tests were run in a lubricating bovine serum containing antibacterial and antifungal agents.[12,43] The cycle motion of each wear station simulated about 46 degrees of flexion-extension, and involved multidirectional motion at the articulating surfaces as described by Medley et al.[45] Testing methods and conditions are described in detail by Chan et al.[12] It should be noted that all implants characterized in the first part of the study were wear tested by

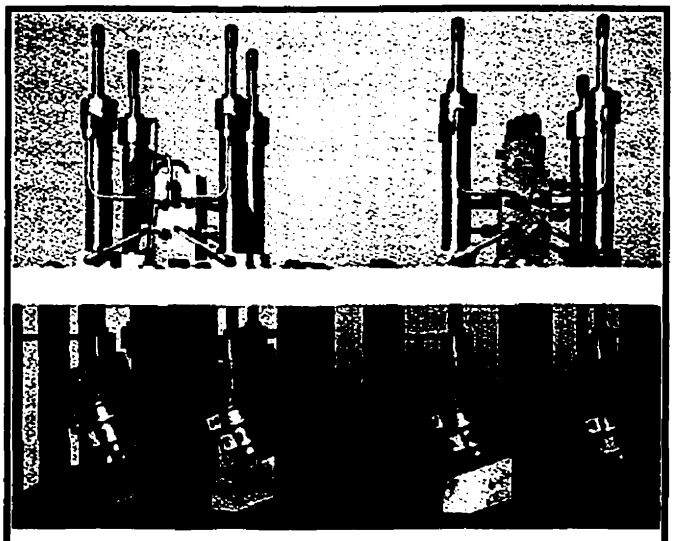

Figure 4.2 – The EW08 MMED hip simulator (taken from Ref. 12).

Chan, and the six implants characterized in the second part of this study were tested according to Chan's procedures. Issues related to the simulator testing were not a subject of this study and will thus not be discussed further.

4.3 IMPLANT SPECIMENS

The samples wear tested in the simulator were 28mm diameter metal heads that were mated with hemispherical metal cups of a slightly larger inner diameter (Fig. 4.3). The inner diameter of the cups was larger in order to allow a diametrical clearance of approximately 40-100μm between the head and the cup. Studies by Chan et al[10, 12] and Medley et al[43,45, 46] have shown that this clearance is essential for the creation of a polar, as opposed to an equatorial contact between the head and cup in order to minimize friction as well as wear. At the same time, the clearance should be as small as manufacturing technology would allow so that the best lubricat-

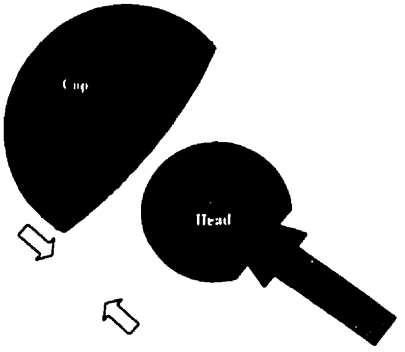

Figure 4.3 – Schematic of implant specimens that were tested in the hip simulator.

ing properties could be achieved, which in turn minimizes the wear.

The implants for this study were manufactured by Wright Medical Technology Inc. (Arlington, TN, USA) using state of the art fabrication techniques. After numerical control machining, the heads were ground to size with roughing stones and finishing stones employed in a rotary fashion, and finally polished with diamond paste. This procedure was a standard superfinishing process for the manufacture of metal-metal hip implants. Final cleaning of the heads was accomplished by ultrasonic immersion in sodium-borate and sodium-hydroxide solution baths, followed by rinsing in water. The components were subsequently passivated according to standard ASTM F86-91 procedures. This entailed immersion of the implants in 20 to 40 vol% nitric acid at room temperature for a minimum of 30 minutes, or at 49-60°C for a minimum of 20 minutes.[4]

The grinding stones used during manufacturing are commonly utilized for metal-metal implant fabrication and were made of SiC abrasives that were bonded with a silica/boron-oxide/alumina glass. They are manufactured by mixing SiC abrasive particles (of a known average size) with a small amount of binder pellets. The desired stone shape is prepared by taking this mixture and pressing it into a mold to form what is called a green component. The green component is subsequently sintered in a high temperature furnace in order to allow the bond pellets to soften and flow around the SiC abrasives, which causes the abrasives to consolidate and form a shape with enough mechanical integrity for its intended use. A schematic diagram of the process can be seen in Fig 4.4. In the sintered condition, the grinding stones had a volumetric density of 50%, which means that 50% of the volume of the stones was in the form of gaps. For esthetic purposes, once consolidated, the grinding stones are dipped in a bath of sulfur, filling the gaps between the abrasives.

The roughing stones contained SiC abrasives that were of an average size of 12-15μm and the finishing stones contained smaller SiC abrasives which were of an average size of 3μm. The bond pellets that are mixed with the SiC abrasives are of a size between the roughing and finishing abrasives. The mix is about 90wt% SiC and

10wt% binder in the roughing stone while in the finishing stone there is 95wt% SiC and 5wt% binder. The compositions of the abrasives and the bond, as given by the manufacturer (Darmann Abrasives, Clinton, MA, USA) are listed in Table 4.1.

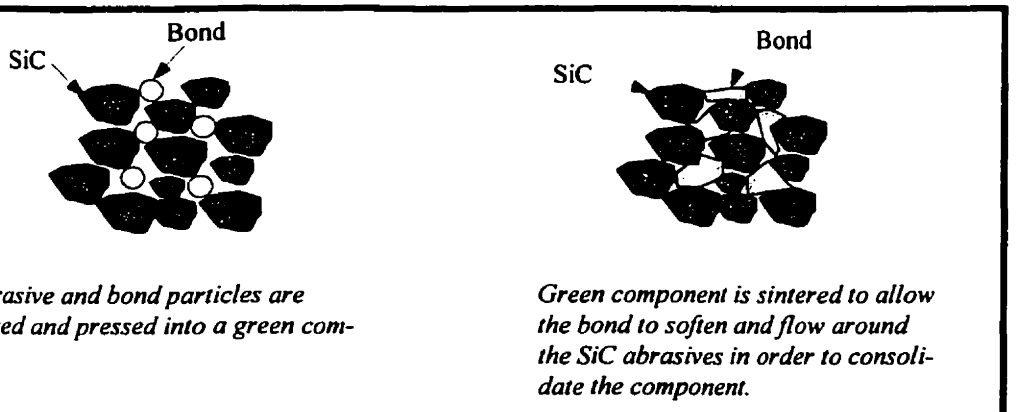

Figure 4.4 – Schematic of grinding stone manufacturing process.

Table 4.1 - Composition of grinding stone constituents as given by the stone manufacturer (Darmann Abrasives, Clinton, MA, USA).

	Composition (Wt%)				
	SiC	SiO_2	B_2O_3	Al_2O_3	Trace
SiC Abrasive (Roughing & Finishing)	99	—	—	—	1% Possibly MgO<0.1%
Binder	—	50	25	10	15% Components unknown Contains no MgO

4.4 SAMPLE INFORMATION

Of the metals that are commonly used as biomaterials, Co-Cr-Mo alloys are the preferred metals for self-bearing applications,[61, 79] and these alloys are classified by ASTM. While the original metal-metal hip implants from three decades ago were

typically made of cast Co-Cr-Mo alloy,[79] the modern generation implants are made from one of three Co-Cr-Mo alloys. All three alloys were included in this study. The implants were made from Co-Cr-Mo alloy which was either cast (ASTM F75-92), low carbon wrought (ASTM F1537-94) or high carbon wrought (ASTM F1537-94). The ASTM composition standards for these alloys are given in Table 4.2. The typical carbon content of the low carbon wrought alloy is 0.05wt% while that of the cast and the high carbon wrought is 0.2wt%. As pointed out in Chapter 2, all three alloys have a large proportion of Cr, which is necessary in order to create a passive oxide film that contributes substantially to corrosion resistance.[65] The alloys also have 5-7wt% Mo for solid solution strengthening.[6] Carbon is added at levels of less than 0.35wt%, also for solid solution strengthening, but more importantly for the formation of carbides, which further strengthen the material and possibly improve wear resistance. The carbides present in the alloys are usually in the form of $M_{23}C_6$, where M is some combination of Co, Cr and Mo.[68]

Of the 15 implants that were characterized, six were cast, six were high carbon wrought and three were low carbon wrought. The flow chart of the study (Fig. 4.5) was edited to show their distribution. In the first part of the study, of those that were characterized before simulator testing, two were cast, two were high carbon wrought and two were low carbon wrought. Of those that were tested to 3 million cycles, there was one of each alloy, and of those that were tested to 6 million cycles, there were three of the cast and three of the high carbon wrought. Unfortunately,

Table 4.2 – ASTM standard compositions of Co-Cr-Mo surgical alloys.[4]

	Composition (Wt%)											
	Cr	W	Mo	C	Fe	Ni	Si	Mn	N	P	S	Co
Cast (F75-92)	27-30	0	5-7	≤ 0.35	≤ 0.75	≤ 1	≤ 1	≤ 1	0	0	0	Bal.
HC Wr (F1537-94)	26-30	0	5-7	≤ 0.35	≤ 0.75	≤ 1	≤ 1	≤ 1	≤ 0.25	0	0	Bal.
LC Wr (F1537-94)	26-30	0	5-7	≤ 0.35	≤ 0.75	≤ 1	≤ 1	≤ 1	≤ 0.25	0	0	Bal.

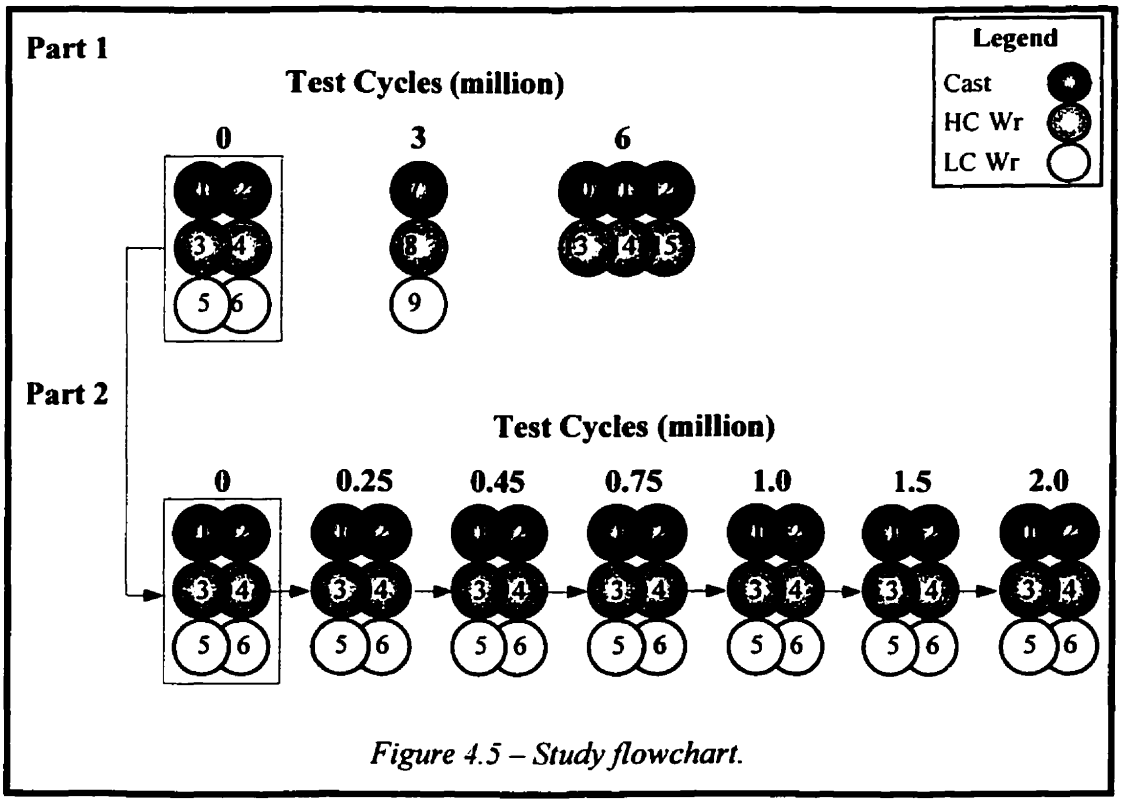

Figure 4.5 – Study flowchart.

there were no low carbon wrought implants available for characterization after 6 million cycles. And of course, the six untested implants from the first part were carried on to the second part of the study.

Each implant started with a certain clearance and a certain surface roughness, all of which are given in Table 4.3. Chan et al[10, 12] have shown that the initial roughness is also a very important variable for minimizing the wear. The smaller the initial surface roughness, the lower the wear. Geometrical effects were not the interest of this study, therefore, the implants chosen had similar diametrical clearance (40-102μm) and similar initial surface roughness (R_a = 2-20 nm).

Table 4.3 – Initial geometry of samples.

1	61	9.0
2	52	6.7
3	76	12.4
4	66	2.6
5	51	9.1
6	36	10.2
7	41	6.8
8	66	2.1
9	102	8.0
10	81	6.4
11	86	5.0
12	86	7.6
13	81	19.8
14	67	10.1
15	76	6.0

4.5 MICROSTRUCTURAL EXAMINATION

After wear testing and prior to characterization, the three heads that were tested to 3 million cycles in the first part were sliced with a low carbon diamond blade into several sections. One section of each head was used for microstructural examination. These sections were mounted in bakelite and were subsequently ground and polished to a final polish of 0.05μm alumina suspension. The polished sections were subsequently electroetched with a solution of 60 vol% nitric acid in water, which was kept at room temperature. The cast alloy was etched for a total of 12s, the high carbon wrought for 18s, and the low carbon wrought for 20s, all at 5V. Prior to examination, the species were sputter coated with gold and palladium in order to render them conductive.

4.6 PREPARATION OF THE HEADS FOR EXAMINATION

Prior to any characterization, the implants were cleaned in order to ensure that there wasn't any bovine serum residue. After wear testing, the implants were first

cleaned according to methods described by Chan,[10] and were subsequently weighed in order to determine their wear rates.[10] After weighing, the implants were rinsed with an acetone stream after which a replicating tape was applied to their surface. Replicating tape is most often used for accurately replicating a surface when it is not possible to examine that surface in any other manner. The tape works by sliding one of it's faces over acetone, which causes that face to soften, while the other remains rigid. The softened face has very good fluid characteristics, and therefore, when placed over a sample surface, the fluid flows into all the features of that surface. Once the tape hardens, it is gently removed from the sample, creating a negative of the sample surface. Because of it's superior fluid characteristics, this technique is sometimes used to clean a surface. While the hardened tape is not likely strong enough to remove a significant amount of metal atoms from the sample, it is capable of removing organic material, leaving the sample surface clean. After using this technique on the implants, they were subsequently immersed in an ultrasonic bath of acetone which ensured that there was no replica tape residue left on them.

4.7 CHARACTERIZATION TECHNIQUES

For the wear surface characterization, two microscopes were used; a scanning electron microscope (SEM) and an atomic force microscope (AFM). For a small part of this study, an x-ray diffractometer (XRD) was also used.

4.7.1 SEM

The first microscope used was a JEOL 840 SEM which was operated in three modes. In the secondary electron mode, it served to examine the morphology of the wear surfaces. In the back scattered electron mode, it was used for compositional imaging. Finally, the energy dispersive spectrometer (EDS) was used for qualitative elemental analysis of the different wear surface features. The EDS used was a NORAN

I2 that was equipped with an ultra thin window for detection of low atomic number elements. The SEM was also used for the microstructural characterization.

Depending on the mode in operation, the accelerating voltages were set to 5, 10 or 15kV. Typically, in secondary electron mode, the wear surfaces were analyzed at 5kV and the microstructural characterization was carried out at 15kV. 15kV provided better resolution than 5kV and would have therefore served better for the wear surface analysis. However, unlike the microstructures, the implant surfaces were not sputter coated with gold and palladium and were thus less conductive. As a result, they charged more readily, which was less prominent at 5kV when compared with 15 or even 10kV. In the back scattered mode, 5kV was used to examine the wear surfaces, once again for the purpose of avoiding charging. The EDS was used at either 5 or 10kV. Typically, when detection of higher atomic number elements was desired, the higher voltage was used.

In the first part of the study, a special SEM mount was not available for examining the heads. When it was desired to examine the pole, the head was placed upright in a standard mount (Fig. 4.6). When the edge or the equator was of interest, the head was rested on its side in that same mount. With this system, it was difficult to find the same region twice, particularly because the head was spherical with no point of reference, and therefore its placement was never the same from one examination to

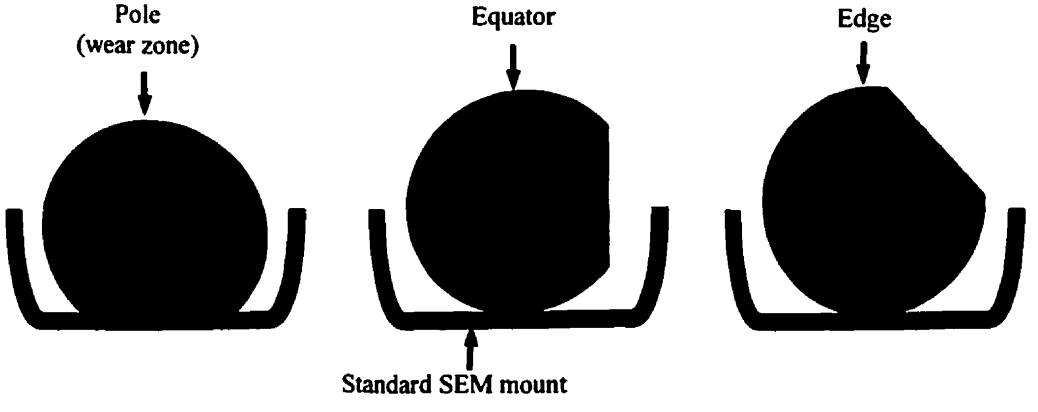

Figure 4.6 – Schematic diagram of the implant head and its placement in the SEM on a standard mount.

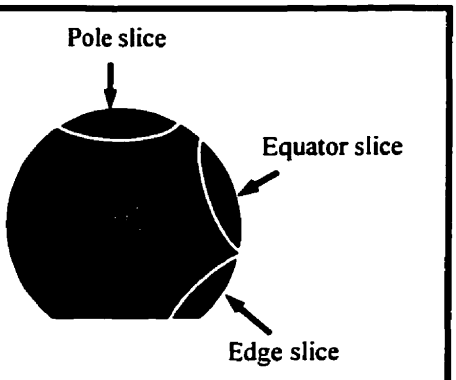

Figure 4.7 – Schematic diagram of transverse slices taken from heads #7, 8 & 9.

another. With the three implants that were tested to 3 million cycles, transverse slices, instead of full heads, were examined (Fig. 4.7). Each slice was placed flat in the same mount. When the pole was to be examined, the slice taken from the pole was mounted, and likewise when the equator or the edge were of interest.

For the second part of the study, a special SEM mount was fabricated in order to create a coordinate system for the heads. This way a particular spot could be viewed more than once and hence progressively followed with continued simulator testing. With this system, the heads were viewed from the top, making the pole, P, the origin. From the pole, the system moved North, (N), South, (S), East, (E), or West, (W). This system, however, was only two dimensional, even though the sample was spherical. Therefore, 1mm moved North meant that the distance viewed along the sphere in the North direction was in fact more than 1mm. The images viewed with the SEM were recorded with Polaroid pictures. In the second part of the study, several numbers were noted on the pictures taken. First, the number of test cycles, written as A (for articulation) followed by a number (ex. 0.75). The number gave the number of test cycles in millions. Next, the location of where the picture was taken was noted. First, the direction was indicated (ex. N), then the distance in that direction away from the pole (ex. 2). The number gave the distance in millimeters. So, if we were to examine an implant that was tested to 0.75 million cycles, and we took a picture 3 mm East of the pole, on the Polaroid, the notation would read A0.75 E3.

4.7.2 AFM

For increased resolution, the characterization was also performed using a Digital Instruments Dimension 3100 atomic force microscope (AFM). The AFM was used in tapping mode and all images acquired were flattened. In the tapping mode, two signals were collected; height and phase. The height revealed the surface morphology, which allowed for some feature quantification by taking line cross-sections of the image. The phase revealed when two or more different phases were adjacent to one another if the phases differed sufficiently in order to be resolved. Unlike the SEM, the images acquired by the AFM were recorded digitally.

In each part of this study, establishing a coordinate system with the AFM was not possible because the heads were too tall for the motorized stage. Also, because the heads did not fit on the stage, an area of only 4 to 5mm^2 around the pole could be examined. In order to examine a larger area, the heads would have to have been tilted on their side. It was not possible to clamp them down in this manner in the absence of the vacuum which was available only on the motorized stage.

4.7.3 XRD

A Rigaku Rotaflex rotating anode x-ray diffractometer was used in order to quantify the volume fraction of FCC and HCP phases that were present on the wear surfaces and to compare that volume fraction to that of the bulk of the material. This was done in order to determine if the articulation caused a phase change from FCC to HCP, as speculated by Chan.[12] This was also performed in order to determine if the manufacturing process (namely grinding and polishing) caused the same above phase change.

The two comparisons were established by having the diffractometer penetrate deep into the sample or just graze the surface of the sample. For the former, the sample was irradiated with a beam perpendicular to its surface. In order to examine a shallow section of the surface, the surface was irradiated with the beam striking at a shallow angle of 1.5°. This examination was done only on the three heads that were

sliced (implants # 7, 8 & 9) as the full heads could not fit in the machine.

The two depth measurement was done both at the wear zone as well as at the edge of the head, where wear did not occur (Figs. 4.6 & 4.7). At the wear zone, the two depth measurement was performed in order to show if articulation changed the FCC and HCP volume fractions. At the edge, the two depth test was performed in order to show the influence of the manufacturing process on the FCC and HCP volume fractions.

4.8 GRINDING STONE EXAMINATION

As a result of some of the findings that were made during the wear surface characterization (which will be discussed later), it became necessary to examine the grinding stones used during manufacturing of the implants. The end sections of a roughing and a finishing stone were supplied for this study by the manufacturer of the implants (Wright Medical Technology Inc.). Fragments of the stones were acquired from random areas of the stones by subjecting the stones to hammer blows in an attempt to produce thin stone fragments. These fragments were anchored to SEM aluminum mounting studs with double sided carbon tape. Once secure, the fragments were sputter coated with gold and palladium in order to render them conductive. A large section from each stone (roughing and finishing) was separately ground to powder with a SIEBTECHNIK ring and puck pulveriser. The powder was subsequently subjected to x-ray diffraction using a PHILLIPS PW 1710 x-ray diffractometer. This was done in order to identify the compounds present in the grinding stones and confirm the composition as given by the manufacturer of the stones.

The grinding stones were further investigated by acquiring bond material from the manufacturer of the stones (Darmann Abrasives). The manufacturer placed a small amount of bond powder in the sintering furnace which caused the powder to agglomerate into a small disk. To investigate the bond, part of this disk was ground in

the SIEBTECHNIK ring and puck pulveriser, and the resulting powder was subjected to atomic absorption spectroscopy (AA) using a Perkin Elmer 3110 model. This technique was used to detect the amount of magnesium (Mg) present in the bond, for reasons that will be discussed later.

Once again, for reasons that will be explained later, the other part of the bond disk was used to attempt to scratch the implant surfaces. This was done by taking the disk and applying a light manual pressure to the surface. The implants subjected to this test were those from the first part of the study that were wear tested to 3 million cycles (implants #7, 8 & 9). This test was done on the remaining portions of the heads after the slices were removed, and was documented using the SEM.

In order to examine some of the effects the grinding stones had on the implants, two additional implant heads, made of the cast alloy, were examined. These heads were not subjected to the complete manufacturing process. One of them was ground only with the roughing stone, after which the manufacturing process was stopped. The other was subjected to grinding by both the roughing and the finishing stones, and once again, manufacturing was stopped after that. These implants were not wear tested, but were examined with the SEM.

4.9 RETRIEVAL EXAMINATION

The last implant head examined in this study was an implant head that was retrieved from a patient after only 3 years of service. Although no information was available on the patient, it is known that the implant failed because of a persistent femoral fracture and not due to osteolysis. The head was part of an all metal Sulzer high carbon Co-Cr-Mo implant. It was examined both with the SEM and AFM. No coordinate system was established for this head as it would not fit on the special SEM mount nor on the AFM motorized stage.

5.0 RESULTS

5.1 MICROSTRUCTURES

The cast microstructure (Fig. 5.1) was the coarsest of the three alloys, having grains with diameter of several hundreds of micrometers. Carbides outlined the grain boundaries and were also found within the grains. Those within the grains were either in chains or were isolated (Fig. 5.1c). The carbide size ranged from about 1 to 10μm in diameter. The cast microstructure, as described here, did not fully resemble that as described in Chapter 2. The cast alloy in the first generation metal-on-metal implants was of a coarser structure. Also, the carbides outlining the grain boundaries were of a eutectic structure, while the carbides in the cast structure examined in this study were not. Furthermore, the carbides within the grains of the first generation alloy were between the dendrites, while in the second generation, the carbides were found either isolated or in chains, a feature not observed in the first generation alloy. The difference in structure is most likely attributed to a secondary operation performed on the current cast alloy that was not performed on the first generation cast implants. The current practice is to solution anneal the cast alloy in order to partially dissolve the carbides in an attempt to make the structure more homogeneous.

When wrought, the grains of the alloy were reduced in diameter to 10μm or less. The high carbon wrought alloy (Fig. 5.2) had carbides that ranged in diameter from about 1 to 5μm and were found in abundance along the grain boundaries as well

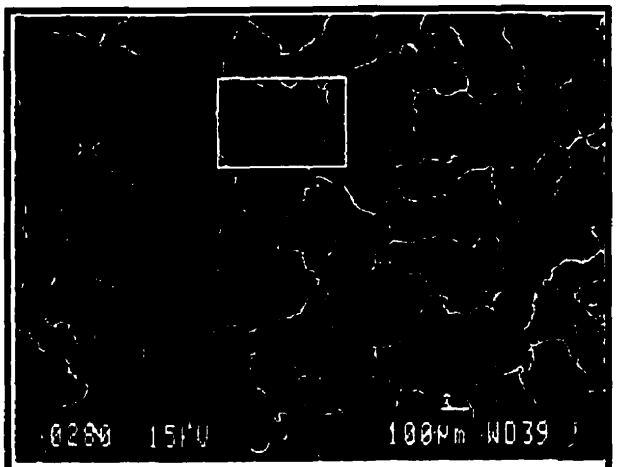

(a)

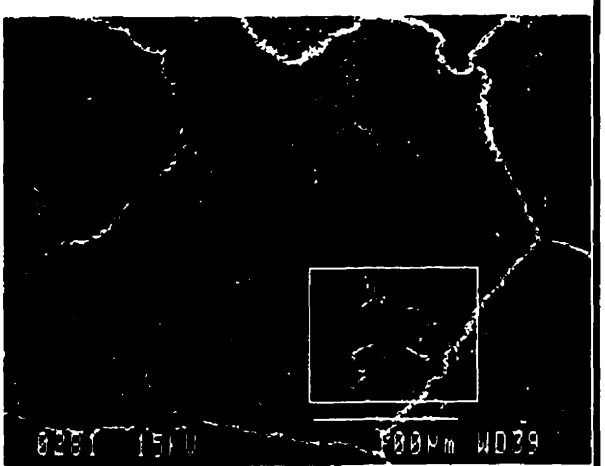

(b) Window seen in a

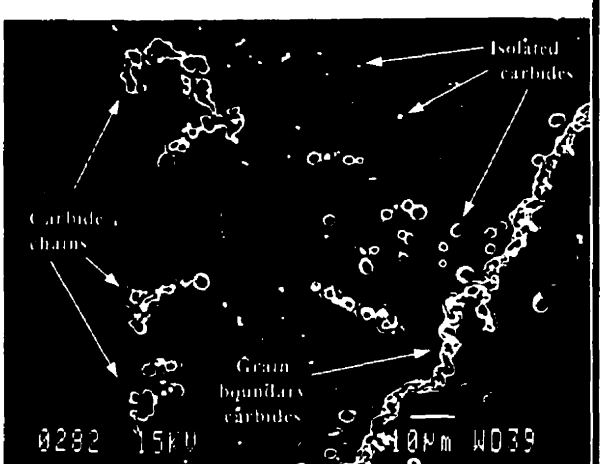

(c) Window seen in b

Figure 5.1 – Cast microstructure as seen with the SEM at 15kV (Head #7).

as within the grains. Unlike the cast alloy, the grain boundaries of the high carbon wrought alloy were not outlined by the carbides. Most of the carbides in the low carbon wrought alloy (Fig. 5.3) were less that 0.5µm in diameter and were found at the grain boundaries as well as within the grains. Some carbides, about 1µm in diameter, were also present and were noted only at the grain boundaries.

The carbides were characterized only after they were chemically identified. The EDS was used for the purpose of identification. When the carbides were analyzed (Fig. 5.5), they were shown to have molybdenum and particularly chromium at levels higher than those seen in an analysis of the matrix (Fig. 5.4). The carbides were also depleted in cobalt, while the matrix was rich with cobalt. When the same analysis was done with the EDS while the ultra-thin-window was inserted, the carbides showed carbon content at a higher level than the matrix. Because of

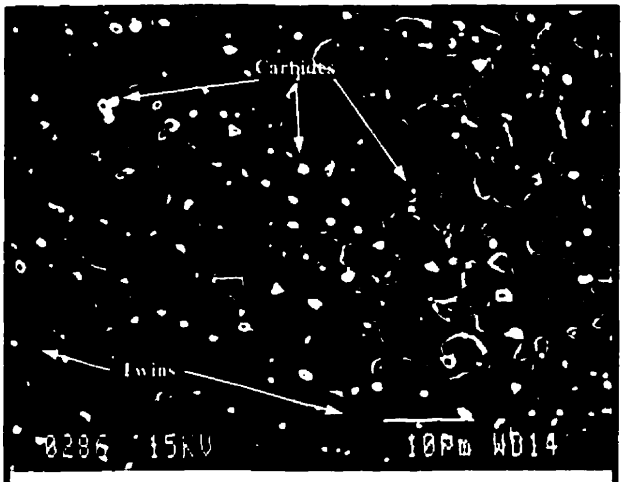

Figure 5.2 – High carbon wrought microstructure as seen with the SEM at 15kV (Head #8).

the elevated levels of carbon and chromium, the particles analyzed were identified as carbides.

Also of interest was the presence of twinning bands seen in the wrought alloys (Figs. 5.2 & 5.3) and the lack of them in the cast alloy (Fig. 5.1). The twinning bands were most abundant in the low carbon wrought alloy. Twinning occurs only in HCP crystal structures and not in that of FCC. The twinning present in the wrought microstructure was most likely an indication of the presence of the HCP phase or at least a precursor to its formation. As discussed in Chapter 2, in these alloys, HCP may form by thermal transformation or through strain induced transformation. Because the wrought alloys are strained during processing and the cast alloy did not show any twinning, the twins present in the wrought structures were most likely a result of strain induced transformations. The pronounced presence of twinning in the low carbon wrought alloy, when compared with the high carbon wrought, was most likely the result of the reduced carbon levels. Because carbon is an FCC stabilizer, its presence in reduced levels would facilitate the formation of HCP.

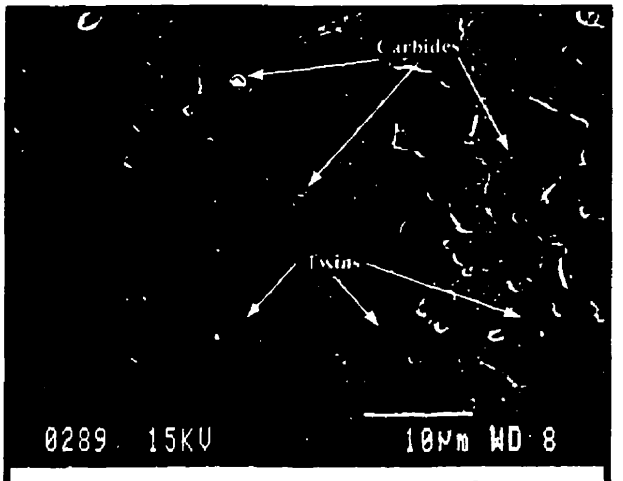

Figure 5.3 – Low carbon wrought microstructure as seen with the SEM at 15kV (Head #9).

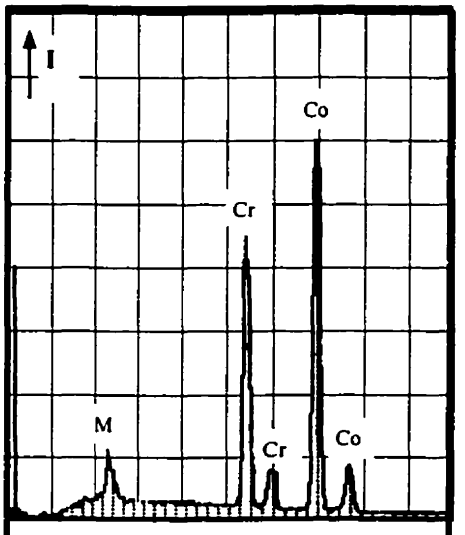

Figure 5.4 – EDS analysis of the matrix. Regular beryllium window used at 10kV.

5.2 PART 1 OF THE STUDY

Of interest in this study was the relationship between surface appearance and volumetric wear as calculated from mass loss. Table 5.1 details the volume of wear released by each implant that was examined in the first part of the study, and this table will be examined in some detail in the next chapter. Aside from the volumetric wear, this part of the study yielded numerous interesting observations. There were several prominent surface features and some less obvious. Some of the features were common to all fifteen heads, regardless of the type of alloy. The presence and the extent of some of the features depended on the number of cycles the implant was subjected to, while other features did not. What follows is a description of the features observed on the surfaces of the 15 heads examined in the first part of the study.

5.2.1 FEATURE #1 – GRINDING MARKS

The whole surface of the untested heads, as well as the surface away from the wear zone of the tested heads were characterized by randomly oriented shallow surface scratches (Fig. 5.6). Although their direction was irregular, many of the scratches were parallel to one another, suggesting that each parallel set was caused by a single action. Their location away from the wear zone and their presence on the untested heads suggested that these shallow scratches were the result of the grinding and polishing operations during manufacturing. In

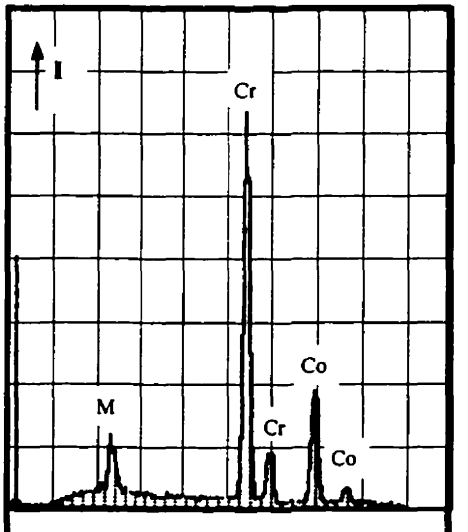

Figure 5.5 – EDS analysis of a carbide. Regular beryllium window used at 10kV.

Table 5.1 – Volumetric wear of the implants examined in Part 1 of study.

1	0	0
2	0	0
3	0	0
4	0	0
5	0	0
6	0	0
7	3	0.16
8	3	0.15
9	3	0.96
10	6	0.70
11	6	0.61
12	6	0.78
13	6	0.70
14	6	0.61
15	6	1.03

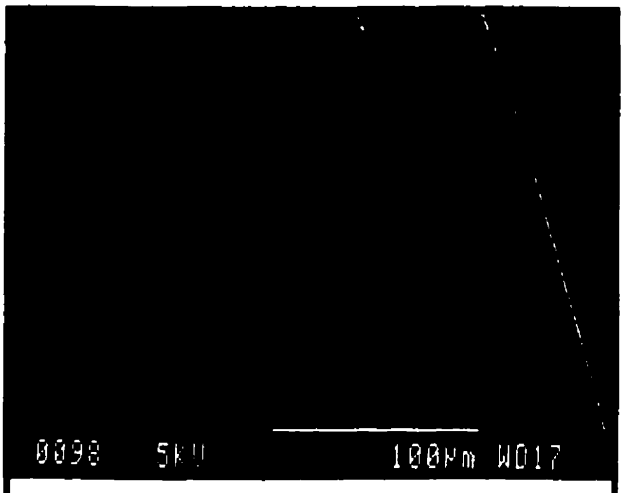

Figure 5.6 – SEM image of shallow scratches on implant surface resulting from grinding and polishing during manufacturing. Implant has not yet been tested in the simulator.

relation to the magnification in Fig. 5.6, the stones used for grinding were relatively large, and therefore one pass (or a single action) of the grinding stone over the surface would likely produce parallel scratches.

Of yet undetermined importance, the presence of the HCP phase may have a bearing on the wear performance of the implants. It is possible that the grinding and polishing operations had a direct effect on the volume fractions of the HCP and FCC at the immediate surface. Because of the potential importance, this was investigated by x-ray diffraction as described in section 4.7.3. If the grinding and polishing operations caused a phase change, the x-ray diffraction pattern of the immediate surface would differ from that of the bulk of the material. The bulk and immediate surface diffraction patterns of the edges of heads # 7, 8 & 9, where articulation had not taken place, were obtained and those of head # 7 (cast alloy) are given in Fig. 5.7. On the graphs, the first feature to note is the dashed vertical lines which illustrate the position of the diffraction peaks of FCC and/or

HCP, and in what relative intensities. Upon examination of the diffraction patterns, it appeared that the peaks were shifted 1 or 2 degrees to the left of their expected positions. Such a shift may occur for several reasons, one of which may be because the surfaces examined were spherical. The second feature of interest was that the two diffraction patterns, namely that of the bulk of the material and that at the immediate surface, differed. Some of the peaks at the immediate surface were absent from the bulk of the material and vice versa. The relative intensities of the peaks were also different when comparing the two diffraction patterns. These two observations were also true for heads # 8 and 9 (high carbon and low carbon wrought). The difference in diffraction patterns suggested that the grinding and polishing did in fact have an impact on the crystal structure of the alloys. The exact effect, however, is unclear, as the diffraction patterns were complex. In general, the higher the peak, the higher the volume fraction of the feature represented by that peak. Unfortunately, some of the FCC and HCP peaks overlapped and therefore it was not quite clear if grinding increased or decreased the fraction of HCP. In order to truly determine the volume fractions of FCC and HCP, the crystallographic texture would have to be examined. In addition, the exact depth of beam penetration would have to be calculated. Both these operations are relatively complex and were not within the scope of this study. What is clear, however, is that grinding and polishing operations did alter the crystal structure.

5.2.2 Feature #2 – Second- & Third-Body Abrasive Scratches

All fifteen heads, even the six untested heads, exhibited regions of deeper, more aggressive scratches than the grinding marks, scratches that were suggestive of abrasive wear (Fig. 5.8). The scratches usually appeared smooth in cross-section and flat at the bottom (Fig. 5.9), suggesting that they were caused by a blunt, rather than a sharp abrasive. The scratches ranged in width from less than 1μm to as wide as 20μm or larger, some of which were large enough to see with the naked eye. The edges of the scratches did not exhibit lips (Fig. 5.9), suggesting that the abrasive action resulted in removal of material as opposed to pile-up along the edges. The ends

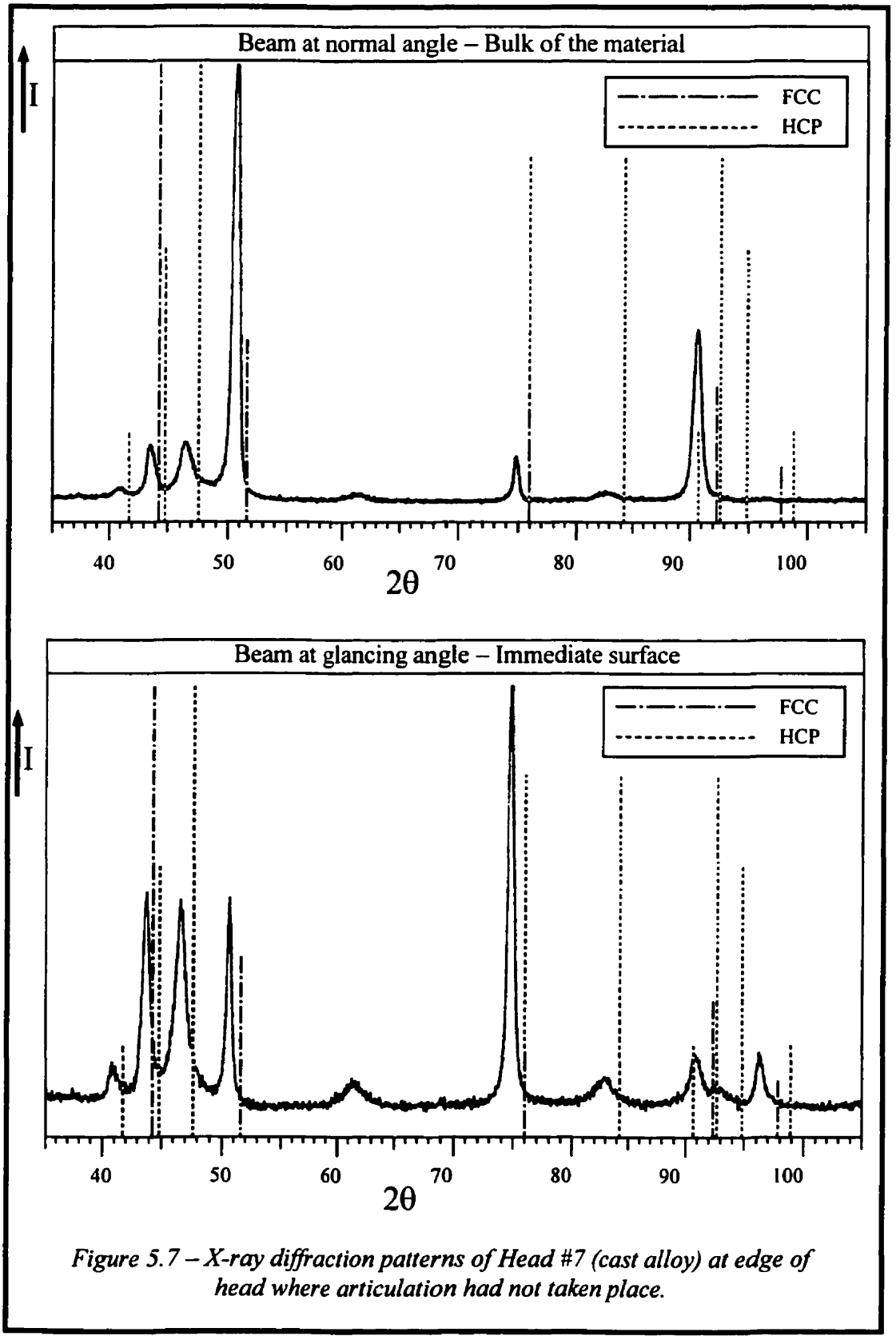

Figure 5.7 – X-ray diffraction patterns of Head #7 (cast alloy) at edge of head where articulation had not taken place.

of the scratches appeared mostly as seen in Fig. 2.2a and c, where the abrasion is shown to have been caused by a blunt particle and one of intermediate sharpness respectively, as opposed to a sharp one. An example of the end of a scratch is given in Fig. 5.10.

Two main types of scratches were observed on the surfaces. Some were straight (Fig. 5.11) thus reminiscent of second-body abrasive wear, where the abrasive body is stationary in one of the surfaces while abrading the other during articulation. Some were tortuous or irregular in shape (Fig. 5.12) thus reminiscent of third-body abrasive wear, where the abrasive is loose between the two articulating surfaces. Often, the tortuous scratches ended abruptly, suggesting that once the load was removed, the free abrasive was flushed from the joint by the lubricant or was relocated to another area. The two types of scratches were seen both individually in different regions (Figs. 5.11 & 5.12), as well as together in the same region (Fig. 5.8).

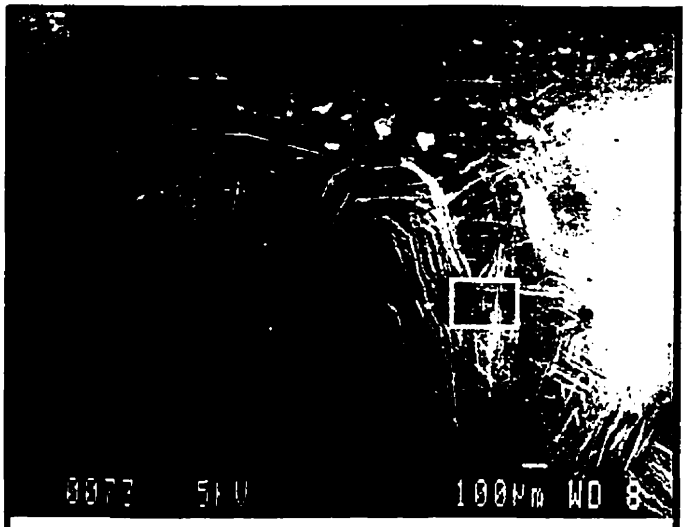

Localized scratches

Image in window above

Figure 5.8 – SEM image of localized abrasive wear at pole proximity of cast alloy after 3 million cycles of testing (head #7).

One of the heads (#15, HC wrought) exhibited straight, near parallel scratches that met at an ori-

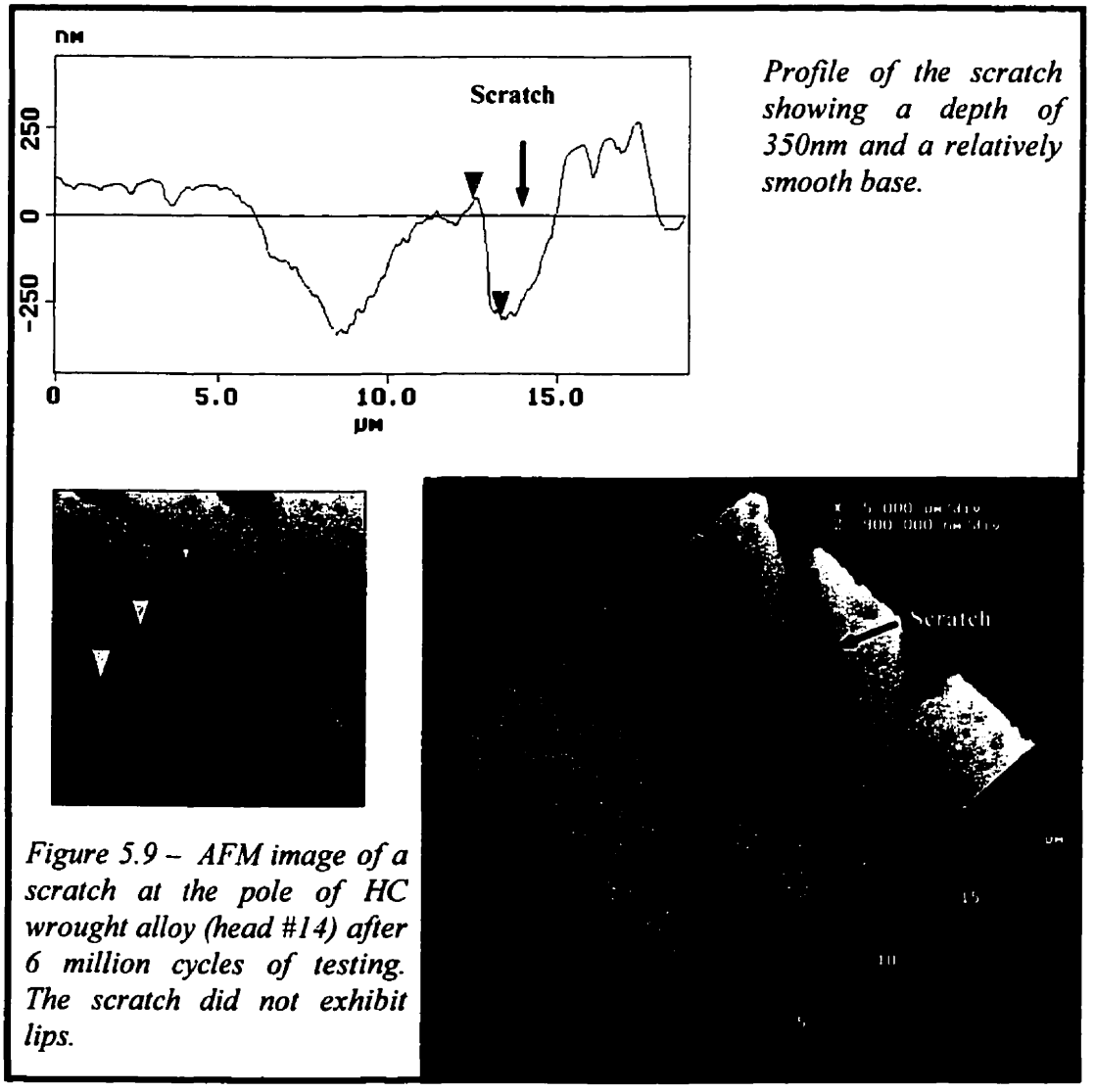

Profile of the scratch showing a depth of 350nm and a relatively smooth base.

Figure 5.9 – AFM image of a scratch at the pole of HC wrought alloy (head #14) after 6 million cycles of testing. The scratch did not exhibit lips.

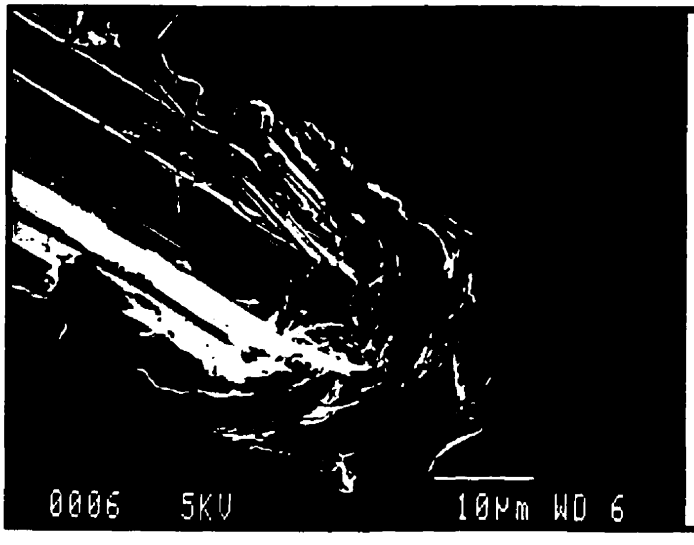

Figure 5.10 – SEM image of the end of a scratch on LC wrought alloy after 3 million cycles of testing (head #9) at the pole. The end of the scratch was similar to that seen in Fig. 2.2c where the scratch in that image was caused by a particle of intermediate sharpness.

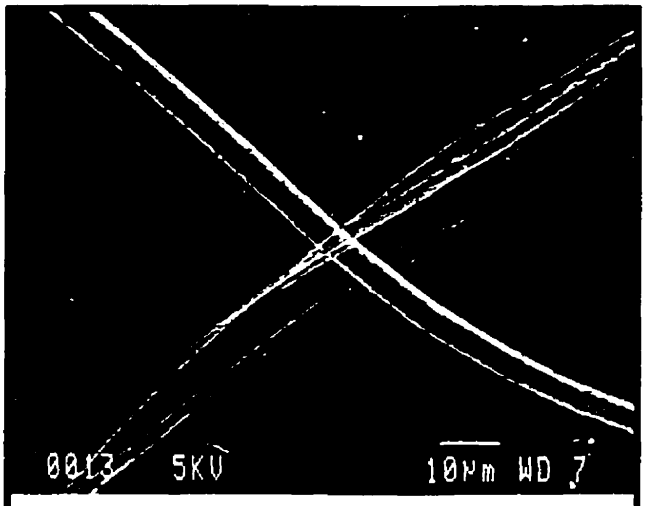

Figure 5.11 – SEM image of straight scratches found on LC wrought alloy after 3 million cycles of testing (head #9).

gin (Fig. 5.13). These scratches were straight and thus were most likely to have been caused by second-body abrasion. This implies that an abrasive particle that was imbedded in the cup was abrading the head as the cup articulated about the head. However, the pattern resulting from the abrasion was not consistent with the movement of the cup. If only one particle was responsible for causing the near parallel scratches, only one scratch would be present because one point on the cup articulates against the same path on the head with each articulating cycle. However, it was occasionally observed that during the first few cycles of testing, the head rotated about its axis until it came to rest against a restraining arm. Therefore, it is possible that the pattern seen in Fig. 5.13 was the result of a single particle abrading the head during the first few cycles of testing while the head was rotating about its axis. Once the arm came to rest, rotation of the head ceased and the particle kept on abrading the same path. This would possibly result in a deeper scratch than those making up the rest of the pattern, one that would appear darker on the SEM image (Fig. 5.13a).

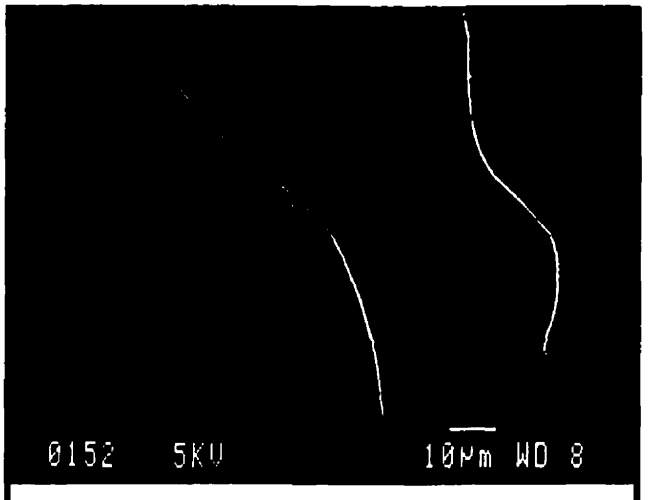

Figure 5.12 – SEM image of tortuous scratches found on HC wrought alloy after 6 million cycles of testing (head #13).

Two scratching trends were observed. First, the three alloys exhibited different amounts

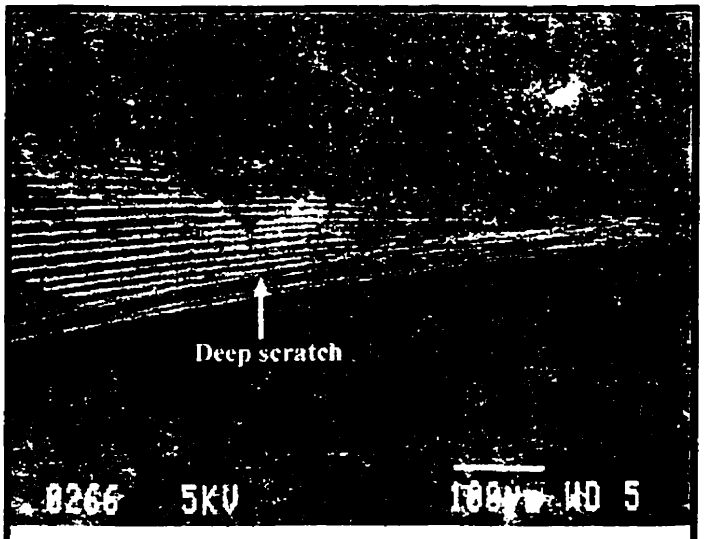

a) Scratches that met at an origin at the pole

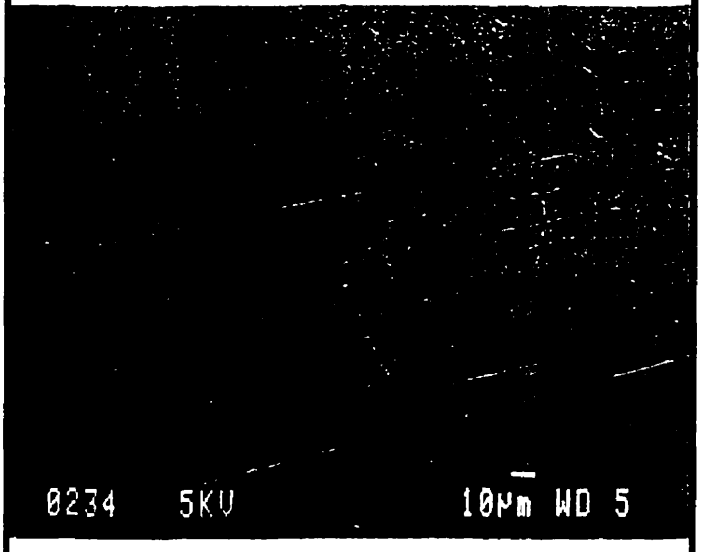

b) Scratches seen in (a) at a higher magnification

Figure 5.13 – Near parallel second-body abrasive scratches observed on HC wrought alloy articulated to 6 million cycles (head #15).

of scratching. By far, the cast alloys were abraded the most, followed by the low carbon wrought and the least scratching was observed on the high carbon wrought. Secondly, the implants were abraded the least before testing, the most scratches were observed after 3 million cycles of testing and the amount of scratching appeared to decrease at 6 million cycles. These trends were based on qualitative observations. To illustrate the trends more clearly, a schematic diagram of the amount of scratching can be seen in Fig. 5.14.

Of interest, it was common for a scratch to pass through the matrix and occasionally along its path there was a carbide. In most instances, the depth of the scratch was shallower through the carbide than through the matrix. The scratching was deeper through the matrix probably because the carbides were harder than the matrix and therefore resisted abrading better than the matrix.

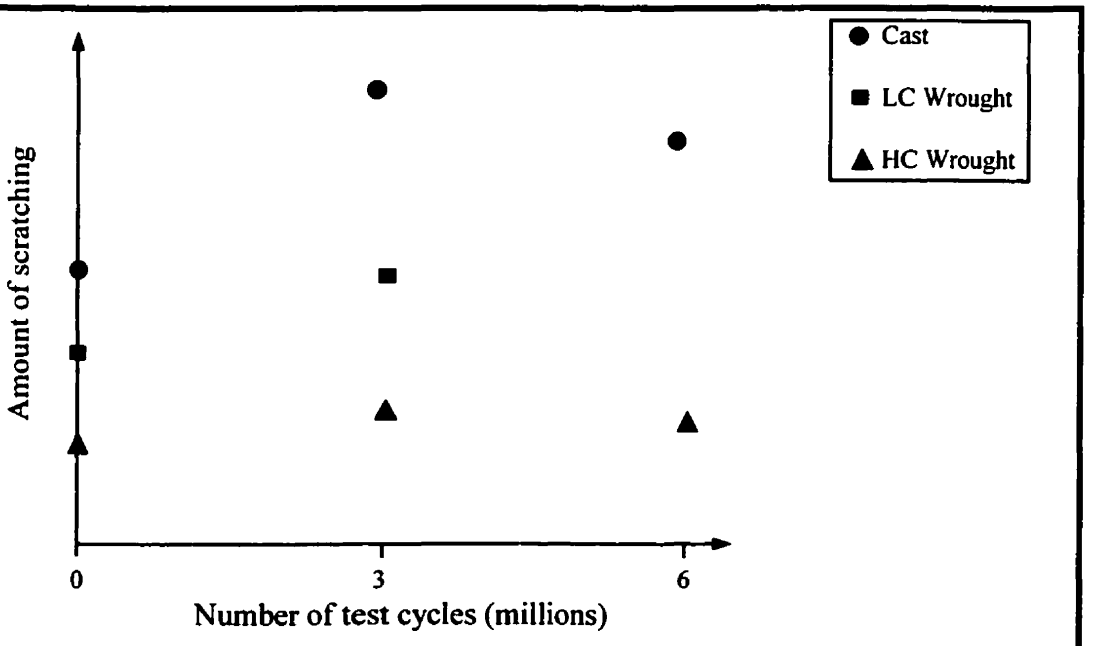

Figure 5.14 – Schematic of the amount of scratching observed on the implant heads. The schematic is based on qualitative observations. The amount of scratching was not quantified.

5.2.3 FEATURE #3 – RESIDUAL GRINDING STONES ON IMPLANT SURFACES

All 15 heads possessed small embedded particles on their surfaces. These particles were not present during the microstructural examination and have therefore been identified strictly as a surface phenomenon. The particles had two distinct appearances. Most were of the spherical kind, which negatively charged when examined in the secondary electron mode with the SEM (Fig. 5.15). Close-up imaging of these particles was difficult due to the charging. When examined at a very low accelerating voltage (2.5 kV) the charging was reduced and it became apparent that the spherical particles were comprised of a shell and a core (Fig. 5.16). The second type of particle, found much less frequently, was irregular in shape and appeared dark when examined with the SEM in the secondary electron mode (Fig. 5.17).

Both types of particles ranged in size from about 1 to 5μm in diameter or greater. Some of the spherical particles appeared as large as 20 or 30μm in diameter.

Figure 5.15 – SEM image of spherical particles detected on cast implant before simulator testing (head #2).

It is possible that some were in fact that large, however, the charging may have caused them to appear larger than they actually were. Accurate measurement of the particles was not possible with the AFM either, as the apparatus would not engage the surface in a location where these particles were present. The cantilever of the AFM would jump away from the particle as approach was attempted.

5.2.3.1 Particle Identification

In order to identify the particles, they were chemically analyzed with the EDS as described in 4.7.1. Figures 5.18, 5.19 and 5.20 are examples of the patterns obtained from analyses of different particles. The particles were shown to have Si, Al, Mg, Co, O and C in their composition. The relative amounts of these elements varied from particle to particle. Most often, the irregularly shaped parti-

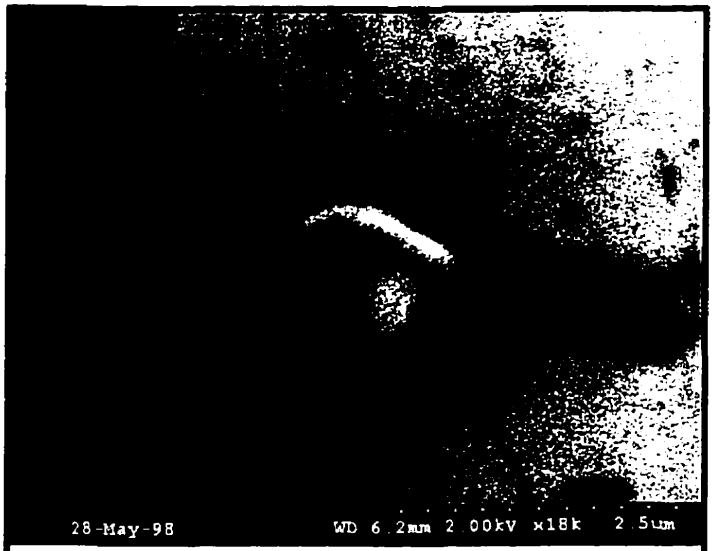

Figure 5.16 – Close-up SEM image of spherical particle detected on cast implant after 6 million cycles of simulator testing (head #11).

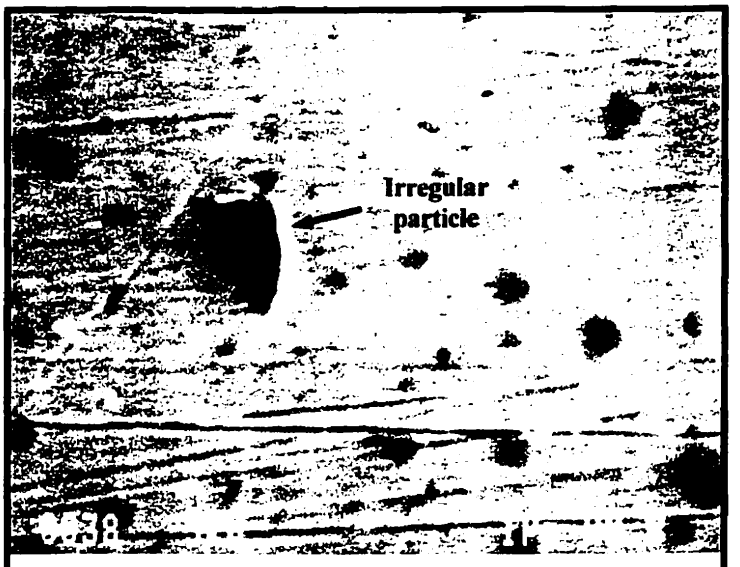

Figure 5.17 – SEM image of irregularly shaped particle detected on HC wrought implant after 3 million cycles of testing (head #8).

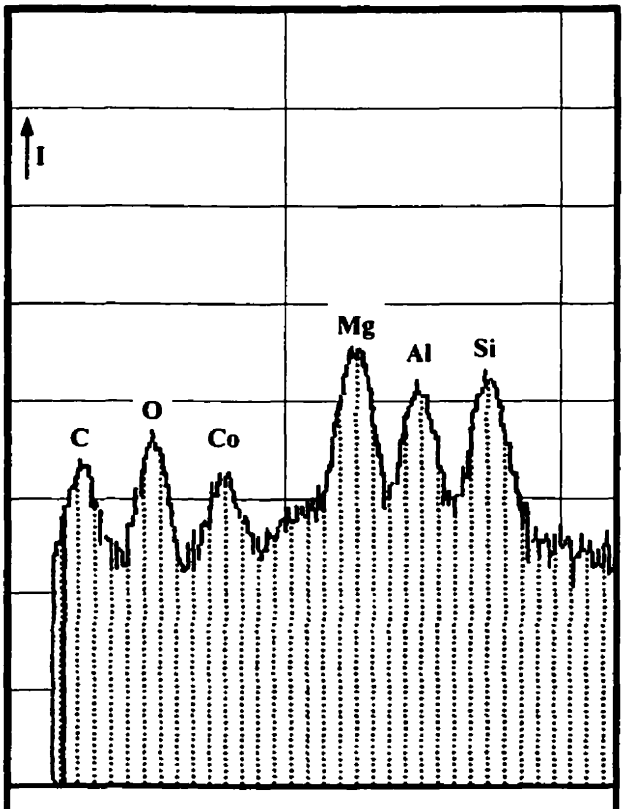

Figure 5.18 – EDS analysis of foreign particle on cast implant prior to simulator testing (head #2). EDS done at 5kV with UTW.

cles contained Si and C (Fig. 5.19) and the spherical particles contained Si, Al and O (Fig. 5.20). Except for the cobalt and carbon, the elements present in the particles were not in the composition of the alloys as given in the standards (Table 4.2). This, coupled with the fact that the particles were strictly a surface phenomenon suggested that their origin was an outside source and not a part of the alloy.

The possibility of these particles originating from an outside source prompted an investigation into the exact process utilized for implant manufacturing. The investigation revealed that the grinding operations were performed with silicon-carbide (SiC) grinding stones as described in section 4.3. The presence of Si and C in the EDS analysis of the particles suggested that the particles on the implant surfaces may

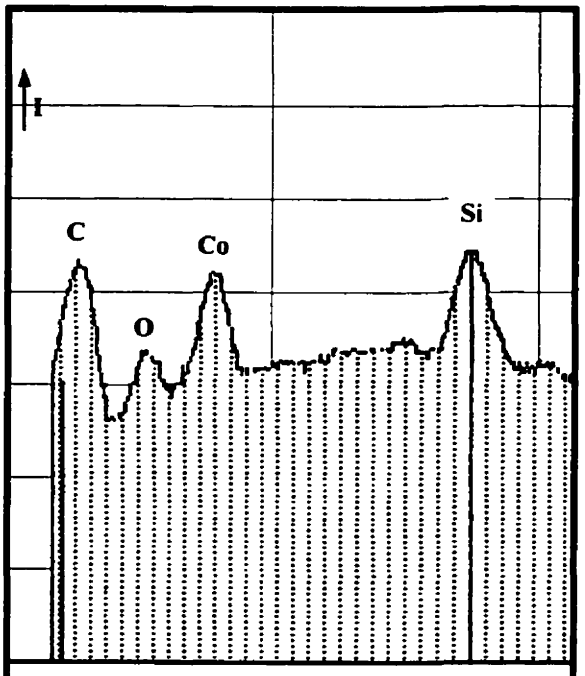

Figure 5.19 – EDS analysis of irregularly shaped particle on LC wrought alloy after 3 million cycles of simulator testing (head #9). EDS done at 5kV with UTW.

bide particles in the grinding stones were bonded with SiO_2-B_2O_3-Al_2O_3 glass binder, as described in 4.3. It is possible that the Al and O as well as some of the Si in the EDS analysis of the particles on the implant surfaces came from embedded bond particles. Boron (B) was not present in the analysis of these particles not necessarily because it was not present in the particles, but rather because it is too low an atomic number element to be detected with the EDS. The source of the Mg at this point was still unclear.

have been residual grinding stones from the manufacturing process. It was probable that the presence of Co in the EDS analysis came from the metal matrix of the implant and not necessarily the particle. The presence of Al, Mg and O in the particles, however, was still unclear.

After a discussion with the manufacturer of the grinding stones (Darmann Abrasives, Clinton, MA, U.S.) the source of Al and O may have been identified. The silicon car-

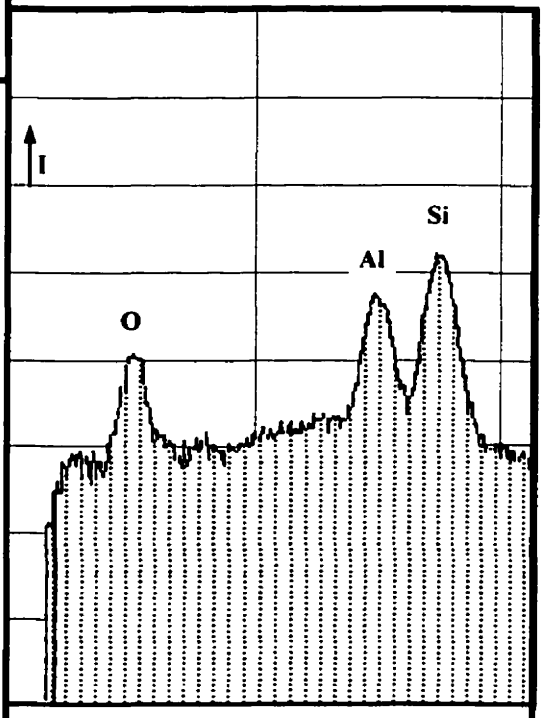

Figure 5.20 – EDS analysis of spherical particle on LC wrought alloy after 3 million cycles of simulator testing (head #9). EDS done at 5kV with UTW.

5.2.3.2 Examination of the Grinding Stones

With the above in mind, it was probable that the round particles on the implant surfaces were SiO_2-B_2O_3-Al_2O_3 glass binder and the irregularly shaped particles were SiC abrasives. In order to verify this, the manufacturer of the implants allowed examination of one of the roughing and one of the finishing grinding stones. As described in section 4.8, the grinding stones were analyzed with the SEM as well as with an x-ray diffractometer. When examined with the SEM, the roughing and finishing grinding stones exhibited similar morphologies (Figs. 5.21 and 5.22). The stones appeared to be comprised of small abrasives that were bonded to one another. The main difference between the two grinding stones was the size of the abrasives. The finishing stone had abrasives an order of magnitude finer than the roughing stone, which were several micrometers in diameter. The sizes of the abrasives were consis-

Figure 5.21 – SEM image of roughing grinding stone used during manufacturing of the implants.

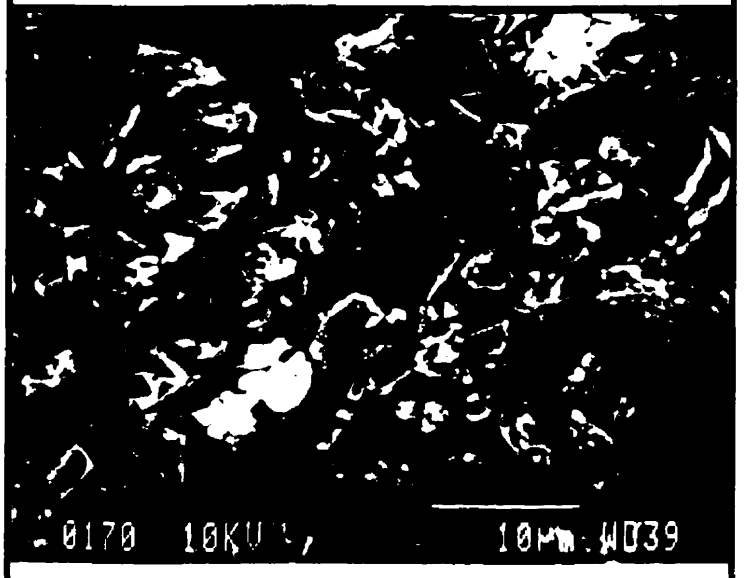

Figure 5.22 – SEM image of finishing grinding stone used during manufacturing of the implants.

tent with those quoted by the manufacturer of the stones (section 4.3).

When analyzed with the EDS, the analysis of the abrasives gave results as shown in Fig. 5.23. The presence of Au and Pd were from the sputter coating process that rendered the samples conductive. The abrasives were probably SiC because both Si and C were present. The morphology of the abrasives in the grinding stones was very similar to the morphology of the irregularly shaped particles on the implant surfaces (Fig. 5.17).

Although the roughing and finishing grinding stones appeared similar, they did have one distinct difference. Occasionally, pockets of spherical particles were found in the roughing stone (Fig. 5.24), a feature that was not detected in the finishing stone. When analyzed with the EDS, the spherical particles were shown to contain Si, Al and O (Fig. 5.25). These particles were probably the glass binder as their composition was consistent with that of the binder as given by the manufacturer. Carbon was present probably because the electron beam picked up on some of the abrasives adjacent to the spherical particles. Sulfur was present because the stones were dipped in sulfur once consolidated. The spherical binder in the grinding stone possessed the same morphology and general size as the spherical particles found on the implant surfaces (Fig. 5.16). In fact, they too were comprised of a shell and a core (arrow on Fig. 5.24).

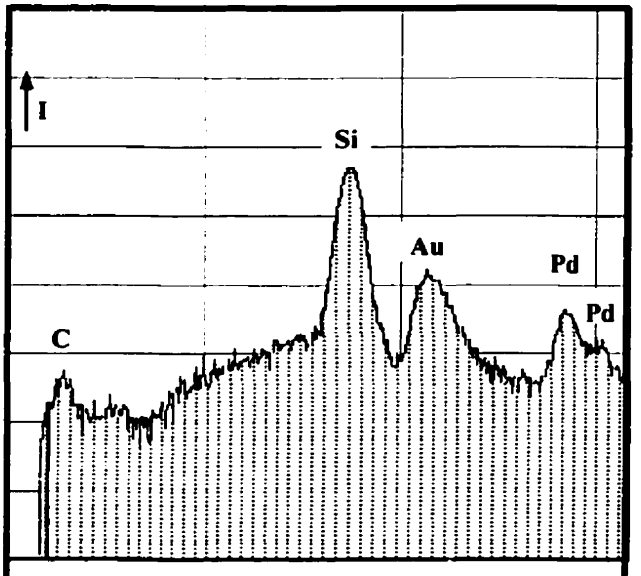

Figure 5.23 – EDS analysis of an abrasive particle in the finishing grinding stone. EDS done at 5kV with UTW.

The examination of the grinding stones suggested that the irregularly shaped particles embedded on the implant surfaces were residual SiC abrasive particles from the roughing and/or finishing grinding process. Simi-

Figure 5.24 – SEM image of a pocket of spherical particles found in the roughing grinding stone. Arrow serves to point out particle similar to that seen in Fig. 5.16.

larly, the spherical particles embedded in the implant surfaces were likely residual binder particles from the roughing grinding process. In order to verify that the binder particles were embedded during the roughing stage of grinding, two additional implants were manufactured for this study, as described in section 4.8. They were both cast alloy, one of which was ground only with the roughing stone and the other with both the roughing and finishing stones. All subsequent standard manufacturing steps were not further employed.

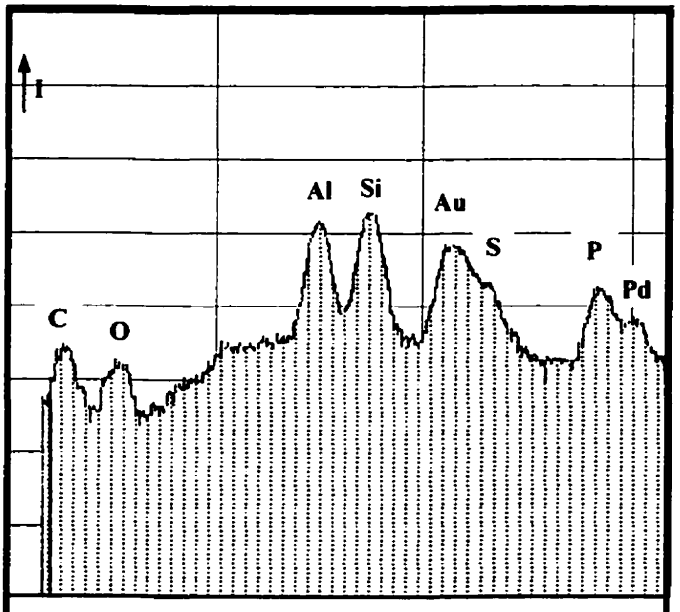

Figure 5.25 – EDS analysis of one of the spherical particles seen in Fig. 5.24. EDS done at 5kV with the UTW.

These two implants were analyzed with the SEM and two of the images are given in Figs. 5.26 and 5.27. One feature that was most prominent was the difference in the polish achieved when the finishing stone was employed after the roughing stone. The features of interest, however, were the residual

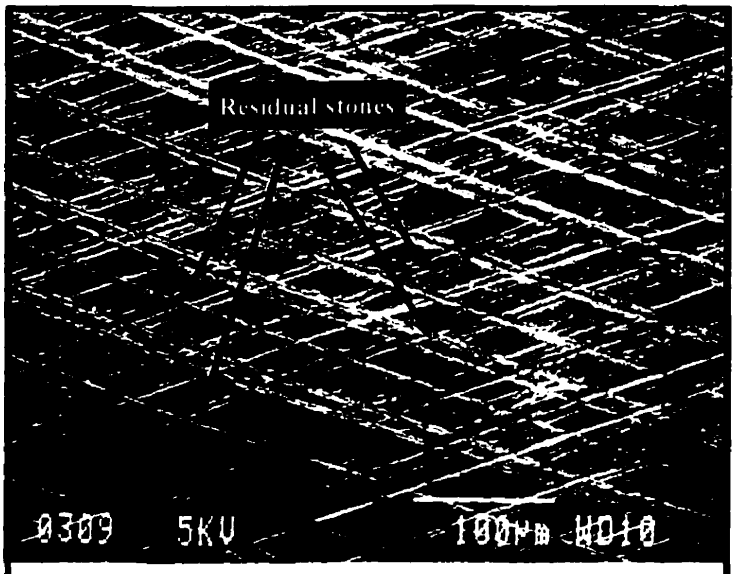

Figure 5.26 – SEM image of first additional cast implant that was ground with the roughing stone only.

grinding stones. Both implants possessed residual grinding stones on their surfaces. On the implant that was ground with only the roughing stone, the residual stones appeared mostly black (Fig. 5.26). On the other implant, the residual stones appeared more exposed and were whiter due to charging (Fig. 5.27). When analyzed with the EDS, the stones on both implants were identified as being almost exclusively of the binder kind.

Qualitatively, the amount of embedded grinding stones was the same on both implants. Because both implants had the same amount of embedded grinding stones and they were almost all of the spherical kind, and the analysis of the finishing stone did not show any binder particles, it is very likely that the stones were deposited during the rough grinding step. Also, the spherical particles on the implant surfaces were more exposed after the finish grinding step. This

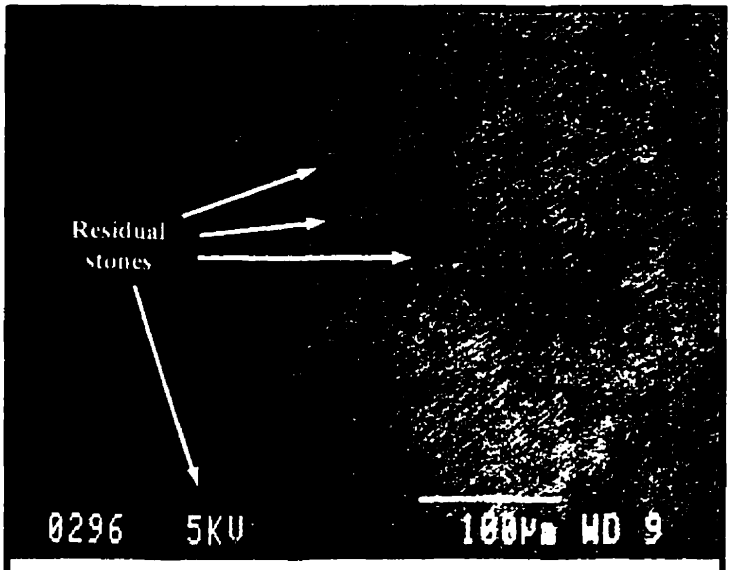

Figure 5.27 – SEM image of second additional cast implant that was ground with the roughing and finishing stones.

suggested that after deposition by the rough grinding step, the finishing stone removed material from the implant, including around the deposited residual binder, causing the spherical particles to stand out more.

5.2.3.3 Source of Magnesium

Examination of the stones, did not explain the source of the magnesium in the residual particles on the implant surfaces. According to the manufacturer of the grinding stones, the SiC abrasives and the binder did not contain enough Mg to correspond to the EDS analysis (refer to Table 4.1 and Fig. 5.18). In order to verify the claims of the manufacturer, the stones were crushed and analyzed by X-ray diffraction as described in section 4.8. The results of this analysis are given in Figs. 5.28 and 5.29. In this analysis, no magnesium compounds were identified, confirming the claims of the manufacturer. These results, however, should be taken with caution, as the resolution of the diffraction patterns was poor. In fact, even SiO_2 was not detected, despite the fact that it was present in significant amounts. Therefore, if any magnesium compounds were present in small amounts, they would probably not have

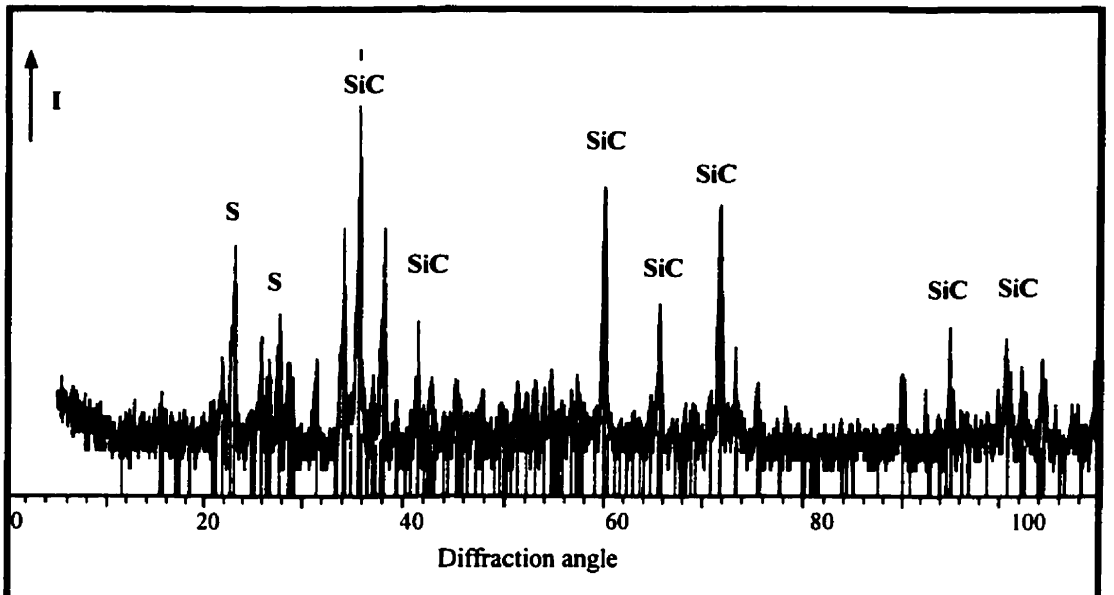

Figure 5.28 – X-ray diffraction pattern of the crushed roughing grinding stone.

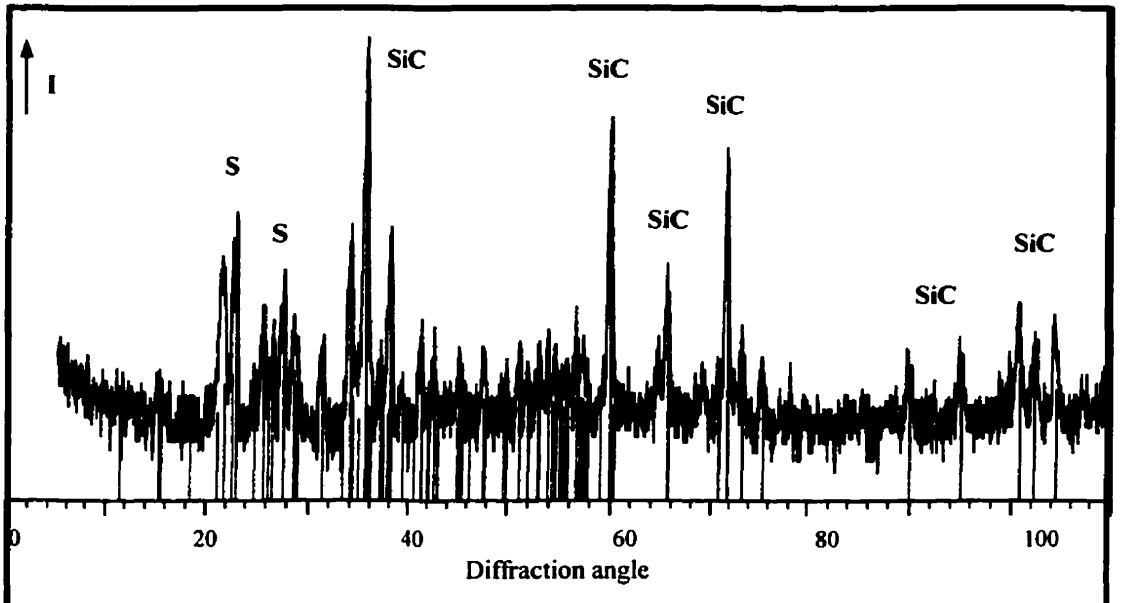

Figure 5.29 – X-ray diffraction pattern of the crushed finishing grinding stone.

been detected by this method.

The search for the magnesium source did not end there. The stone manufacturer supplied some consolidated bond material (no SiC abrasives) which was analyzed with AA as described in 4.8. The analysis yielded a magnesium content of 0.31% by weight, probably not enough to produce the peaks seen in the EDS analysis of the residual grinding stones on the implant surfaces (Fig. 5.18). With these tests, the source of magnesium was not identified and remained unknown.

5.2.3.4 Residual Grinding Stone Trend

Two trends in the amount of residual grinding stones on the implant surfaces were observed. Qualitatively, the cast implants exhibited by far the greatest amount of residual stones. The low carbon wrought implants had a moderate amount and the high carbon wrought implants showed the least amount. In fact, the high carbon wrought had very few residual stones on the surfaces. The fact that the cast implants consistently had more stones than the two wrought alloys embedded on the surface might be due to the differences in surface hardness between the alloys. The second

trend observed was the decrease in the number of stones with progression of wear testing. More precisely, before testing, the implants had the greatest amount of residual stones, followed by those that were tested to 3 million cycles, with the smallest amount being found on those tested to 6 million cycles. This, once again, was a qualitative observation. To show these trends more clearly, Fig. 5.30 gives a schematic indication of the amount of stones present on the implant surfaces as a function of test cycles. This trend suggested that as the implants were articulating, the embedded residual stones were being released from the surface and were ejected out of the joint into the lubricant. Also of interest, the residual stones remaining on the implant surfaces after 6 million cycles tended to be of the larger size. This was perhaps because the larger stones were embedded deeper into the surface and were therefore more difficult to dislodge.

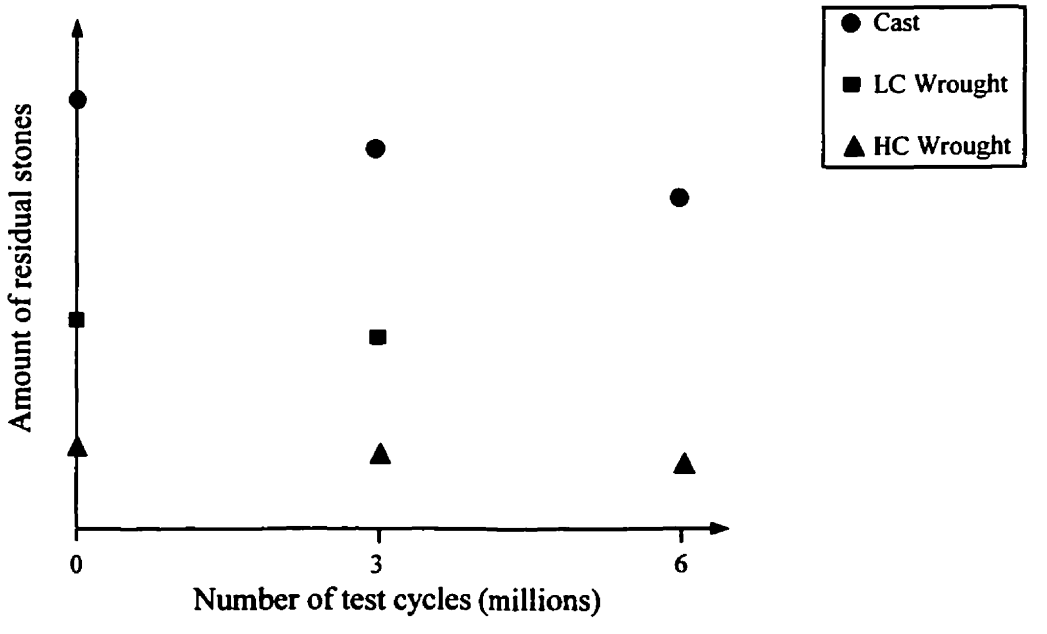

Figure 5.30 – Schematic of the amount of residual grinding stones observed on the implant heads. The schematic is based on qualitative observations. The amount of stones was not quantified.

5.2.4 FEATURE #4 – CARBIDES

When examining the implant heads with the SEM in the secondary electron mode, the carbides on the implant surfaces always appeared darker than the matrix regardless of whether they were proud, flush or below the matrix (ex. Fig. 5.31). Despite the fact that secondary electron imaging primarily reveals topographical features, it was believed that the carbides were always darker than the matrix because of a back-scattering electron effect.[30] The lower the atomic element of the feature being examined, the darker it appears. Because the carbides were of a lower atomic number element than the matrix, they appeared darker. This effect was lessened when the sample was coated with a heavy element such as Au or Pd. That is the reason why the proud carbides in the sputter coated microstructures appeared light (Figs. 5.1, 5.2 & 5.3) while those in the uncoated implant surfaces appeared dark even when proud.

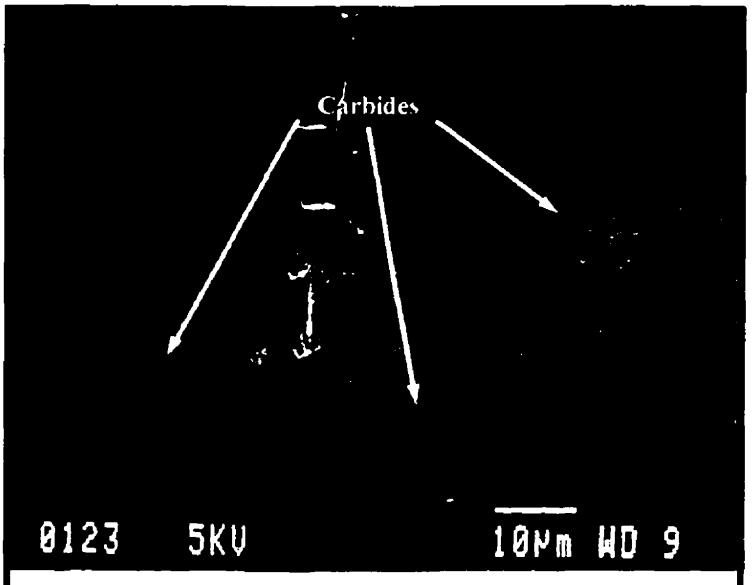

Figure 5.31 – SEM image of carbides on cast implant surface prior to simulator testing (head #2).

The appearance of the carbides on the implant surfaces changed with increasing test cycles. As such, what follows is a description of the carbides as a function of test cycles.

5.2.4.1 Carbides Before Simulator Testing

Prior to simulator testing, the SEM examination seemed to suggest that the detectable surface carbides in the as-manufactured cast and high carbon wrought components were flush with the surface (Fig. 5.31). However, AFM examination

Figure 5.32 – AFM image of proud carbides on cast implant surface prior to simulator testing (head #2).

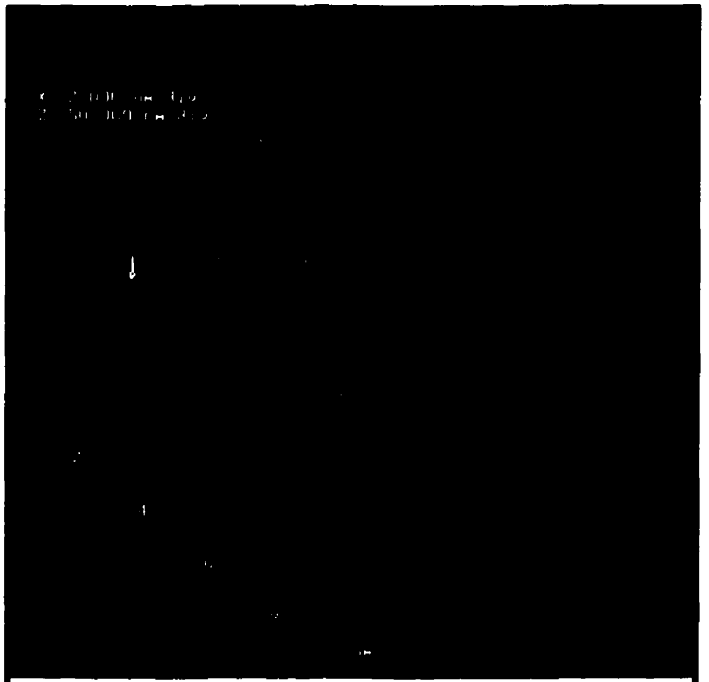

Figure 5.33 – AFM image of proud carbides on HC wrought implant surface prior to simulator testing (head #4).

showed them to be standing proud (Figs. 5.32 and 5.33). Cross-sectional analysis of the carbides showed them to be protruding several tens of nanometers on the cast components, and less than 10nm on the high carbon wrought components. The proud nature of the carbides may be a reflection of their resistance to abrasion. During manufacturing, the grinding operation, which is abrasive in nature, may not have been as effective on the carbides as it was on the matrix. As a result, the grinding stones may not have removed as much material from the carbides as they did from the matrix, resulting in proud carbides.

The carbides on the surfaces of the low carbon wrought heads were not seen with the SEM, nor with the AFM. This suggested that the carbides did

not exist at the surfaces of the low carbon wrought alloy heads. However, it should be noted that the surfaces of the implants were not sputter coated with Au and Pd. In the absence of a coating, the resolution with the SEM is most often not as sharp compared to when a coating is applied. It is probably for this reason that the carbides in the low carbon wrought alloy were visible during SEM microstructural examination, but not during SEM surface examination. The carbides, however, were not detected with the AFM either. Unlike the SEM, the AFM has sufficient resolution to detect features as small as the carbides in the low carbon wrought alloy. This once again suggested that the carbides did not exist on the surfaces of the low carbon wrought alloy heads. The carbides may have appeared to be absent simply because they might have been flush with the surface. If that was the case, the AFM would not have shown them as they would not have had a significant topography to be detected. As such, with the two techniques used for surface analysis, the behavior of the carbides in the low carbon wrought could not be characterized and will therefore not be discussed further.

5.2.4.2 Carbides After 3 Million Cycles of Simulator Testing

After 3 million cycles of testing, it appeared that aside from abrasive scratching, the wear occurred primarily at the apex of the implant heads. In this wear zone, all of the carbides on the surface of the high carbon wrought alloy (head #8) were no longer proud of the surface, but were now below the surface of the matrix (Fig. 5.34). This indicated that the carbides had been worn at a faster rate than the surrounding matrix.

Unlike the high carbon wrought alloy, only part of the carbides in the wear zone of the cast component (head #7) were worn below the matrix surface. Only the carbides in chains were worn below the matrix surface and those that were isolated remained proud (Fig. 5.35). This suggested that the two different carbide types in the cast implant had different wear characteristics. Perhaps the carbides in chains were M_7C_3 and those isolated were $M_{23}C_6$ or vice versa. Or maybe the two different car-

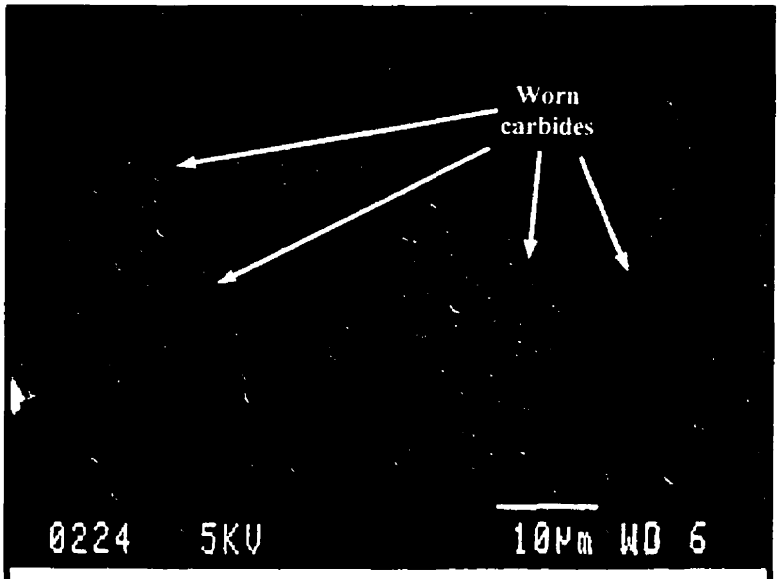

Figure 5.34 – SEM image of worn surface of high carbon wrought implant (head #8) after 3 million cycles of testing. Featured are carbides worn below matrix surface.

bide types were of a different composition and/or crystal structure. Analysis of the carbides with the EDS did not show a difference between the two types of carbides and therefore it is not known if the carbides in fact differed at all. The difference in wear behavior may also have been caused by different load bearing characteristics. In composites, it is known that fibrous phases take more of the load from the matrix than do spherical phases. In the same manner, the carbides in chains may have acted as fibers, taking more load from the matrix than the isolated round carbides. As a result, the higher loads experienced by the carbides in chains may have translated to higher wear rates of those carbides.

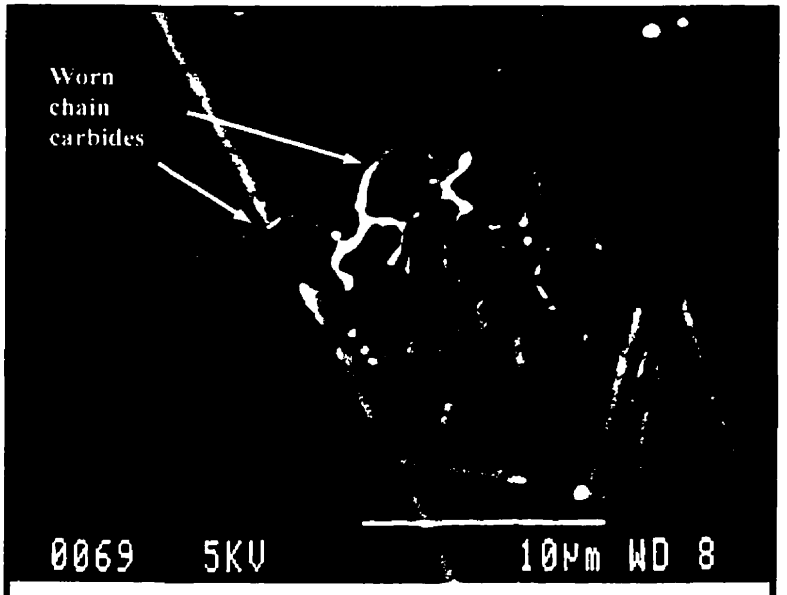

Figure 5.35 – SEM image of worn surface of cast implant (head #7) after 3 million cycles of testing. Featured are chain carbides worn below matrix surface.

Unfortunately, the implants tested to 3

million cycles were not examined with the AFM. For this reason, it was not clear if the worn carbides had a rough or smooth surface. Their topography may have been of some importance. If rough, it would have suggested that they were worn by some mechanical means, while if smooth, they could have possibly been worn or partially removed by chemical means. The images obtained with the SEM (Figs. 5.34 and 5.35) did not reveal if the topography of the worn carbides was rough or smooth. As a result, at this stage it was difficult to speculate as to the wear mechanism responsible for the worn carbides.

5.2.4.3 Carbides After 6 Million Cycles of Simulator Testing

Similar to the observations after 3 million cycles of testing, the carbides in the high carbon wrought heads after 6 million cycles still appeared to be worn below the matrix surface, as was seen with the SEM (Fig. 5.36). This time, the implants were also examined with the AFM, and the examination confirmed the SEM findings that the carbides were worn below the surface matrix (Fig. 5.37). Cross-sectional analysis of the worn carbides revealed that they were worn to a depth of about 30 to 40nm. The cross-section also showed that the worn carbides had a rough surface, suggesting that they were worn by mechanical means, possibly fracture caused by fatigue.

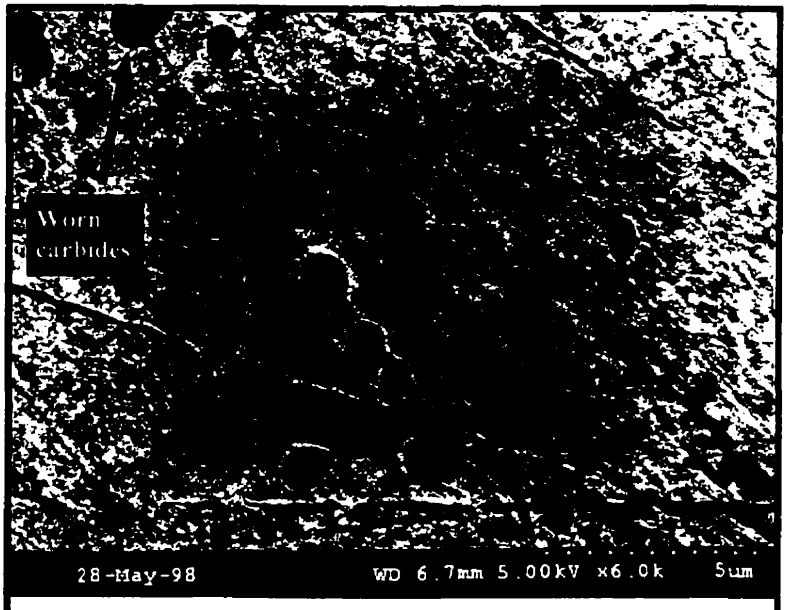

Figure 5.36 – SEM image of the wear zone of HC wrought implant after 6 million cycles of testing (head #13). Featured are carbides worn below the matrix surface.

The three cast implants examined after 6 million cycles of testing (heads #10, 11 &12) showed car-

Figure 5.37 – AFM image of wear zone on HC wrought alloy (head #13). Featured are carbides worn below matrix surface.

bide wear of a more complicated nature. Head #12 appeared to have a microstructure that was different from the other 2 cast implants tested to 6 million cycles, a microstructure that was also different from the cast implants examined at 3 million cycles and prior to testing. Head #12 had many isolated carbides and very few in chains, while the other cast implants had significantly more carbides in chains.

This different microstructure also exhibited somewhat different carbide wear behavior. The two implants with many carbides in chains exhibited carbide wear very similar to that seen on the cast implant after 3 million cycles of testing. That is, the carbides in chains were once again worn below the matrix surface while most of those isolated were still proud of the surface. There was one distinct difference, however, as the chains also appeared pitted (Figs. 5.38 and 5.39). AFM cross-sectional analysis of the pits showed them to have a depth of around 100 to 200 nm. The few carbide chains on the implant with many isolated carbides (head #12) showed the same wear behavior as the chains on the other two heads. On this implant, however, almost all of the isolated carbides were not proud of the surface, but rather experienced partial or full pull-out (Fig. 5.40). This pull-out resulted in pits having a depth of 100 to 200 nm, similar to the pits in the carbide chains. There was a distinct difference between the appearance of the pits at isolated carbide sites and those in the

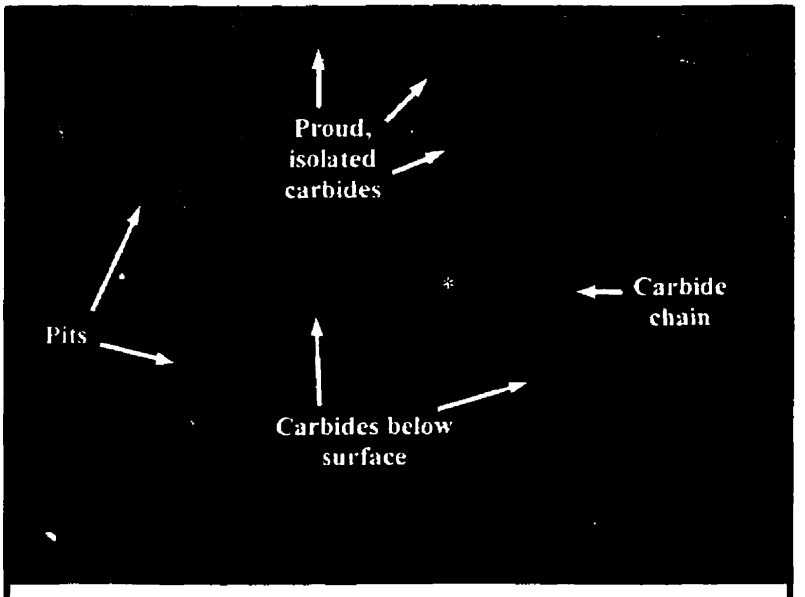

Figure 5.38 – SEM image of cast implant after 6 million cycles of testing (head #11). Featured is a carbide chain with pits and worn carbides, as well as proud isolated carbides.

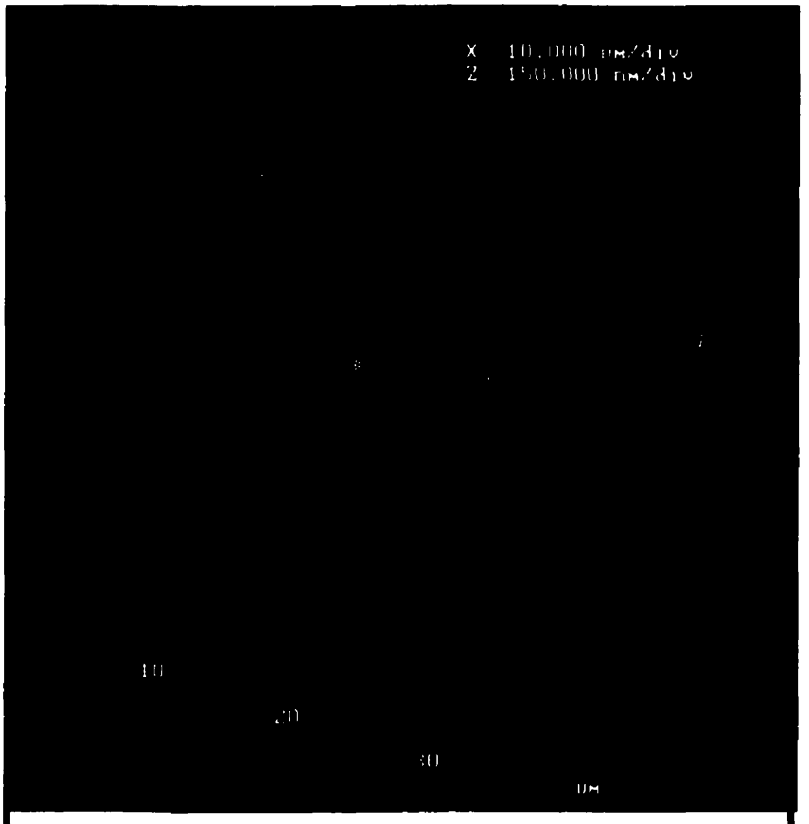

Figure 5.39 – AFM image of carbide chain shown in Fig. 5.38. The asterisk serves to orient the two images.

carbide chains. The pits resulting from isolated carbide pull-out had considerably rougher edges than the pits resulting from the partial carbide pull-out in the carbide chains (Fig. 5.41).

As with the high carbon wrought, the pits at carbide sites had a rough surface, once again suggesting that the wear was caused by a mechanical mechanism, possibly fracture caused by fatigue. Because the depth of the pits was an order of magnitude smaller than the carbides, it is likely that carbides still existed at the bottom of the pits, both in the cast and the high carbon wrought heads. In order to

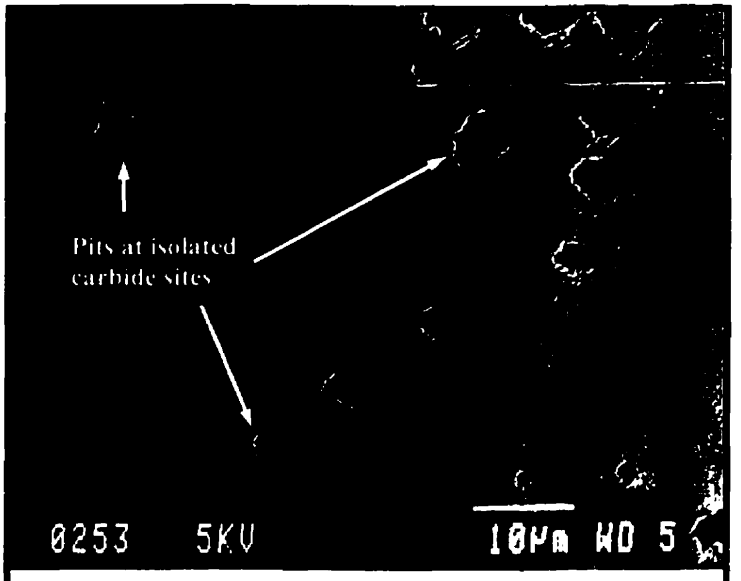

Figure 5.40 – SEM image of the wear zone of cast alloy after 6 million cycles of testing (head #12). Featured are pits at isolated carbide sites.

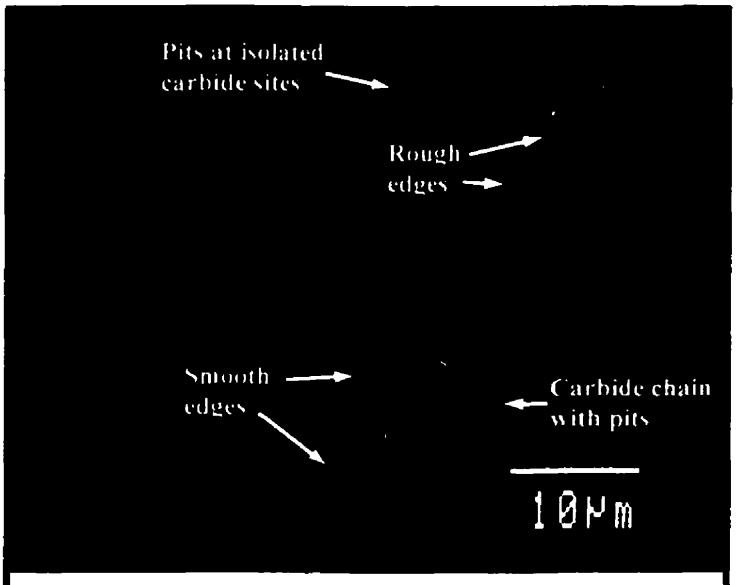

Figure 5.41 – SEM image of the wear zone of cast alloy after 6 million cycles of testing (head #12). Featured are pits at isolated carbide sites and those within carbide chains.

confirm this, it was attempted to analyze the composition inside the pits with the EDS. The signal coming out of the pits was very weak, probably because the walls of the pit absorbed the signal. As a result, it was not possible to analyze the composition and therefore it could not be confirmed if carbides still existed at the bottom of the pits.

5.2.5 FEATURE #5 – PITTING

As discussed in the previous section (5.2.4), pitting was observed on the surface of the cast implants after 6 million cycles of testing. The pits observed were mainly in the carbide chains and were 100 to 200 nm in depth. The pits were rough in cross-section, suggesting that they were caused by mechanical means. The edges of the pits were smooth, indicating that removal of material was due to brittle fracture. This was true for only the carbides in

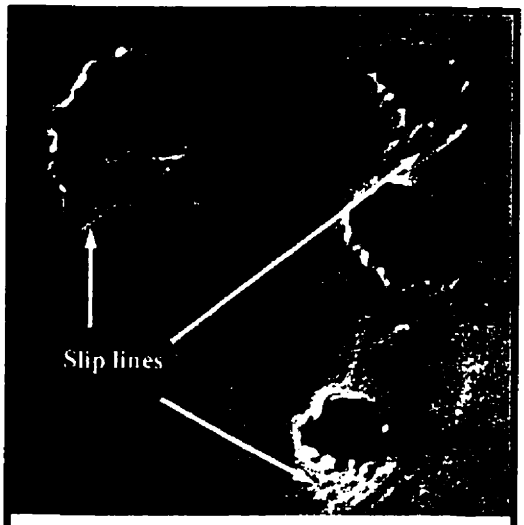

Figure 5.42 – SEM image of pits at isolated carbide sites on cast implant after 6 million cycles of testing (head #12). Featured are slip lines in the matrix adjacent to the pits.

chains. The isolated carbides that experienced pitting did not have smooth edges. The matrix around these pits appeared to have experienced plastic deformation as indicated by what appeared to be slip lines in the matrix adjacent to the pits (Fig. 5.42). This suggested that removal of material at isolated carbide sites was more difficult than at carbide chains. In either case, it appeared that the pits were no larger than the carbides, implying that only carbide material was removed to form the pits.

Like the cast implants, pitting was observed on the high carbon wrought heads after 6 million cycles of testing (Fig. 5.43). The pits on these implants appeared to be located at carbide sites. However, it did not appear that only carbide material was removed to form the pit, as was speculated for the cast implants. The pits on the high carbon wrought appeared to originate at carbide sites, but spread into the matrix (Fig. 5.44), implying that matrix material was also removed to contribute to the creation of the pits. AFM analysis of these pits showed them to be

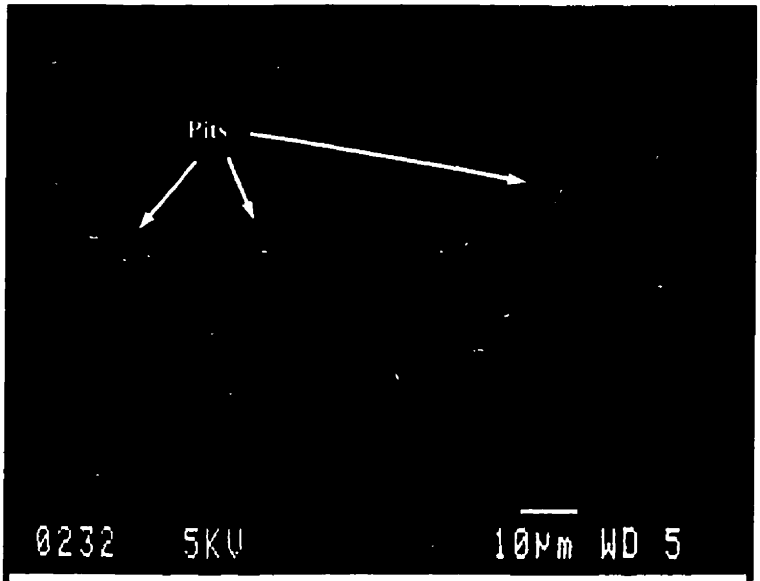

Figure 5.43 – SEM image of pits on high carbon wrought implant after 6 million cycles of testing (head #15).

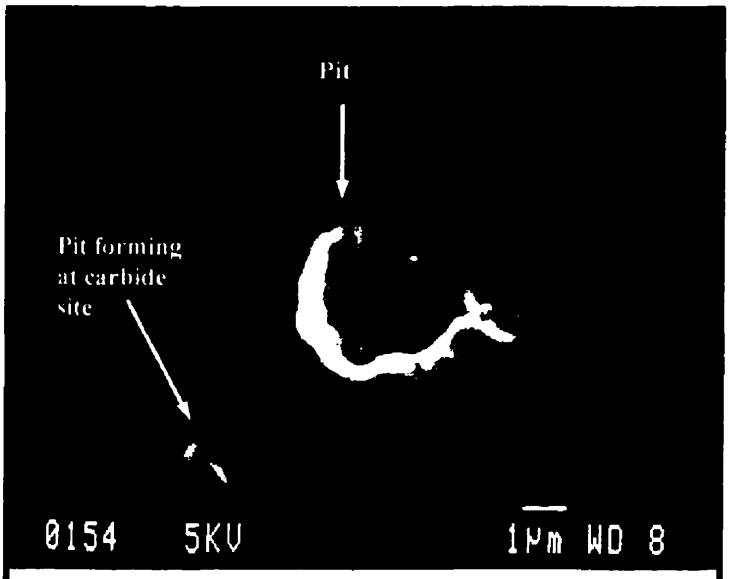

Figure 5.44 – SEM image of high carbon wrought implant after 6 million cycles of testing (head #13). Featured are pits originating at carbide sites.

of a similar depth to those observed on the cast heads (100 to 200 nm) and appeared as shown in Figure 5.45. Because the depth of the pits, both in the cast and the high carbon wrought, was two orders of magnitude smaller than the size of the carbides, it was likely that the carbides still existed at the bottom of the pits. EDS analysis in the pits did not confirm this, as the signal from the pits was insufficient for the analysis. Cross-sections of the pits on the high carbon wrought heads (as observed with the AFM) were also rough, suggesting that they too were caused by mechanical means.

The edges of the pits in the high carbon wrought heads were rougher than those in chains in the cast, but not as rough as the pits at isolated carbide sites on the cast. This indicated that removal of material to form pits in the high carbon wrought was not as difficult as at isolated carbide sites on the cast, but more difficult than at the carbides in chains. This is under the assumption that the

Figure 5.45 – AFM image of pit on high carbon wrought implant after 6 million cycles of testing (head #13).

mechanical properties of the matrix in the high carbon wrought material were similar to those of the cast material.

Pitting was not detected on any of the implants after 3 million cycles of testing, nor on any before simulator testing. The pitting appeared to be dependent on the number of test cycles. Perhaps if the low carbon wrought heads, which did not exhibit pitting at 3 million cycles of testing, were allowed to articulate to 6 million cycles, they too would have exhibited pitting.

5.2.6 Feature #6 – Matrix Delamination

After 3 and 6 million cycles of testing, all the implant heads of all three alloys displayed what appeared to be a discontinuous fragmented upper layer that rested on a non-fragmented lower layer (Figs. 5.46 & 5.47). In other words, the surfaces appeared to be missing plates from the upper layer. As described in section 2.3.1.4, a surface with this appearance could be the result of wear through a mechanism known as delamination.

This wear was most obvious at a zone away from the pole but still in the zone where wear occurred. The delaminating layer was most obvious away from the pole probably because the delaminating upper layer was thicker there than at the pole and therefore was more easily detected with the SEM. The delaminating layer appeared to increase in thickness with increasing distance from the pole. This was likely because the plane of maximum shear was moving deeper with the increasing distance. The plane of maximum shear moves deeper as the load at the surface is decreased.[85] The further away from the pole, the lower the load, the deeper the plane of maximum shear and therefore the thicker would be the delaminating layer. AFM analysis showed the delaminating layers to be several tens of nanometers in thickness.

Of interest was the fact that in the cast and high carbon wrought heads, delamination appeared to take place only after the carbides were relieved below the matrix surface. As seen in Figures 5.46 and 5.47, the carbides in the delaminating upper layer were worn below the matrix surface, and those in the lower layer were flush with the surface. AFM analysis showed that the depth to which the carbides were worn was similar to the thickness of the delaminating layer (Fig. 5.48). This phenomenon was not observed on the surface of the low carbon wrought head as the car-

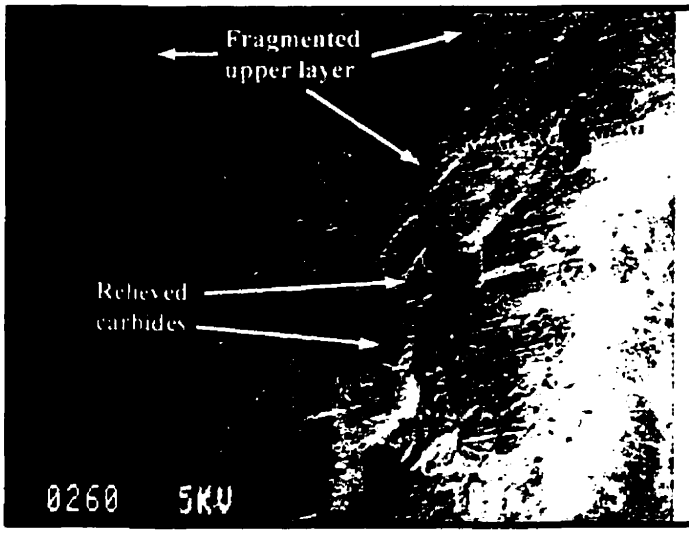

Figure 5.46 – SEM image of cast implant tested to 6 million cycles (head #12). Featured is a fragmented upper layer resting on a non-fragmented lower layer. Carbides in the upper layer were relieved below matrix surface.

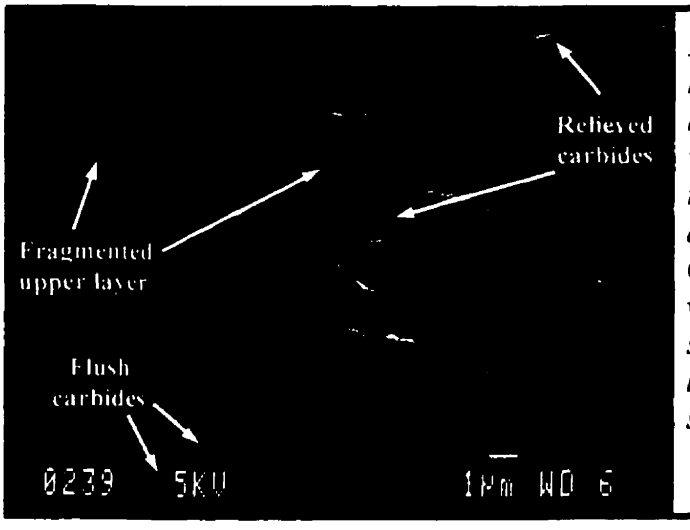

Figure 5.47 – SEM image of high carbon wrought implant tested to 6 million cycles (head #15). Featured is a fragmented upper layer resting on a non-fragmented lower layer. Carbides in the upper layer were relieved below matrix surface and those in the lower layer were flush with matrix surface.

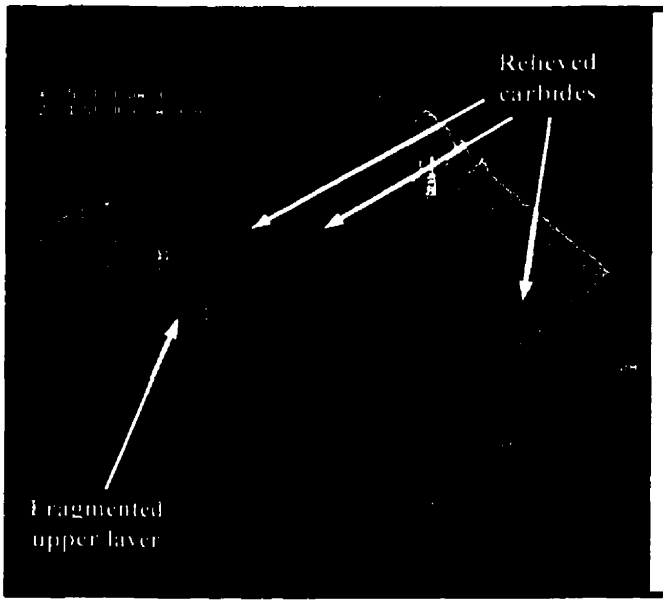

Figure 5.48 – AFM image of high carbon wrought implant tested to 6 million cycles (head #13). Featured is a fragmented upper layer resting on a non-fragmented lower layer. Carbides in the upper layer were relieved below matrix surface. The depth of carbide relief was similar to the thickness of the upper layer.

bides were not detected.

It was of interest to determine if the delaminating layer had a volume fraction of FCC and HCP that differed from that of the bulk of the material. In other words, did articulation cause a phase change? This was examined with x-ray diffraction as described in section 4.7.3. Diffraction patterns were obtained for all three alloys in the wear zone at the pole, both deep into the surface and at the immediate surface (Fig. 5.49). The diffraction patterns deep into the surface were very similar to those obtained deep into the surface at the edge of the implant where articulation did not occur (ex. top of Fig. 5.7 compared with top of Fig. 5.49). This showed that the volume fractions of FCC and HCP in the bulk of the material, whether at the pole or at the edge, were consistent. Figure 5.49 shows that the diffraction patterns of the bulk material and of the immediate surface at the pole were not the same. Some of the peaks at the immediate surface were absent from the bulk of the material. The relative intensities of the peaks were also different when comparing the two diffraction patterns. That means that it was likely that the delaminating layer had a different volume fraction of FCC and HCP when compared with the bulk of the material. This suggested that articulation caused a phase change at the immediate surface. The exact phase change was unclear because the diffraction patterns are complex. Nevertheless, it is likely that with the phase change, the wear properties of the material changed as well.

5.3 PART 2 OF THE STUDY

As in the first part of the study, it was of interest to establish a relationship between surface appearance and volumetric wear. Figure 5.50 shows the volumetric wear shed by the six heads (not cups) as they were progressively wear tested. For this set of 6 heads, the low carbon wrought alloy experienced more wear than the cast and the high carbon wrought, both of which experienced similar amounts of wear. At some of the points when the wear was measured, a surface examination of the samples was performed with the SEM and AFM and what follows is a description of the observations made.

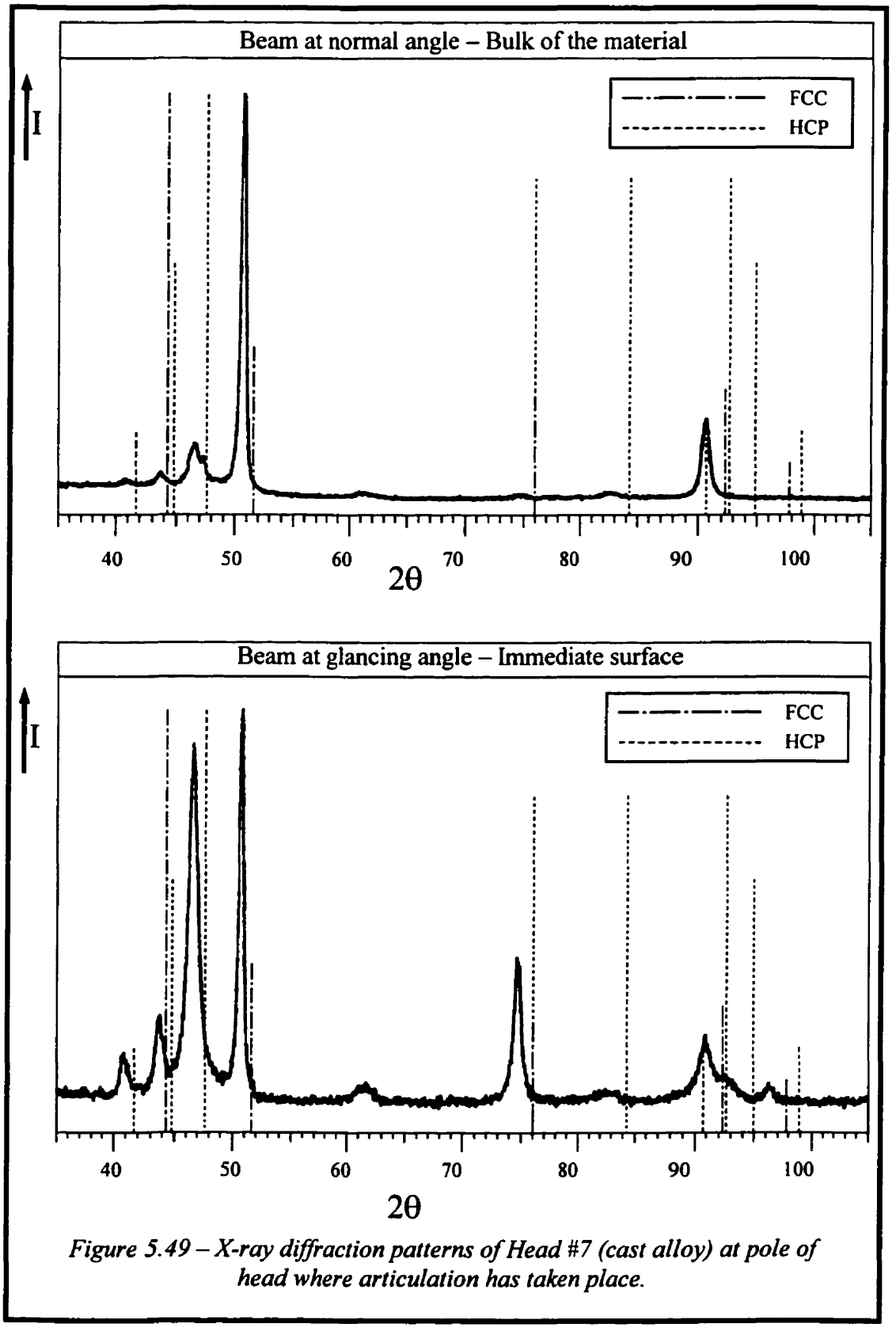

Figure 5.49 – X-ray diffraction patterns of Head #7 (cast alloy) at pole of head where articulation has taken place.

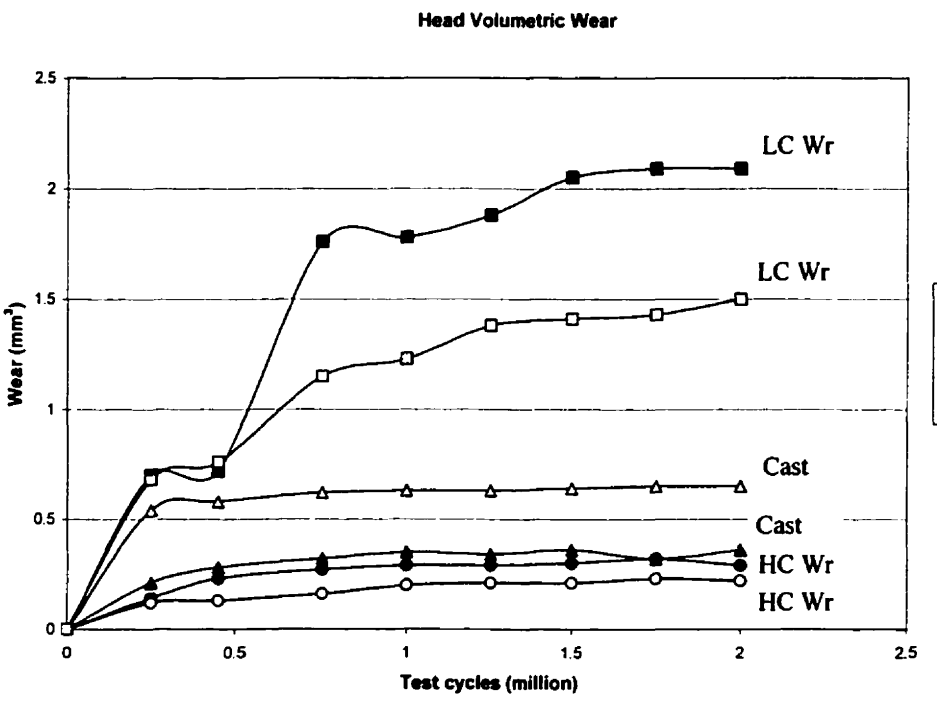

Figure 5.50 – Volumetric wear of the six heads examined in the second part of the study.

5.3.1 FEATURES #1, 2, 3, 4 & 6

Features #1, 2, 3, 4 and 6 refer to the same as those in section 5.2, namely grinding marks, second & third-body abrasive scratches, residual grinding stones, carbides and delamination respectively. The six implants examined in this part of the study were those examined in the first part prior to simulator testing. As such, some of the features described in the first part were therefore the same. Grinding marks after manufacturing were as described in 5.2.1. The amount of scratches and grinding stones prior to simulator testing was the same as described in 5.2.2 and 5.2.3 respectively. The carbides were also the same prior to testing and were therefore as described in 5.2.4.1.

With testing, some of the features did not exhibit the same behavior as in the first part. The residual grinding stones did not appear to reduce in number as the im-

plants were progressively tested. For example, Figures 5.51 and 5.52 show that there were the same number of stones, still in the same locations, at 2 million cycles as there were at 0.75 million cycles of testing. Perhaps the implants were not worn enough at 2 million cycles to allow release of the stones from the surface. If the testing would have been carried out to the same duration as in the first part of the study, perhaps some of the stones would have been released from the surface and their number would have decreased. It can also be argued that the implant heads examined after 3 and 6 million cycles in the first part of the study had fewer stones on the surface to begin with and therefore exhibited fewer stones than the implants that were examined prior to testing. Also, the fact that the implants were articulated at a higher load in the second part of study may also have influenced the lack of release of stones from the surface. Figure 5.53 shows the same lo-

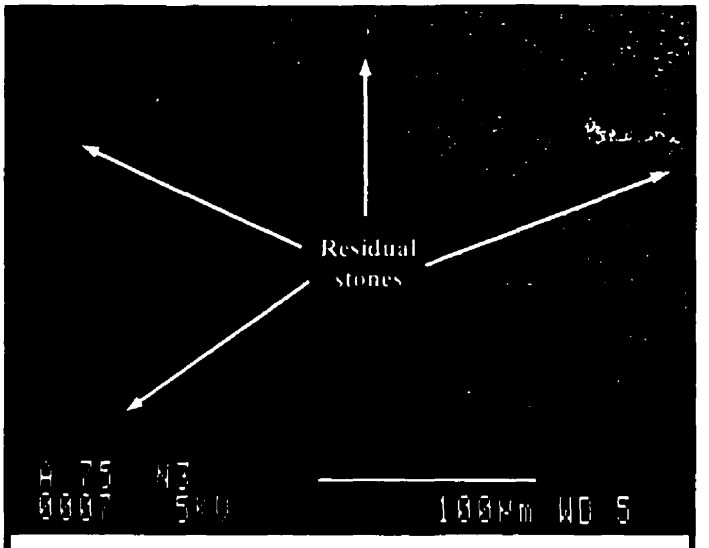

Figure 5.51 – SEM image of cast implant after 0.75 million cycles of testing (head #1). Featured are embedded residual grinding stones.

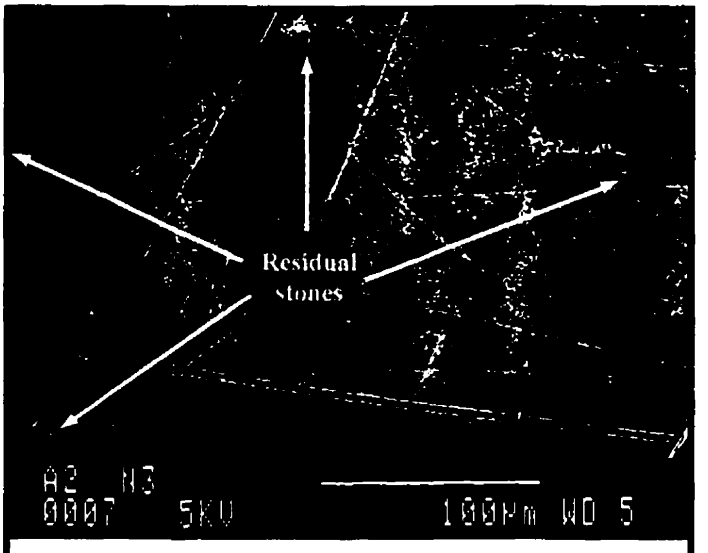

Figure 5.52 – SEM image of cast implant after 2 million cycles of testing (head #1) taken at the same location as in Figure 5.51. Featured are the same embedded residual grinding stones. Also featured are straight, second-body abrasive scratches.

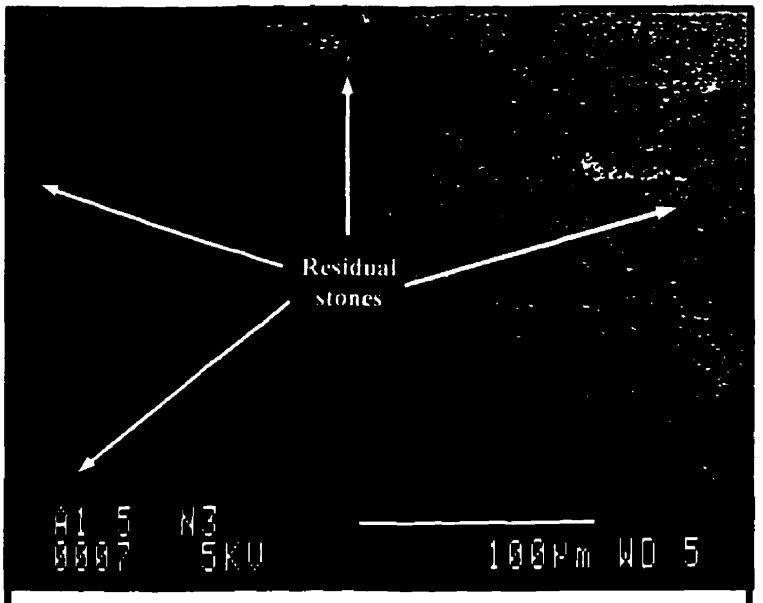

Figure 5.53 – SEM image of cast implant after 1.5 million cycles of testing (head #1) taken at the same location as in Figures 5.51 and 5.52. Featured are the same embedded residual grinding stones which appear to have been pushed further into the surface.

cation as in Figures 5.51 and 5.52 but after 1.5 million cycles of testing. At this point in the testing, it appeared as though the stones were pushed further into the surface. Perhaps the higher loads used in this part of the study did not allow the release of the stones, but rather forced them further into the surface, continually preventing their release.

Second and third-body abrasive scratching were also somewhat different in this part of the study. The most obvious difference was the lack of tortuous scratches, implying that third-body abrasion did not take place. That means that loose abrasives were probably not present between the articulating bodies. Only straight scratches were observed on the surfaces of the six implants (Fig. 5.52). The cast still exhibited the greatest amount of scratching and the high carbon wrought the least. The overall amount of scratching on these six implants appeared to be less than the scratching observed in the first part of the study. This may be because third-body abrasion did not take place. Figures 5.51 to 5.53 show that abrasive scratching did not occur until 2 million cycles of testing. In fact, all six implants did not exhibit significant scratching until 1.5 or 2 million cycles of testing. What this suggests is that either the abrasives were not present until 1.5 or 2 million cycles of testing, or that the surfaces had a better resistance to abrasion up to this point. This may have been related to the effect grinding during manufacturing had on the matrix, as shown in

Figure 5.7. Although the effect of grinding discussed in section 5.2.1 was not clear, it may have increased the hardness of the matrix, which in turn may have improved the matrix's resistance to abrasion. It is possible that once the affected material was worn, the unaffected material underneath was exposed, making the surface susceptible to abrasion, perhaps at 1.5 to 2 million cycles.

Also in the second part of the study, the carbides in the cast behaved very similarly to those in the first part of the study. The behavior, however, was significantly accelerated. The carbides in chains were relieved below the matrix surface very early into the testing, as early as 0.25 million cycles (Fig. 5.54). The depth of relief appeared to be 2 or 3 times greater than the depth observed after 3 million cycles of testing in the first part of the study (Fig. 5.35). The pitting in the chains also appeared very early. They were present already at 0.75 million cycles and grew in size and number as the implants were progressively tested (Figs. 5.55 & 5.56). The depth of the pits was similar to that observed after 6 million cycles in the first part (100 to 200 nm). Before the whole carbide chain had a chance to pit, however, further testing appeared to cause a layer that was at least as deep as the pits to be removed. As Figure 5.57 shows, the pits that were present at 1 million cycles (Fig. 5.56) were no longer present at 2 million cycles. That implies that the pits were either filled with material again, or that a layer was removed, removing the pits along with it. The isolated carbides on the cast implants were not clearly detected with testing and therefore their behavior could not be determined.

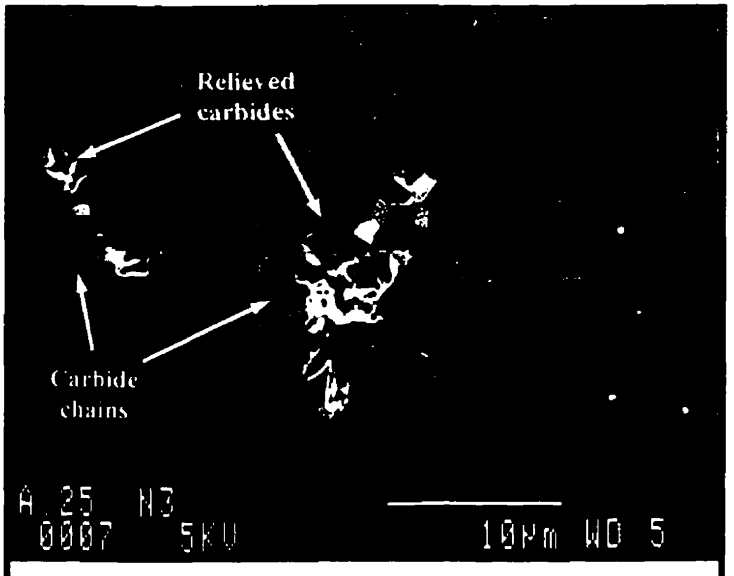

Figure 5.54 – SEM image of cast implant after 0.25 million cycles of testing (head #1). Featured are chain carbides that were worn below matrix surface.

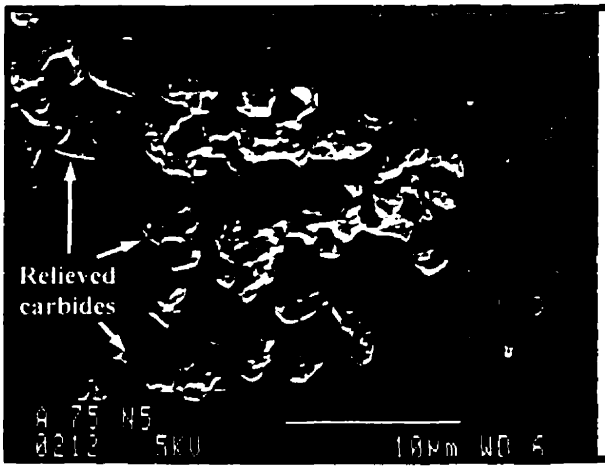

Figure 5.55 – SEM image of cast implant after 0.75 million cycles of testing (head #2). Featured is a relieved carbide chain with pits.

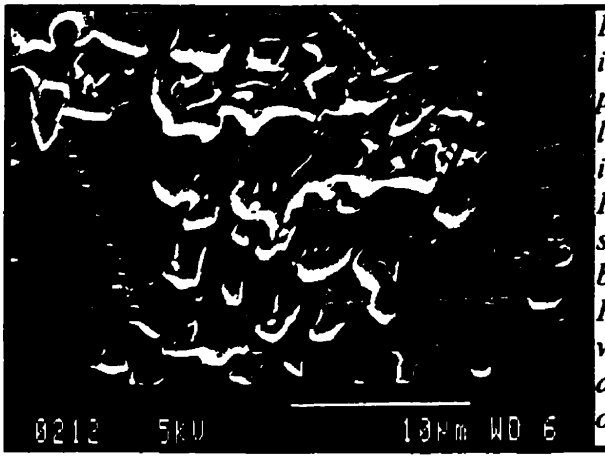

Figure 5.56 – SEM image of cast implant after 1 million cycles of testing (head #2). Featured is the same relieved carbide chain as in Fig. 5.55. Pits were now larger and more numerous.

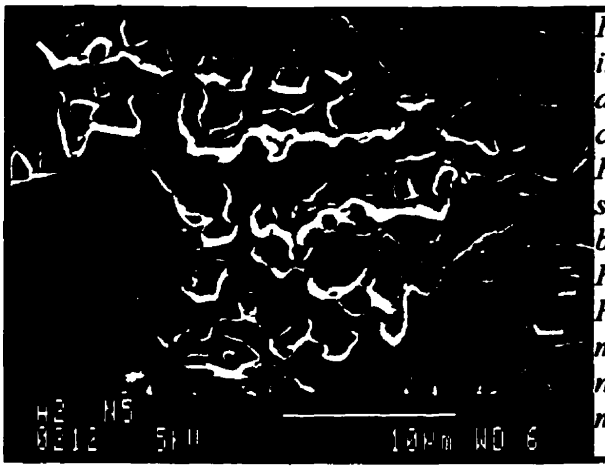

Figure 5.57 – SEM image of head #2 after 2 million cycles of testing. Featured is the same relieved carbide chain as in Figs. 5.55 & 5.56. Pits present at 1 million cycles were not present at 2 million cycles

The carbides in the high carbon wrought implants did not exhibit the same behavior as those in the first part of the study. The carbides appeared to remain flush with the matrix surface at all times once testing commenced. As in the first part, they did not remain proud of the surface with testing, but they were not relieved below the matrix surface with testing as was observed in the first part. Once again, the carbides in the low carbon wrought heads were not detected.

Feature #6, that is delamination, was not readily observed on the six implants tested in the second part of the study. As was discussed in section 5.2.6, the higher

the load, the thinner the delaminating layer. In this part of the study, the loads used were five times body weight instead of three times body weight. Because of the higher loads, it is possible that the delaminating layer, if any, was too thin to detect with the SEM. AFM analysis did reveal a fragmented upper layer that rested on a non-fragmented lower layer (Fig. 5.58). However, this layer had a distinctly different appearance than the delaminating layers observed in the first part of the study. For lack of a better description, this layer appeared more powdery. It did not appear to be missing plates as in Figures 5.46, 5.47 & 5.48. This powdery surface will be discussed in more detail in a later section. From the observations made with the SEM and AFM, it did not appear that the matrix of the implants was wearing through delamination.

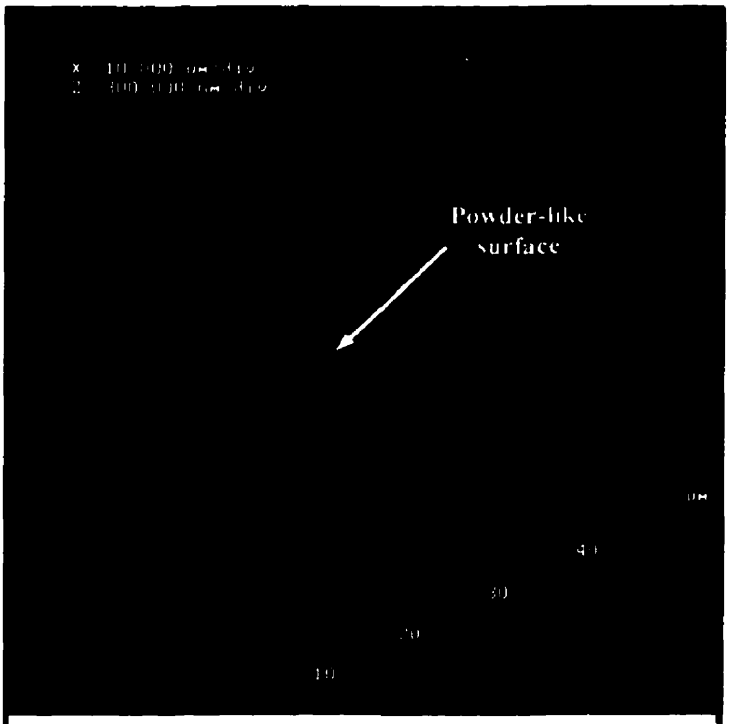

Figure 5.58 – AFM image of high carbon wrought surface after 0.25 million cycles of testing (head #3). Featured is a fragmented upper layer that appeared powder-like.

5.3.2 FEATURE #5 – PITTING

With testing, the most prominent feature seen on the six implant heads was pitting. Unlike the first part of the study, where pitting was observed only after 6 million cycles of testing, all six implants exhibited pitting after only 0.25 million cycles. As for the first part of the study, the pits were rough in cross-section, suggesting that they were caused by mechanical means. The pitting size and depth varied from

alloy to alloy, as well as from head to head of the same alloy. Tables 5.2 to 5.7 give the average pitting depth as measured with the AFM. The depth not only varied from head to head, but also from cycle to cycle. The depth did not increase with increasing test cycles nor did it decrease with increasing test cycles. In fact, the average pit depth fluctuated with testing. The tables also give the deepest and most shallow pits sampled. As for the average depth, there was no consistency in this range, neither from cycle to cycle, nor from head to head.

Table 5.2 – Wear data for Head #1 (cast).

0	0	0	0	-	-	-
0.25	0.211	3.5	5500	183	9	21 to 646
0.45	0.066	6	580	195	16	102 to 312
0.75	0.045	6	400	199	15	108 to 446
1.0	0.025	6	220	146	13	95 to 263
1.5	0.014	5	170	138	10	96 to 229
2.0	0	4	0	-	0	-

Table 5.3 – Wear data for Head #2 (cast).

0	0	0	0	-	-	-
0.25	0.537	4	10700	469	17	199 to 950
0.45	0.045	4	900	203	12	38 to 420
0.75	0.037	4.5	580	452	5	229 to 709
1.0	0.011	3.5	290	219	9	51 to 425
1.5	0.010	3.5	260	105	16	53 to 165
2.0	0.013	4	260	-	0	-

Table 5.4 – Wear data for Head #3 (HC Wrought).

0	0	0	0	-	-	-
0.25	0.139	4	2760	143	12	102 to 213
0.45	0.091	6	800	105	4	85 to 121
0.75	0.042	5.5	440	115	9	36 to 283
1.0	0.013	6	110	101	12	41 to 189
1.5	0.017	3	600	295	6	250 to 487
2.0	-0.008	1	0	-	0	-

Table 5.5 – Wear data for Head #4 (HC Wrought).

0	0	0	0	-	-	-
0.25	0.121	5	1540	243	14	142 to 460
0.45	0.008	6	70	253	2	244 to 261
0.75	0.030	6	270	256	3	203 to 284
1.0	0.036	6	320	201	14	128 to 386
1.5	0.012	3	420	291	10	196 to 414
2.0	0.012	3	420	-	0	-

Table 5.6 – Wear data for Head #5 (LC Wrought).

0	0	0	0	-	-	-
0.25	0.700	2	55700	179	12	102 to 281
0.45	0.024	2	1910	150	6	116 to 258
0.75	1.039	5.5	10930	211	13	147 to 259
1.0	0.019	5.5	200	-	0	-
1.5	0.264	6	2330	358	6	57 to 455
2.0	0.042	2	3340	-	0	-

Table 5.7 – Wear data for Head #6 (LC Wrought).

0	0	0	0	-	-	-
0.25	0.682	1	217000	345	19	232 to 583
0.45	0.079	3	2790	356	10	183 to 479
0.75	0.389	3	13760	171	9	112 to 301
1.0	0.080	2	6370	60	5	50 to 68
1.5	0.184	4	3660	574	8	465 to 719
2.0	0.088	2	7000	-	0	-

Aside from the distinct pitting of the carbide chains in the cast heads (section 5.3.1), the pits present on the six implant heads did not appear to form at any particular location. That is, the pitting did not appear to be associated with carbide sites nor any other alloy features. There were two types of pitting distributions observed. Five of the heads (excluding head #6) exhibited pits that were evenly distributed throughout the wear zone, gradually reducing in frequency at the periphery (Fig. 5.59). Head #6 exhibited isolated islands of wide pits that were surrounded by some smaller, isolated pits (Fig. 5.60). These pits also subsided at the periphery.

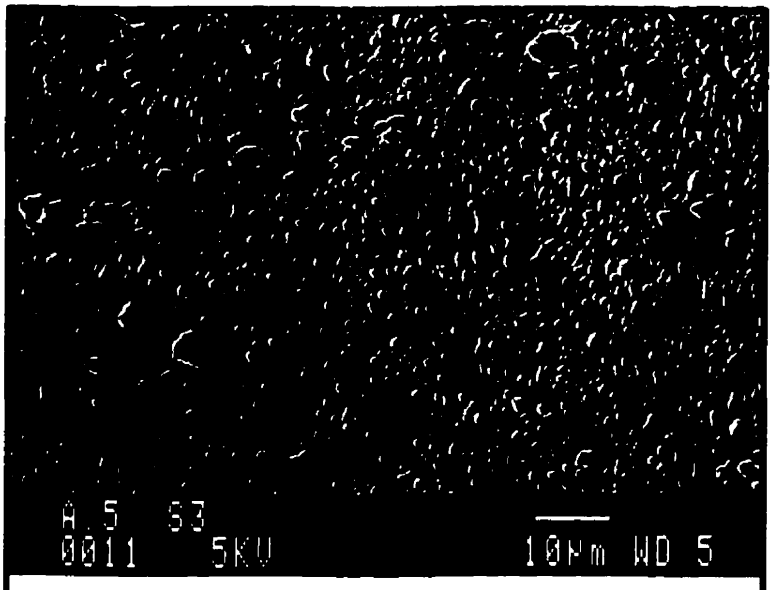

Figure 5.59 – SEM image of high carbon wrought implant after 0.45 million cycles of testing (head #4). Featured are varying size pits that were evenly distributed on surface.

An interesting phenomenon, one that

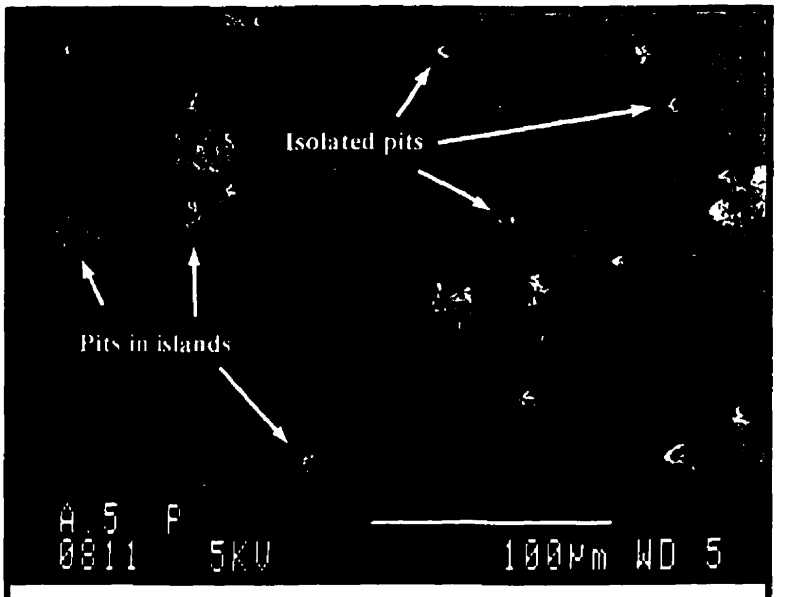

Figure 5.60 – SEM image of low carbon wrought implant after 0.45 million cycles of testing (head #6). Featured are isolated islands of wide pits surrounded by smaller, isolated pits.

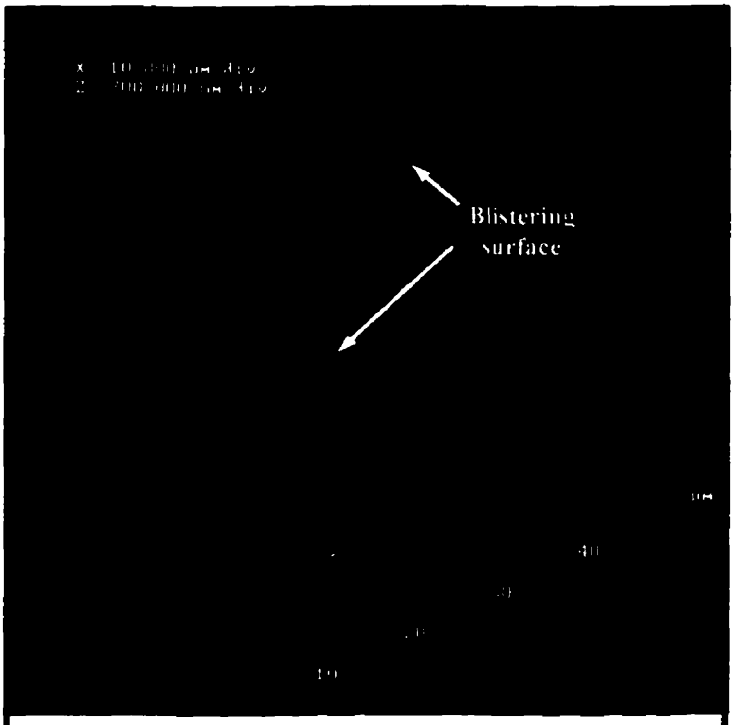

Figure 5.61 – AFM image of high carbon wrought surface after 0.25 million cycles of testing (head #3). Featured is a blistering surface. (This image was seen in Fig. 5.58).

was not observed in the first part of the study, was the feature that appeared to be a precursor to pitting. This feature can best be described as a blistering or a powdery surface (Figs. 5.61 & 5.62). This blistering was described in section 5.3.1 as a fragmented upper layer that did not appear to be delamination. It was thought that the blistering was a precursor to pitting because the pits were present only where blisters were present. A good example of this can be seen in Figures 5.63 and 5.64. At 0.25 million cycles, where the surface was blistered, a pit appeared at 0.45 million cycles in the same formation as the blisters. Another good example is given in Figures 5.65 and 5.66. The pits were present only where there were blisters.

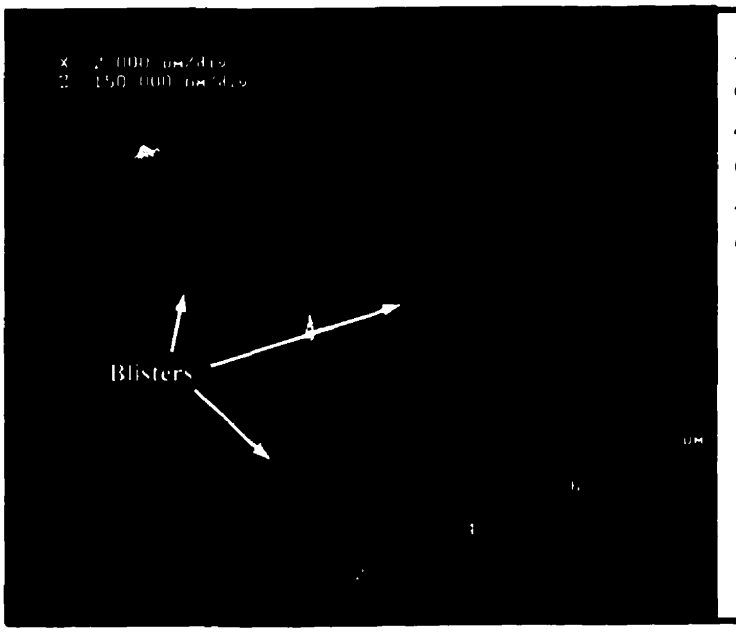

Figure 5.62 – AFM image of high carbon wrought surface after 0.25 million cycles of testing (head #4). Featured are blisters on the surface.

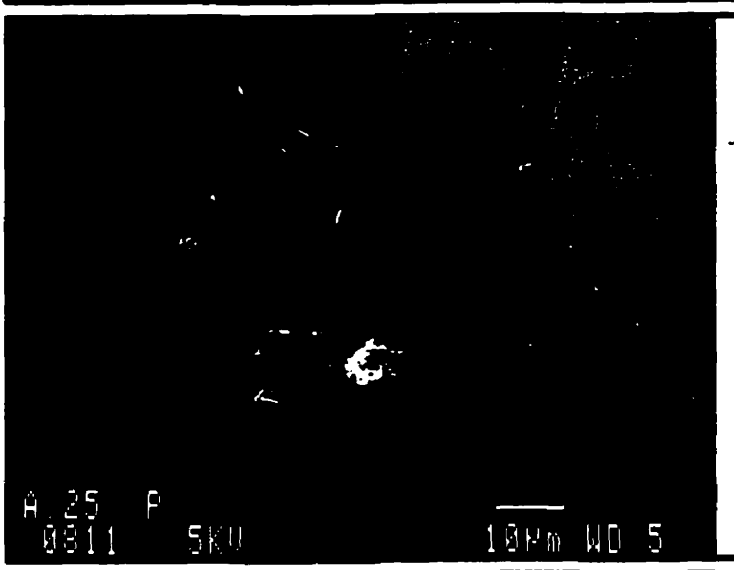

Figure 5.63 – SEM image of low carbon wrought surface after 0.25 million cycles of testing (head #6). Featured are blisters on the surface.

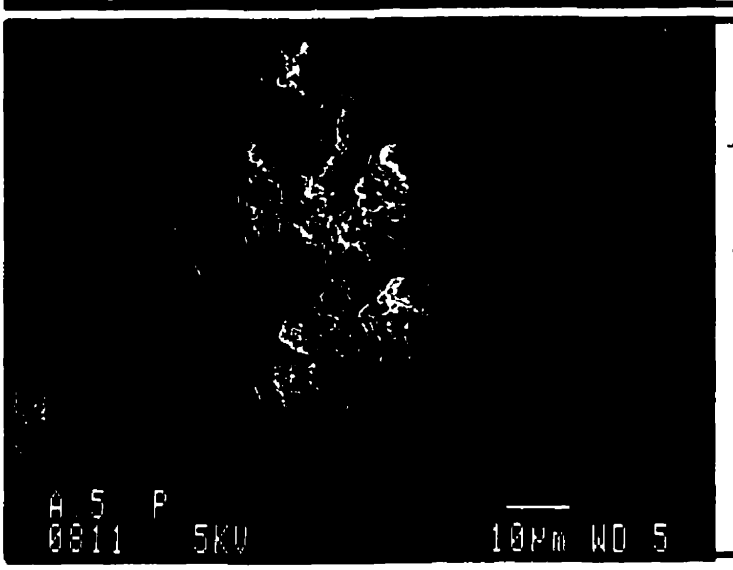

Figure 5.64 – SEM image of low carbon wrought surface after 0.45 million cycles of testing (head #6). Featured are pits in the same location where the blisters were at 0.25 million cycles of testing (Fig. 5.63).

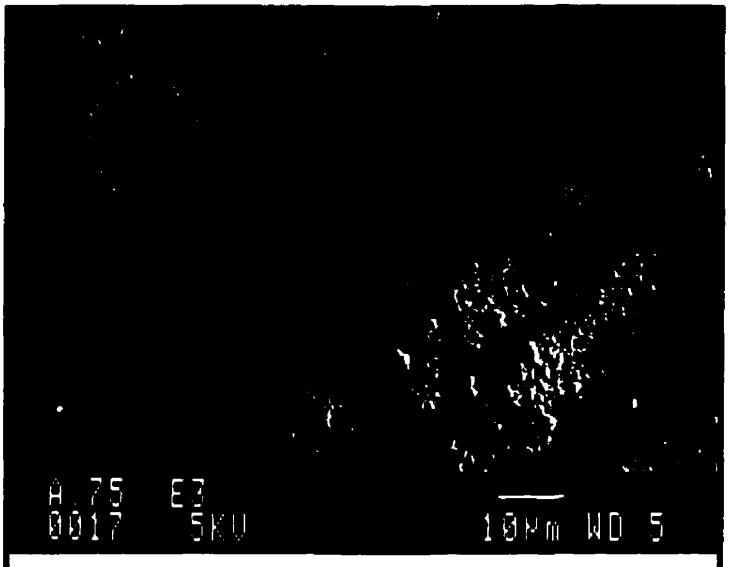

Figure 5.65 – SEM image of low carbon wrought surface after 0.75 million cycles (head #5). Featured are pits that were restricted to areas that were blistered.

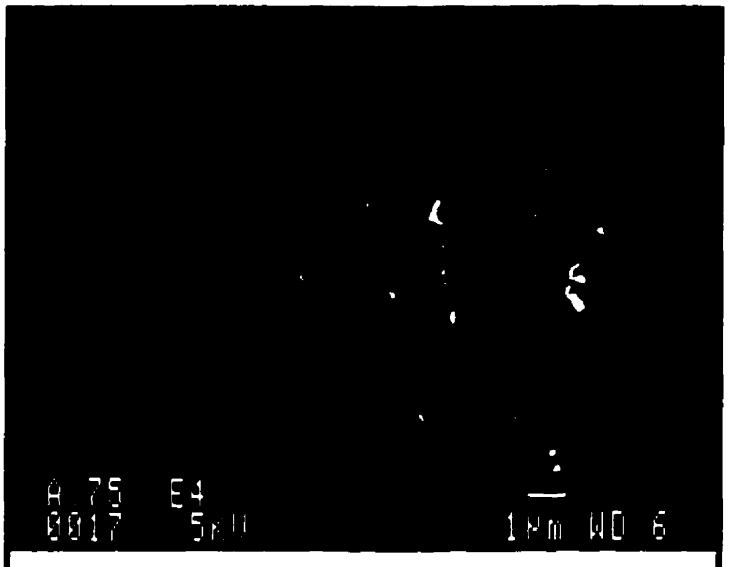

Figure 5.66 – SEM image of low carbon wrought surface after 0.75 million cycles (head #5). Featured are blisters close-up.

The implant heads appeared to undergo pitting cycles. The cycles would start with blistering, followed by pitting and then by removal of a layer of material at least as thick as the depth of the pits. The heads were thought to go through these cycles because at certain test cycles, the surface would not exhibit much pitting and the pits that were previously present were gone. For example, Figure 5.67 shows the same location as Figures 5.63 and 5.64 but after 0.75 million cycles. The pits, which were first a blister, were no longer there. At this stage in the testing, this particular head did not exhibit much pitting. In order for the pits to have disappeared, one of two things had to have happened. Either they would have to be back-filled with material during articulation, or the matrix surrounding them would have to wear away to at least the same depth as the pits. As Tables 5.2 to 5.7 show, according to gravimetric

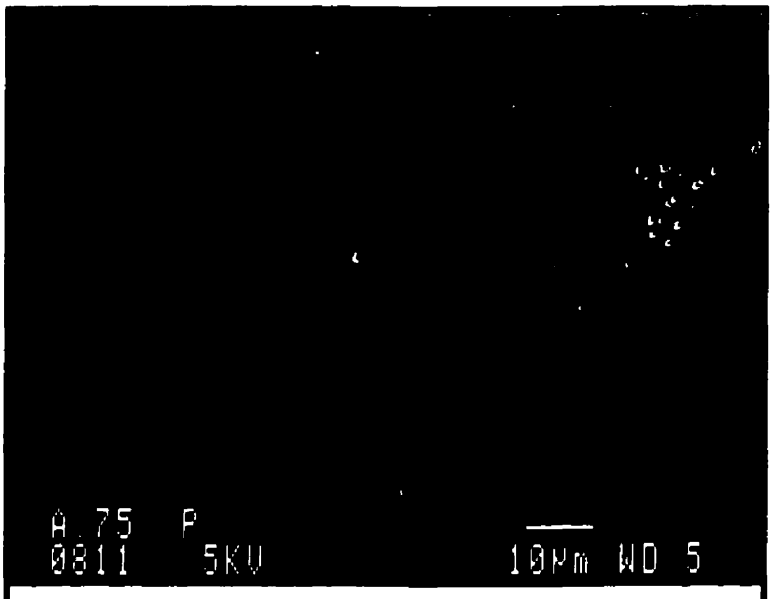

Figure 5.67 – SEM image of low carbon wrought surface after 0.75 million cycles (head #6). Featured is the same area seen in Figs. 5.63 and 5.64. The pits that were present at 0.45 million cycles were no longer present at 0.75 million cycles.

measurements, the heads continuously lost material and therefore it is likely that the pits disappeared because the matrix around them had worn away.

As discussed in section 3.0, one of the objectives of the study was to determine if examination of the wear surfaces may quantitatively reveal the volumetric wear. The fact that the heads appeared to go through pitting cycles may allow for quantitative measurements of volumetric wear. That is, if at 0.25 million cycles, for example, an implant head exhibited pits of a depth d, and those pits were gone at 0.45 million cycles, a layer of a thickness t would have to have been worn away, and this thickness t would have to have been at least as deep as d (i.e.: $t \geq d$). If a layer of thickness t wears over a surface area A, then the volume shed would be $V = tA$. The surface area, A, can be determined with the SEM by determining how far from the pole the wear zone spans. This distance can be called r, and is determined somewhat subjectively. The linear area, A (not the projected) would then be πr^2. The volume would then be $\pi r^2 t$. The thickness may be assumed to be the pit depth, d, from the previous examination. That is, $V_{at\ 0.45} = \pi r_{at\ 0.45}^2 d_{at\ 0.25}$.

This theory was put to the test. Tables 5.2 to 5.7 give the parameters necessary to check this assumption. Given are the volumetric wear that was determined gravimetrically, the radius of the wear zone (as determined during the SEM examina-

tion), the calculated layer thickness that would have to be shed in order to produce the corresponding volumetric wear, and the average pit depth. In order for the assumption to be valid, the pit depth at test cycle x (d_x) would have to be similar to the layer thickness at test cycle x+1 (t_{x+1}). The arrows in the tables serve to allow for easy comparison.

What quickly became apparent was that this theory does not hold. The depths and thicknesses were not sufficiently similar. Not even the deepest measured pits would fit this theory. This theory did not work for several reasons. First, there is no way to determine how many pitting cycles the heads experienced between surface examinations. In order to be able to apply this theory, examination would have to be performed after pit formation, and immediately after a layer was shed. There is no way to determine when this occurs during testing. Also, this examination is limited to the heads, and therefore the wear produced by the cups would not be accounted for. Finally, as was seen in the first part of the study, pitting does not necessarily take place. Therefore, the volumetric wear, if produced by abrasion, delamination and carbide pitting, could not be determined by this method.

5.3.3 Feature #7 – Spherical Oxide Nodules

In this part of the study, it was attempted to examine the implant heads with a very high magnification. This was made possible with the AFM and was done on the heads from 0.25 million cycles and on. Figures 5.68 and 5.69 show a feature consistently found on the heads at the high magnification. The surface appeared to be covered in spherical nodules that ranged from 80 to 350 nm in diameter and from about 1 to 20 nm in depth. These nodules were found on all of the heads and after every stage in the wear testing.

The nodules were found in the wear zone, implying that they were continuously removed. That means that either the alloy was made entirely of these nodules and as one nodule layer was removed, the one underneath became apparent, or the nodules were a feature that kept reforming once removed. These nodules were not visible with the SEM because the necessary resolution could not be achieved. As

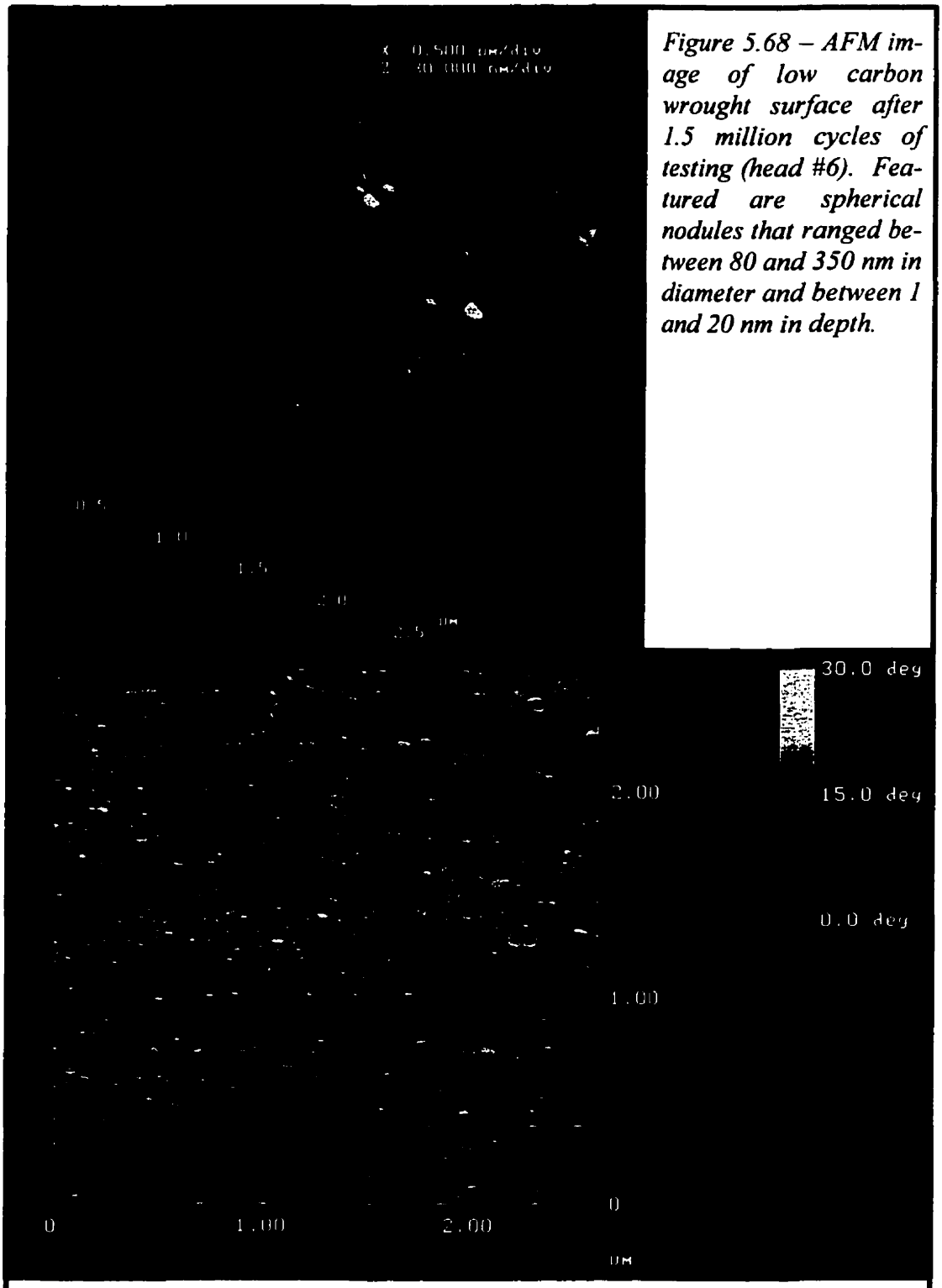

Figure 5.68 – AFM image of low carbon wrought surface after 1.5 million cycles of testing (head #6). Featured are spherical nodules that ranged between 80 and 350 nm in diameter and between 1 and 20 nm in depth.

Figure 5.69 – AFM phase image of low carbon wrought surface after 1.5 million cycles (head #6). This image was taken in the same location as that seen in Fig. 5.68. The phase imaging gave a better resolution of the nodules.

such, their composition could not be determined using the EDS.

As discussed in section 2.3.2.3, the implant alloys have a chromium addition of 27-30 wt% in order to create a passive oxide film which contributes to corrosion resistance. With this in mind, it is possible that the nodules found on the surfaces were the result of passive oxide growth on the alloy. In fact, the surfaces appeared very similar to that of nickel after deliberate oxidation.[19] Nickel too forms nodules of oxide. Fehlner and Graham[24] described that the transition to an oxide film is a gradual one in the sense that islands of oxide first nucleate and then grow laterally across the surface. Such growth can result in the formation seen in Figures 5.68 and 5.69 and as such, it is quite possible that the nodules seen on the implant surfaces were in fact the result of oxide growth.

5.4 RETRIEVAL EXAMINATION

SEM examination of the high carbon wrought Sulzer retrieval revealed a similar appearance to the Wright Medical high carbon wrought implants. As seen in Figure 5.70, the alloy was rich with carbides which were of a similar size to those

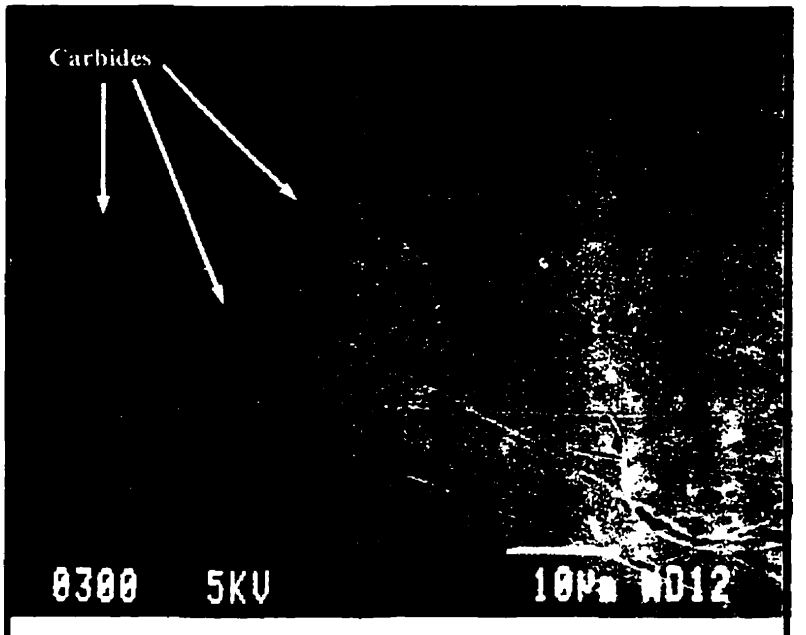

Figure 5.70 – SEM image of Sulzer, high carbon wrought retrieval. Featured are carbides in the wear zone that appeared to be flush with the matrix.

in the Wright Medical implants. However, although the implant was in service for 3 years, the carbides in the wear zone appeared flush with the matrix surface when examined with the SEM (Fig. 5.70). They were not relieved below the surface as was observed after 3 million cycles of testing in the first part of the study (Fig. 5.34). In fact, when examined with the AFM, the carbides were still proud (Fig. 5.71) and were protruding 10 to 40 nm. What was interesting was that on one side of the carbides, consistently the same side, the matrix was also proud (Fig. 5.71). This gave the carbides a comet-like appearance. This suggested that the matrix on the proud side did not wear at the same rate as the rest of the matrix. This may be suggestive of hip motion that was not simulated in the simulator.

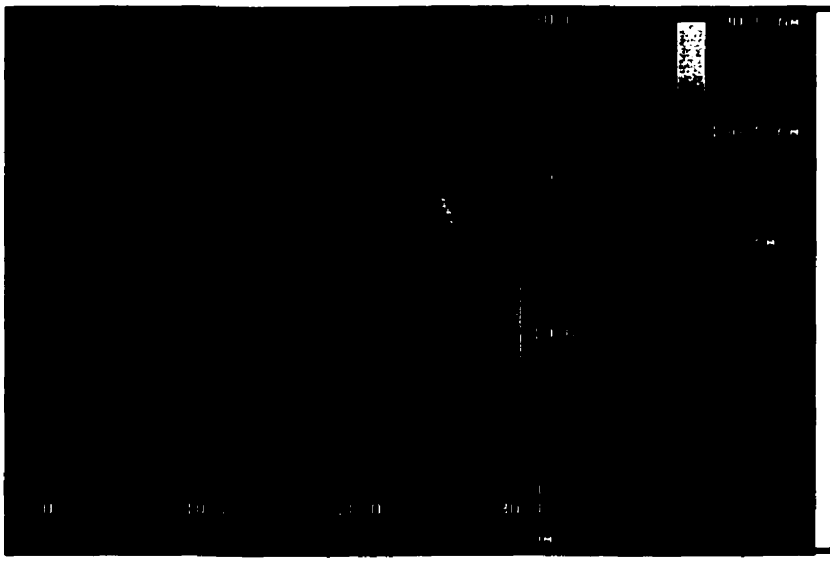

Figure 5.71 – AFM image of Sulzer, high carbon wrought retrieval. Featured are proud carbides that had a comet-like appearance.

As with the Wright Medical implants, the retrieval exhibited both second and third-body abrasive scratching (Figs. 5.72 & 5.73). Although the amount of scratching was small, it was more prevalent than observed on the other high carbon wrought implants examined in this study. The scratches were very similar in appearance to those on the other implants, exhibiting no pile-up on the edges.

Figure 5.74 shows some residue on the implant that could not be removed with the cleaning methods employed in this study. This area appeared to have a concentration of abrasive scratching. Close-up imaging (Fig. 5.75) revealed the presence

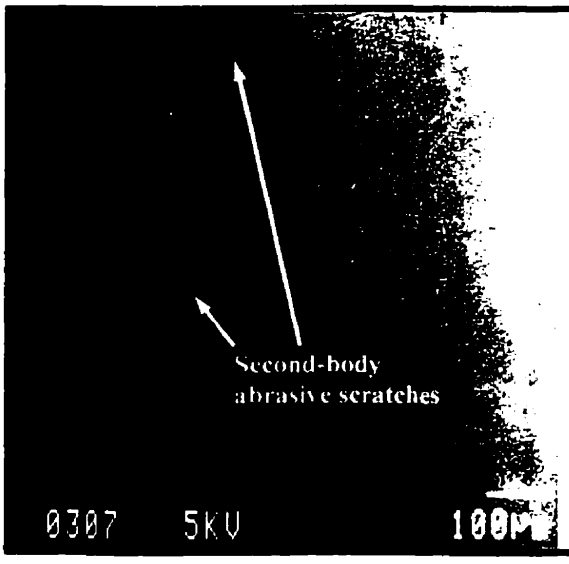

Figure 5.72 – SEM image of Sulzer, high carbon wrought retrieval. Featured are second-body abrasive scratches.

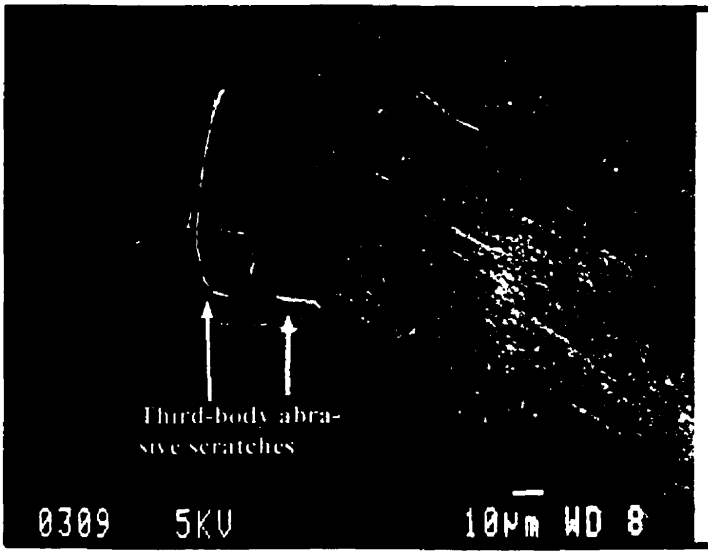

Figure 5.73 – SEM image of Sulzer, high carbon wrought retrieval. Featured are third-body abrasive scratches.

of white particles amidst the black residue. EDS analysis of the particles (Fig. 5.76) showed them to contain Co, Cr and Mo (which were likely from the matrix of the alloy), as well as Zn, Cu, Cl, Si, Al, O and C. The presence of Si, Al, O and C were suggestive of residual grinding stones from the manufacturing process. It is probable that the Sulzer implant was manufactured in a similar manner to the Wright Medical implants. It is therefore feasible that it too would have residual grinding stones on its surface. The source of Zn, Cu and Cl could not be determined, but may have been residue from organic tissue. Because the carbon was present in a much larger quan-

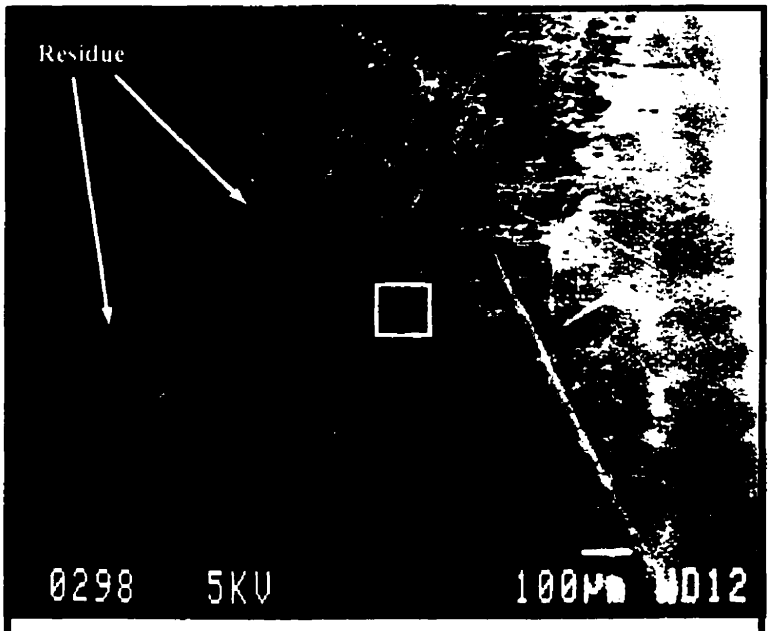

Figure 5.74 – SEM image of Sulzer, high carbon wrought retrieval. Featured is residue that could not be removed as well as a high concentration of abrasion.

Figure 5.75 – SEM image of Sulzer, high carbon wrought retrieval. Featured are white particles amidst the black residue outlined in the window in Fig. 5.74.

tity than the Si, some of it was likely also from organic residue.

A feature unique to the retrieval can be seen in Figures 5.77 and 5.78. The parallel clusters of alternating proud and relieved material were possibly caused by slip deformation, and may simply be slip lines. Alternatively, the clusters may also have been the result of twinning, a precursor to strain induced phase transformation. Regardless of the mechanism, it was clear that the surface was experiencing some form of deformation.

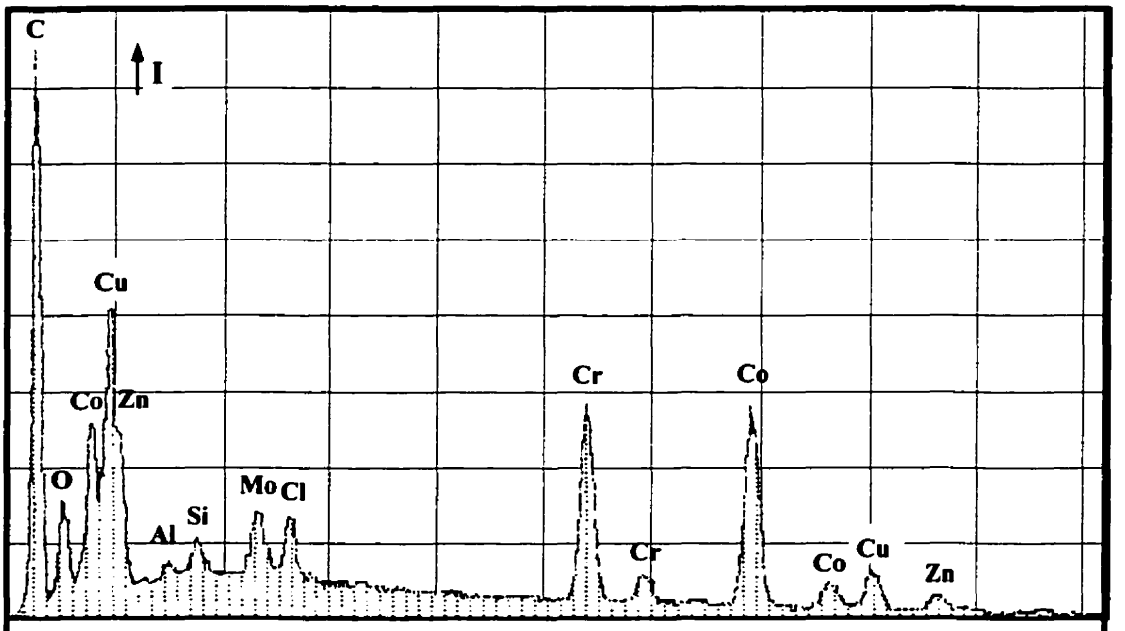

Figure 5.76 – EDS analysis of the white particles seen in Fig. 5.75.

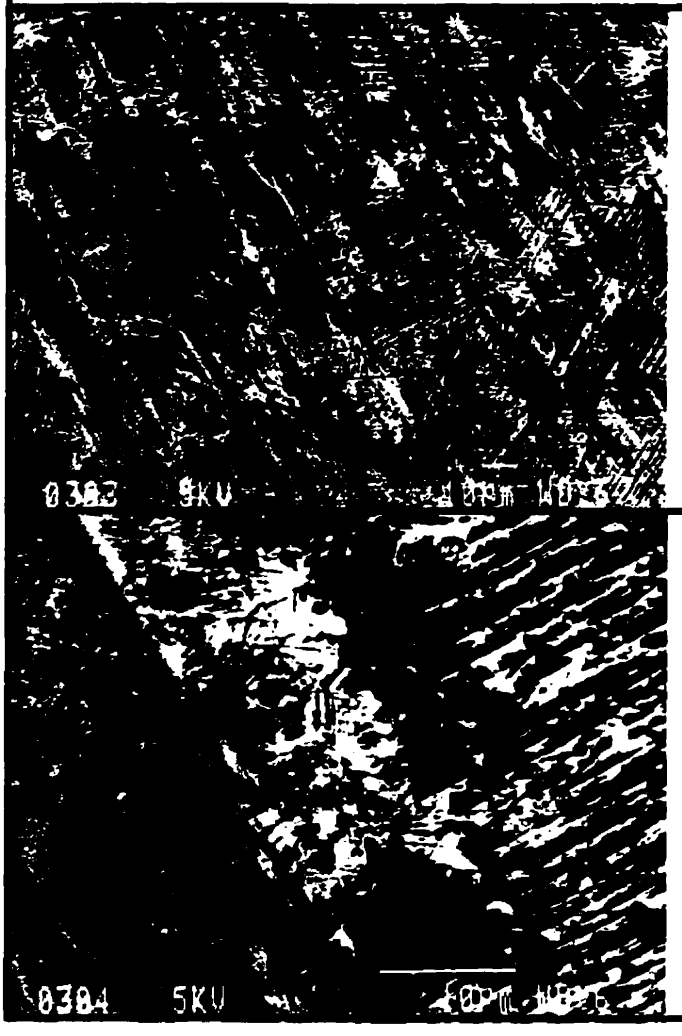

Figure 5.77 – SEM image of Sulzer, high carbon wrought retrieval. Featured is a surface that appears to have undergone some kind of deformation.

Figure 5.78 – Close-up SEM image of Fig. 5.77. Exhibited are slip lines or twinning.

6.0 DISCUSSION

The purpose of the present study was to analyze the surfaces of Co-Cr-Mo alloy heads before and after simulator testing in an attempt to determine the wear mechanisms responsible for particle release during metal-metal hip implant articulation. What follows are the proposed wear mechanisms experienced by the implants as suggested by the morphology of the wear surfaces and the consequences of those mechanisms.

6.1 CONSEQUENCES OF GRINDING DURING MANUFACTURING

The grinding operations during manufacturing appeared to have several effects on the alloy surface and wear. Figures 5.26 and 5.27 clearly show that the grinding operations had a positive effect on the surface finish, reducing the surface roughness. Chan et al[10, 11, 12] and Medley et al[46] have shown that improved surface roughness reduces overall wear.

It was also clear that grinding resulted in residual stones being embedded in the implant surfaces, particularly during the rough grinding stage. With such abrasives present on the surface, one must question their effect during articulation. Several authors[10,11,12,41,50,56,65,70,74,79] had previously reported scratches that seemed simi-

lar to the ones observed in the present study. Schmidt et al[65] and Park et al[50] have proposed that the scratches were caused by carbide fragments that were released from the implant surface during articulation. Walker and Gold[79] were less specific, but did suggest that the scratches were caused in part by wear particles formed during the running-in period of wearing. While these scratches might have occurred as previously proposed, the finding of residual grinding stone material on the implant surfaces strongly indicated an additional mechanism. This was supported by the finding that the extent of scratching correlated directly with the amount of residual grinding material on the component surfaces in the first part of the study. This can best be seen when superimposing Figures 5.14 and 5.30 (Fig. 6.1). When superimposed, it becomes apparent that as the amount of stones decreased between 3 and 6 million cycles, so did the amount of scratching. Furthermore, the cast alloy, which exhibited the greatest amount of scratching also had the largest number of stones. The opposite was true for the high carbon wrought, having the least amount of scratching corresponding to the smallest amount of residual stones. Also of importance, the widths of the scratches were compatible with the stone sizes. St. John et al[70] had reported finding a large scratch that was of 150 μm in width on a high carbon wrought head that they were wear testing. They had initially speculated that the scratch was due to a carbide being removed from one of the bearing surfaces, a carbide that became a third-body. However, they further went on to say that this width of a scratch was inconsistent with the size of the carbides in the high carbon wrought alloy and no likely site of carbide or grain loss was found on either the head or cup components.

In the first part of the study, the extent of second and third body scratching was greatest after 3 million cycles and decreased between 3 and 6 million cycles of testing. This study showed that in the first part, only a small amount of carbide release was observed in the first 3 million cycles of testing, but relatively more carbide release was seen between 3 and 6 million cycles. If carbides were the main source of the scratching, as was speculated by several authors, it would be expected that an increase in carbide release would result in an increase in scratches, but this was not the

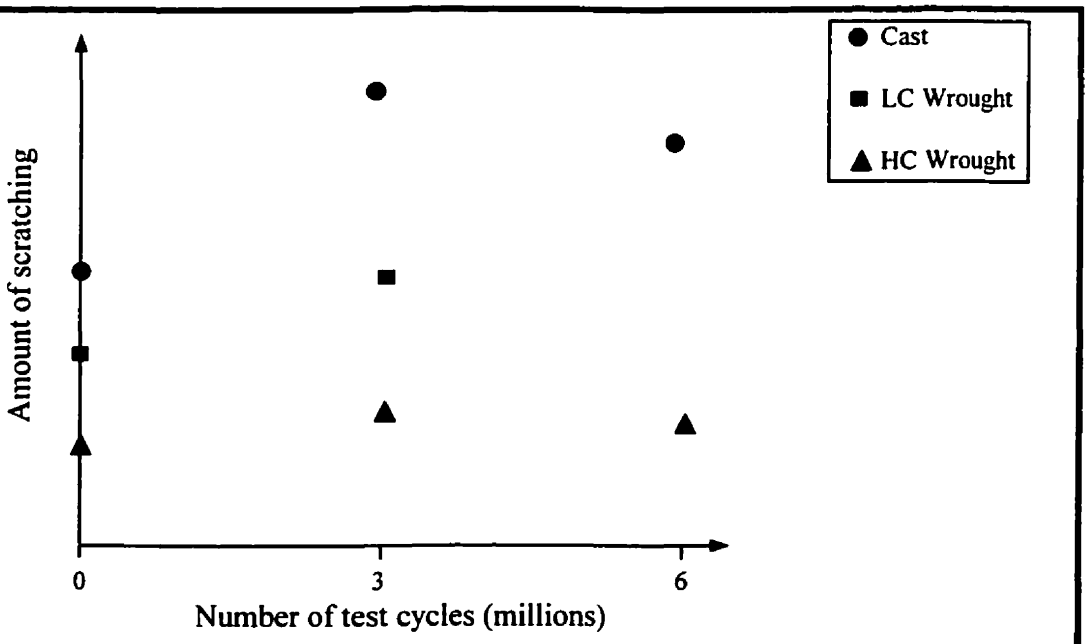

Figure 5.14 – Schematic of the amount of scratching observed on the implant heads. The schematic is based on qualitative observations. The amount of scratching was not quantified.

Figure 6.1 – Figures 5.14 and 5.30 superimposed in order to illustrate how the amount of residual grinding stones directly correlated to the amount of scratching on the implants surfaces.

case. Also, a substantial number of carbides was released early in the second part of the study, yet very little scratching was observed. It is also important to note that scratches were readily seen on the surfaces of the low carbon wrought heads that did not have large enough carbides to cause such wide scratches. Furthermore, the low carbon wrought displayed more scratches than did the high carbon wrought despite the fact that the high carbon wrought had a lot more carbides. These findings together imply that the carbides were not the main cause of the abrasive scratching.

There were two main types of stones found on the implant surfaces: irregularly shaped stones made mostly of SiC and spherical stones made mostly of SiO_2-B_2O_3-Al_2O_3. It was clear that the SiC stones were capable of scratching the implant

surfaces, since the SiC was the abrasive of choice for grinding during manufacturing. However, the SiC stones were found in a far fewer number than the SiO_2-B_2O_3-Al_2O_3 bond stones. Because it was speculated that the grinding stones were causing the abrasive scratches, it was important to determine if the bond material was capable of scratching the implant alloys. As described in Section 4.8, a scratch test using consolidated bond disks (without SiC) was conducted in order to determine if the bond material was hard enough to be able to abrade the implant alloys. The test was done by taking the consolidated bond disk and applying a light manual pressure to the implant surface. All three alloys were easily scratched as illustrated in Figure 6.2 of the test performed on the high carbon wrought alloy. Surrounding the scratched area were many fragments of the bond material that were not removed with light air pressure from an air gun (Fig. 6.3). This test illustrated that not only was the bond material able to abrade the alloys, but also the ease with which it embedded itself in the alloys.

Thus far, all the arguments pointing at the residual grinding stones as being responsible for abrasive scratching have been speculative. Figure 6.4, which illustrates the end of a series of scratches found on one of the heads after testing, showed conclusively that the residual stones did in fact cause abrasive scratching on the implant surfaces. Found at the end of the scratches were fragments of embedded stones that were of the bond type. This phenomenon was not restricted to the implants that were tested in the hip simulator. The retrieval also showed areas of high concentration of abrasive scratching, areas which also had high concentrations of residual grinding stones (Figs. 5.74 & 5.75).

Now that the cause of the abrasive scratching is better understood, a clear recommendation would appear to be finding methods of reducing or eliminating the residual stones in an attempt to reduce the amount of abrasion. However, Table 5.1 shows that the amount of wear produced by the cast implants did not significantly differ from that of the high carbon wrought. This was despite the fact that the cast implants had significantly more abrasive scratching. Perhaps during abrasion, the al-

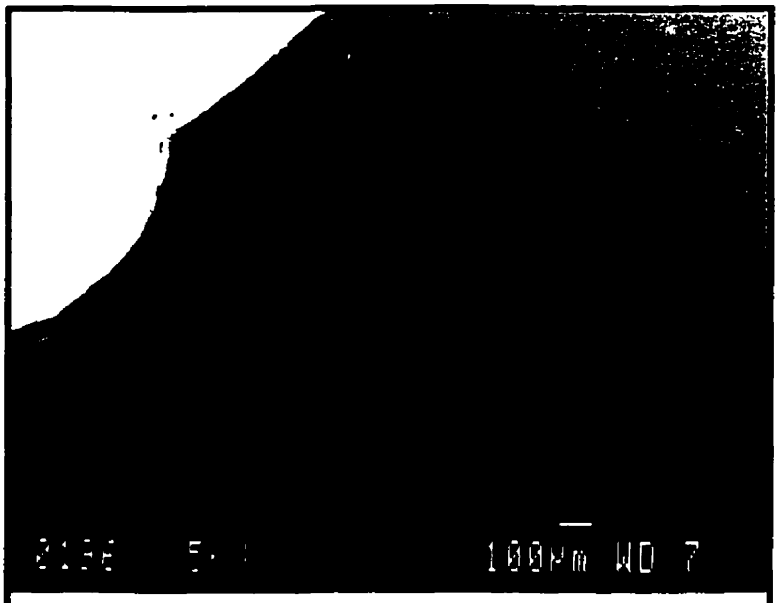

a) Prior to scratching

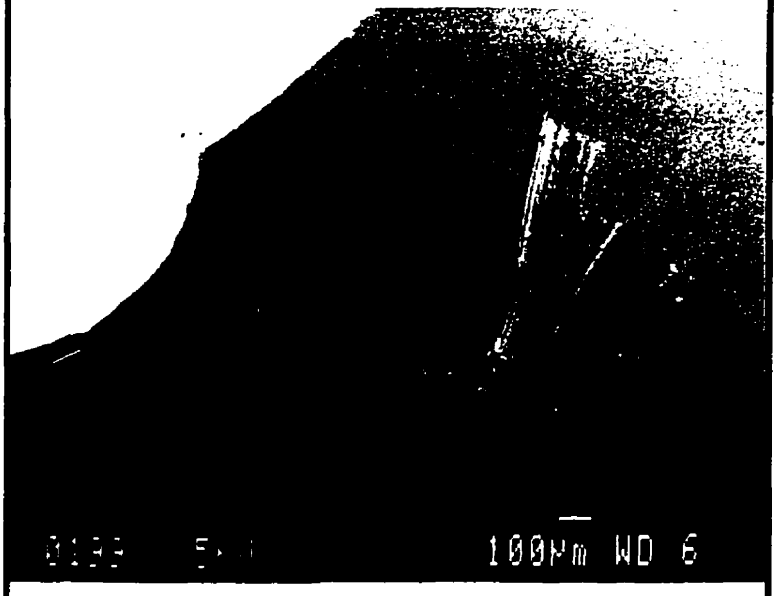

b) After scratching

Figure 6.2 – SEM images showing a high carbon wrought surface before and after scratching with bond material using light manual pressure (head #8).

loy did not experience any wear, but rather a displacement of material. Also, it is possible that the scratches provided channels for ingress and egress of lubricating fluid which may have reduced the effect of other wear mechanisms. Thus, even though it is clear that the residual grinding stones caused abrasive scratching, it is unclear if they had a detrimental effect on wear.

It appeared that grinding during manufacturing had one additional effect on the alloys. As discussed in Section 5.1, grinding changed the relative amounts of the HCP and FCC phases at the immediate surface. The consequences of the change in the relative amount is unclear. The second part of the study, however,

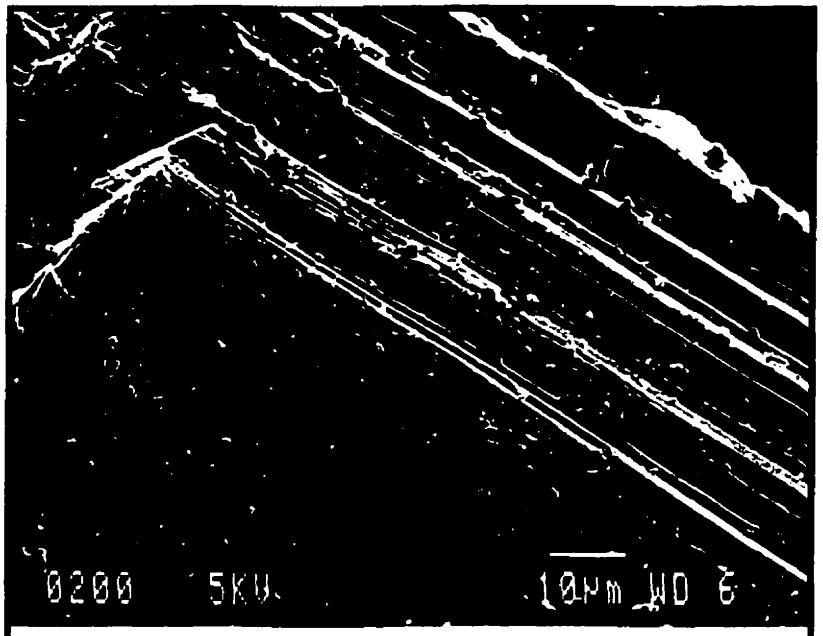

Figure 6.3 – Close-up SEM image of the scratch seen in Figure 6.2b. Illustrated were many bond fragments that were embedded in the implant surface.

seemed to suggest that the phase change increased the hardness because the alloys were not susceptible to abrasive scratching early in the testing. This was despite the fact that residual stones were present on the surfaces, carbides were proud and were being released, rendering them free to cause abrasion, and running-in material was also released. Regardless of which material is generally responsible for abrasion, abrasion did not take place early during testing probably because the surfaces were hardened by the grinding process. On the other hand, the extensive presence of pitting may have helped lubrication which in turn may have prevented abrasion. However, the extent of pitting did not decrease later in the testing, yet abrasion was beginning to take place. This, once again, suggested that grinding during manufacturing increased hardness which helped the alloys resist abrasion. The consequences of hardening on other wear mechanisms, however, was not determined.

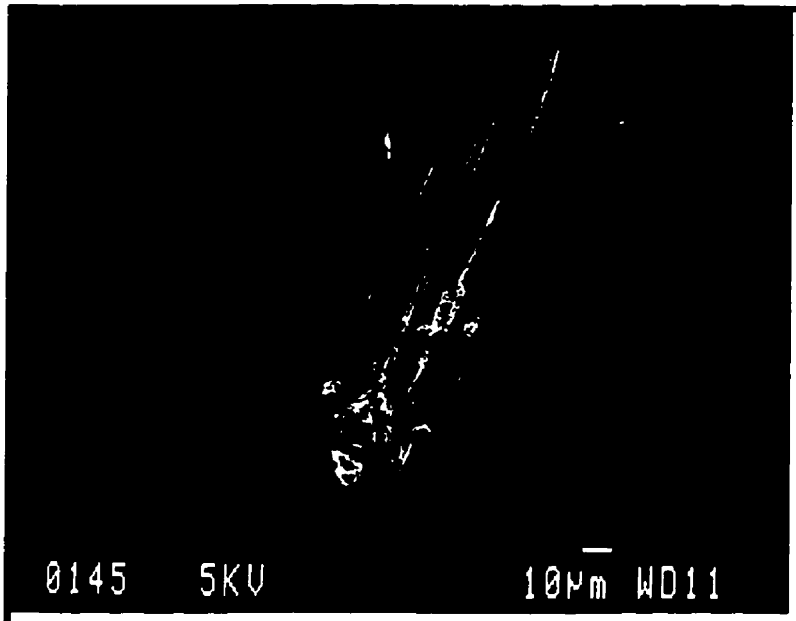

Figure 6.4 – SEM image of high carbon wrought alloy before simulator testing (head #4). Illustrated is a set of scratches.

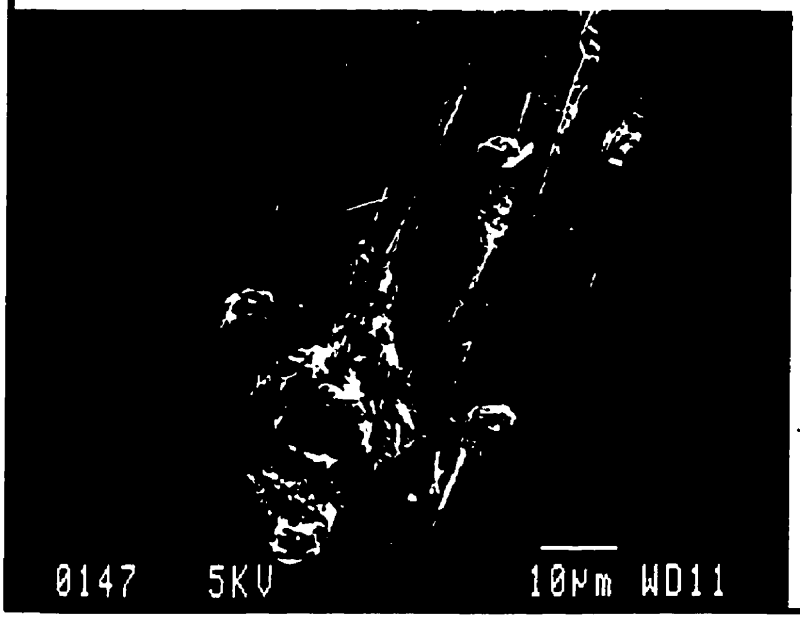

Close-up SEM image of the scratch seen above. At the end of the scratch were found fragments of bond material left behind from grinding during manufacturing.

6.2 Consequences of Carbon Level and Carbide Morphology

The carbon level and carbide morphology appeared to have several consequences on the wear mechanisms of the implant alloys. As was discussed in Section

5.2.6, matrix delamination appeared to be a wear mechanism that was shared by all three alloys, regardless of the carbon level. What was interesting, however, was the manner in which delamination was occurring in the cast and high carbon wrought alloys. A delaminating layer appeared to be present only where the carbides were relieved below the matrix surface (Figs. 5.46, 5.47 & 5.48). One could then speculate that delamination in those two alloys occurred only once the carbides had been worn. The fact that the delaminating layer was of a thickness similar to the depth of carbide relief suggested that the layer wore only once the carbides were relieved to a depth similar to that of the maximum shear. What all this implies is that the presence of carbides retarded the delamination process, slowing down the wear rate. This assumption was strengthened by the fact that in this study, the low carbon wrought implants consequently exhibited a higher wear rate than the cast and the high carbon wrought implants, as was evident from Table 5.1 and Figure 5.50. Although other factors aside from carbon level may have influenced the wear rate of the implants, particularly geometry, this study did attempt to restrict the geometric variables. Other authors, such as Medley et al,[44] have also found that the low carbon wrought implants wore at a higher rate than the high carbon alloys. This, as discussed above, may be due in part to the lack of carbide support that is enjoyed by the matrix of the high carbon alloys.

The size of the carbides also appeared to have an influence on the wear. At low loads, as in the first part of the study, fatigue pitting in the cast components appeared to be restricted to carbide sites. In the high carbon wrought, fatigue pitting appeared to have originated at carbide sites, however, did progress into the matrix. Although one would anticipate this to mean that the high carbon wrought should have worn at a faster rate than the cast, the wear rates, as given in Table 5.1 showed that it did not. Perhaps the wear produced by pitting in the high carbon wrought was offset by the abrasion experienced by the cast heads. This could only be ascertained if the experiment was repeated in the absence of residual grinding stones.

In the second part of the study, the wear surfaces were dominated by pits.

What this suggested was that pitting was a major contributor to the generation of wear debris. Figure 5.50, which showed the wear rates of the implant heads examined in the second part, revealed that the low carbon wrought, had by far the highest wear rate. However, as shown in section 5.3.2, the pits in the low carbon wrought heads did not differ in depth, size or number from those in the cast or high carbon wrought. It is thus difficult to explain why the low carbon wrought experienced a higher wear rate than the cast and high carbon wrought if the pitting was similar in all three alloys. As discussed in Section 5.3.2, it appeared that the heads were experiencing pitting cycles. Perhaps the low carbon wrought experienced the pitting cycles more frequently and therefore experienced a higher wear rate. This would suggest that the pitting cycles were slowed down by the presence of carbon in solution and/or carbides. The fact that the cast and high carbon wrought experienced similar wear, suggests that the pitting cycles were experienced at a similar rate for both. Since scratching in the second part of the study was not a factor, the cast and high carbon wrought can be compared more easily when regarding the influence of the pitting.

A less obvious contributing factor to the higher wear rate of the low carbon wrought alloy may be the chromium levels in the matrix. Chromium is added to all three alloys in quantities of 27-30 wt% in order to render the alloys corrosion resistant. That is, when the alloy comes in contact with oxygen, the chromium in the alloy forms a layer of protective oxide film (mainly Cr_2O_3). In the cast and high carbon wrought alloys, more of the chromium becomes trapped in the carbides. Thus, less chromium is present in the metal matrix of the cast and high carbon wrought alloys when compared to that in the matrix of the low carbon wrought. Therefore, more chromium is available for oxidation in the low carbon wrought alloy. As discussed in Section 5.3.3, the oxide that forms on the surface of the implants wears away. Because more chromium is available for oxidation in the low carbon wrought, it is possible that more oxide forms on the low carbon wrought surface and therefore more of it wears away, contributing to the higher wear rate of the low carbon wrought implants. Authors such as Campbell et al[9] have reported finding chromium oxide parti-

cles during analysis of bovine serum taken from simulator implant testing. The oxide particles found were of a similar size and morphology as the oxide nodules seen on the surfaces of the implants (Figs. 5.68 & 5.69). In fact, results of ongoing studies by Isabelle Cattellas, of the Department of Biomedical Engineering, McGill University, strengthened the argument that more oxide particles are released from the low carbon wrought alloy. She has examined the bovine serum used in this study and her examination revealed that the serum from the low carbon wrought testing contained more chromium oxide particles than in that of the cast or the high carbon wrought serum. Perhaps if the chromium content in the low carbon wrought alloy was reduced, so would its wear rate. However, it must be remembered that chromium is added in order to render the alloy corrosion resistance. Therefore, if the chromium level is reduced in order to observe any change in wear rate, the corrosion rate would also have to be monitored.

6.3 CONSEQUENCES OF LOADING

Because this study examined implants that were articulated under 3 times and 5 times body weight, it was possible to consider the consequences of loading. The most profound difference between the implant heads that were articulated at 3 times body weight and those that were articulated at 5 times body weight was the fatigue pitting. At the higher loads, pitting was the prominent feature seen on the surfaces and was seen very early in the testing. All other wear mechanisms were difficult to detect because of the pitting. At the lower loads, pitting appeared only after 6 million cycles of testing. The pits were not as numerous nor as large as those observed on the implants subjected to the higher loads. What this suggested was that for these alloys, an increase in loading from 3 to 5 times body weight increased fatigue wear.

Not only did the surfaces appear more worn, but the volumetric wear measured was also greater. Despite the fact that Table 5.1 reported the volumetric wear of

the combined head and cup, measured at 3 and 6 million cycles, it showed that the volumetric wear of the implants was less than that of only the heads tested to 2 million cycles at 5 times body weight (Fig. 5.50). To give an example, implant #7, a cast implant tested to 3 million cycles at 3 times body weight wore 0.16 mm^3 from the cup and head combined. Heads #1 and 2, which were cast heads tested at 5 times body weight, wore about 0.4 mm^3 and 0.6 mm^3 respectively at 2 million cycles from the head alone. This was observed with all the implants when comparing testing at 3 and 5 times body weight. Needless to say, further studies into material and design are required in order to accommodate heavier patients.

From the above, it can be speculated that the individual from which the retrieval was extracted and examined in this study was likely of relatively light weight or was very inactive. As shown in Section 5.4, the retrieval implant showed very little evidence of wear. No fatigue pits were found, not in the matrix nor at carbide sites. In fact, the carbides were still proud after 3 years of service. The large amount of twinning observed on the surface of the retrieval (Figs. 5.77 & 5.78) may have been the result of the manufacturing process as opposed to articulation. However, it was contradictory to find such extensive evidence of deformation without much evidence of wear. Perhaps, the deformation seen on the surface was the result of the manufacturing process, and perhaps it contributed to the lack of wear observed on the surface.

7.0 CONCLUSIONS

Grinding during manufacturing resulted in an improved surface finish. While surface finish was improved, grinding also resulted in deposition of residual grinding stones on the implant surfaces. Most of the stones were deposited during the rough grinding stage. The stones were mainly of the bond type, but some were also silicon carbide abrasives. The implant surfaces experienced second and third-body abrasive scratching, possibly caused by the residual grinding stones that were deposited during the manufacturing of the implants.

The manufacturing process rendered the carbides proud of the surface in the cast and high carbon wrought implants. With testing, the carbides in the high carbon wrought did not stay proud of the surface in the wear zone. the carbides were worn below the matrix surface likely by some mechanical means, probably fatigue fracture. In the cast wear zone, the isolated carbides remained proud of the surface with testing, while those in chains were relieved below the matrix surface. The behavior of the carbides in the low carbon wrought could not be ascertained, as the carbides were not detected during implant examination.

The manner by which the matrix wore is somewhat speculative. Aside for abrasive scratching, it is believed that the matrix wore because of three additional mechanisms. At lower loads, the matrix wore mainly through delamination. At higher loads, the main mechanisms was fatigue pitting and pitting cycles. It appeared that the carbides in the cast and high carbon wrought served as an origin for fatigue pitting. However, at the higher loads, pitting was not restricted to carbide sites. It

also appeared that those carbides also served as matrix stabilizers, which slowed down delamination as well as the pitting cycles. It is believed that the low carbon wrought implant experienced higher wear because of the lack of supporting carbides. Lastly, it appeared that when the metal matrix was exposed to oxygen by the above two wear mechanisms, oxide nodules formed on the surface and eventually wore, contributing to the matrix wear.

This study showed that when higher loads were applied during testing, the implants wore at a faster rate, and this was reflected in the surface appearance. The retrieval implant showed very little evidence of wear. It is therefore possible that the patient from whom the implant was retrieved was a light and/or inactive individual.

8.0 FUTURE WORK

While this study revealed numerous mechanisms by which the Co-Cr-Mo alloy implants wear, it also brought up some new questions. First and foremost, it is of interest to determine the consequences of the residual grinding stones left behind by the manufacturing process. Are they detrimental to wear or are the abrasive scratches they inflict on the surfaces of a benefit to lubrication? This can only be answered by testing and examining implants that are devoid of residual stones. That would require investigation of the manufacturing process. Perhaps employing less pressure when grinding would result in fewer stones embedded on the surface. Also, the manufacturer of the grinding stones may have to examine methods for eliminating pockets of unconsolidated bond material from the rough grinding stones, in an attempt to reduce the amount of bond particles embedded on the implant surfaces.

It may also be beneficial to examine the effect grinding and manufacturing, in general, have on the hardness of the implant surfaces. How does the process affect the relative amounts of FCC and HCP at the immediate surface? Does this influence improve the alloy's resistance to wear? The first step would be to devise a technique to quantify the phases at the immediate surface. Once that is established, the next step would be to determine how to control the relative amounts and then investigate the effect different relative amounts would have on the wear behavior.

While investigating manufacturing process variables, it may also be beneficial to compare implants from different manufacturers. If from this it is found that the performance differs from manufacturer to manufacturer, then the manufacturing tech-

niques should be compared and contrasted.

Lastly, it would likely be beneficial to further investigate the spherical nodules found on the surfaces. Are they in fact oxide? If so, how quickly do they form and at what rate do they wear? Is this mechanism a significant contributor to the overall wear? Would the wear rate differ if the chromium level is changed? If so, how would a change in the chromium level affect the corrosion resistance?

REFERENCES

1. Ahlroos, T., and Saikko, V., "Wear of Prosthetic Joint Materials in Various Lubricants", *Wear*, Vol. 211, 1997, pp. 113-119.

2. Amstutz, H. C., Campbell, P. A., McKellop, H., Schmalzried, T. P., Gillespie W. J., Howie, D., Jacobs, J., Medley J. B., and Merritt, K., "Metal on Metal Hip Replacement Workshop Consensus Document", *Clinical Orthopaedics and Related Research*, No. S329, 1996, pp. S297-S303.

3. Amstutz, H. C., and Grigoris, P., "Metal on Metal Bearings in Hip Arthroplasty", *Clinical Orthopaedics and Related Research*, No. S329, 1996, pp. S11-S34.

4. Annual Book of ASTM Standards – Medical Devices, Vol. 13.01, American Society for Testing and Materials, 1994, pp. 6-9, 230-231.

5. Arnell, R. D., Davies, P. B., Halling J., and Whomes, T. L., Tribology – Principles and Design Applications, Macmillan Press, London and Basingstoke, 1991.

6. Atamert, S., and Stekly, J., "Current Status Review – Microstructure, wear Resistance, and Stability of Cobalt Based and Alternative Iron Based Hardfacing Alloys", *Surface Engineering*, V. 9, No. 3, 1993, pp. 231-240.

7. Berry, G., Bolton, J. D., Brown, J. B., & Mcquaide, S., "The Production and Properties of Wrought High Carbon Co-Cr-M0 Alloys", Cobalt-Base Alloys for Biomedical Applications, ASTM STP 1365, J. A. Disegi, R. L. Kennedy, R. Pilliar, Eds., American Society for Testing and Materials, West Conshohocken, PA, 1999, pp. 11-31.

8. Bobyn, J. D., Tanzer, M., Krygier, J. J., Dujovne, A. R., and Brooks, E., "Concerns with Modularity in Total Hip Arthroplasty", *Clinical Orthopae-*

dics and Related Research, No. 298, 1994, pp. 27-36.

9. Campbell, P., McKellop, H., Alim, R., Mirra, J., Nutt, S., Dorr, L, and Amstutz, H. C., "Metal-on-Metal Hip Replacements: Wear Performacne and Cellular response to Wear Particles", Cobalt-Base Alloys for Biomedical Applications, ASTM STP 1365, J. A. Disegi, R. L. Kennedy, and R. Pilliar, Eds., American Society for Testing and Materials, West Conshohocken, PA, 1999, pp. 193-209.

10. Chan, F. W., "Wear and Lubrication of Metal-Metal Bearings for Total Hip Arthroplasty", *Ph.D. Thesis*, Department of Biomedical Engineering, McGill University, 1999.

11. Chan, F. W., Bobyn, J. D., Medley, J. B., Krygier, J. J., Podgorsak, G. F., and Tanzer, M., "Metal-Metal Hip Implants: Investigation of Design Parameters that Control Wear", *Clinical Orthopaedics and Related Research*, 1999, (in press).

12. Chan, F. W., Bobyn, J. D., Medley, J. B., Krygier, J. J., Yue, S., and Tanzer, M., "Engineering Issues and Wear Performance of Metal on Metal Hip Implants", *Clinical Orthopaedics and Related Research*, No. 333, 1996, pp. 96-107.

13. Chan, F. W., Medley, J. B., Bobyn, J. D., and Krygier, J. J., "Numerical Analysis of Time-Varying Fluid Film Thickness in Metal-Metal Hip Implants in simulator Tests", Alternative Bearing Surfaces in Total Joint Replacement, ASTM STP 1346, J. J. Jacobs and T. L. Craig, Eds., American Society for Testing and Materials, 1998, pp. 111-128.

14. Chen, C. J., Introduction to Scanning Tunneling Microscopy, Oxford University Press, NY, 1993, pp.313-324.

15. Cipera, W. M., and Medley, J. B., "Tribological Investigations of Cobalt-Based Alloys in Metal-on-Metal Contacts Using a Reciprocating cylinder-on-Flat Apparatus with Bovine Serum Lubricants", Alternative Bearing Surfaces in Total Hoint Replacement, ASTM STP 1346, J. J. Jacobs and T. L. Craig, Eds., American Society for Testing and Materials, 1998, pp. 76-91.

16. Collins, J. A., Failure of Materials in Mechanical Design - Analysis, Prediction, Prevention, 2nd Ed., John Wiley & Sons, 1993, pp.504-643.

17. Crook, P., "Cobalt-Base Alloys Resist Wear, Corrosion, and Heat", *Advanced Materials & Processes*, Vol. 4, 1994.

18. Crowninshield, R. D. & Anderson, P. J., "Mechanical Properties & Manufacturing Techniques for Orthopaedic Implants", Advanced Concepts in Total Hip Replacement, Harris, W. H., Ed., SLACK, NJ, 1985, pp. 181-189.

19. Czerwinski, F., "The Growth and Structure of Thin Oxide Films on Nickel Superficially Modified With Ceria and Cerium", *Ph.D.*, Metallurgical Engineering Department, McGill University, 1997.

20. Doorn, P. F., Campbell, P. A., and Amstutz, H. C., "Metal Versus Polyethylene Wear Particles in Total Hip Replacements", *Clinical Orthopaedics and Related Research*, No. S329, 1996, pp. S206-S216.

21. Doorn, P. F., Campbell, P. A., Worrall, J., Benya, P. D., McKellop, H. A., and Amstutz, H. C., "Metal Wear Particle Characterization from Metal on Metal Total Hip Replacements: Transmission Electron Microscopy Study of Periprosthetic Tissues and Isolated Particles", *Journal of Biomedical Materials Research*, Vol. 42, No. 1`, 1998, pp. 103-111.

22. Doorn, P. F., Mirra, J. M., Campbell, P. A., and Amstutz, H. C., "Tissue Reaction to Metal on Metal Total Hip Prostheses", *Clinical Orthopaedics and Related Research*, No. S329, 1996, pp. S187-S205.

23. Duff-Barclay, I., and Spillman, D. T., "Total Human Hip Hoint Prostheses – A Laboratory Study of Friction and Wear", *Proceeding of the Institution of Mechanical Engineers*, Vol. 181, Part. 3F, 1666-67, pp. 90-103.

24. Fehlner, F. P., and Graham, M. J., "Thin Oxide Film Formation on Metals", Corrosion Mechanisms in Theory and Practice, P. Marcus & J. Oudar, Eds., Marcell Dekker, 1995, pp. 123-141.

25. Firkins, P. J., Tipper, J. L., Ingham, E., Farrar, R., and Fisher, J., "Wear and Debris Analysis of Low and High Carbon Content Cobalt Chrome Alloys for Use in Metal on Metal Total Hip Replacements", *Proceedings of the Orthopaedic Research Society*, 1998, pg. 370.

26. Frenk, A, and Kurz, W., "Microstructural Effects on the Sliding Wear Resistance of a Cobalt-Based Alloy", *Wear*, Vol. 174, 1994, pp. 81-91.

27. Friedman, R. J., Black, J., Galante, J. O., Jacobs, J. J., and Skinner, J. B., "Current Concepts in Orthopaedic Biomaterials and Implant Fixation", *Journal of Bone and Joint Surgery*, Vol. 75-A, No. 7, 1993, pp.1086-1109.

28. Gerwith, A. A., and LaGraff, J. R., "Atomic Force Microscopy", The Hand-

book of Surface Imaging and Visualization, A. T. Hubbard, Ed., CRC Press, 1995, pp. 23-31.

29. Goldring, S. R., Clark, C. R., and Wright, T. M., "The Problem in Total Joint Arthroplasty: Aseptic Loosening", *The Journal of Bone and Joint Surgery*, Vol. 75-A, No. 6, 1993, pp.799-801.

30. Goldstein, J. I., Newbury, D. E., Echlin, P., Joy, D. C., Romig, A. D., Lyman, C. E., Fiori, C., and Lifshin, E., Scanning Electron Microscopy and X-Ray Microanalysis – A Text for Biologists, Materials Scientists, and Geologists, 2 nd Ed., Plenum Press, NY, 1992.

31. Gross, T. P., and Lennox, D. W., "Osteolytic Cyst-Like Area Associated with Polyethylene and Metallic Debris after Total Knee Replacement with an Uncemented Vitallium Prosthesis", *Journal of Bone and Joint Surgery*, Vol. 74-A, No. 7, 1992, pp.1096-1101.

32. Hirakawa, K., Bauer, T. W., Stulberg, B. N., Wilde, A. H., and Secic, M., "Characterization and Comparison of Wear Debris from Failed Total Hip Implants of Different Types", *Journal of Bone and Joint Surgery*, Vol. 78-A, No. 8, 1996, pp.1235-1243.

33. Jacobsson, S.-A., Djerf, K., and Wahlström, O., "20-Year Results of McKee-Farrar Versus Charnley Prosthesis", *Clinical Orthopaedics and Related R esearch*, No. S329, 1996, pp. S60-S68.

34. Jayson, M., Ed., Total Hip Replacement, J. B. Lippincott, Philadelphia and Toronto, 1971.

35. Khurshudov, A., and Kato, K., "Wear Mechanisms in Reciprocal Scraching of Polycarbonate, Studied by Atomic Force Microscopy", *Wear*, Vol. 205, 1997, pp. 1-10.

36. Kilner, T., "The relationship of Microstructure to the Mechanical Properties of a Cobalt-Chromium-Molybdenum Alloy Used for Prosthetic Devices", *Ph.D. Thesis*, Department of Biomaterials, University of Toronto, 1984.

37. Kostick, J. A., Segaii, A. E., Conway, J. C. Jr., and Amateau, M. F., "The Sliding Wear Behavior of Cobalt-Based Hardfacing Alloys Used in Steam Valve Applications", *Triboloby Transactions*, Vol. 40, No. 1, 1997, pp.168-172.

38. Ling, R. S. M., and Timperley, A. J., "Cemented Total Hip Replacement", Postgraduate Textbook of Clinical Orthopaedics, N. H. Harris, Ed., Bristol,

Boston: Wright-PSG, 1983, pp. 645-685.

39. MacDougall, B., and Graham, M. J., "Growth and Stability of Passive Films", Corrosion Mechanisms in Theory and Practice, Marcel Dekker, 1995, pp. 143-173.

40. Mai, M. T., Schmalzried, T. P., Dorey, F. J., Campbell, P. A., and Amstutz, H. C., "The Contribution of Frictional Torque to Loosening at the Cement-Bone Interface in Tharies Hip Replacements", *Journal of Bone and Joint Surgery*, Vol. 78-A, No. 4, 1996, pp. 505-511.

41. McKellop, H., Park, S.-H., Chiesa, R., Doorn, P., Lu, B., Normand, P., Grigoris, P. and amxtutz, H., "In Vivo Wear of 3 Types of metal on Metal Hip Prostheses During 2 Decades of Use", *Clinical Orthopaedics and Related Research*, No. S329, 1996, pp. S128-S140.

42. McMinn, D., Treacy, R., Lin, K., and Pynsent, P., "Metal on Metal Surface Replacement of the Hip", *Clinical Orthopaedics and Related Research*, No. S329, 1996, pp. S89-S98.

43. Medley, J. B., Chan, F. W., Krygier, J. J., and Bobyn J. D., "Comparison of Alloys and Designs in a Hip simulator Study of Metal on Metal Implants", *Clinical Orthopaedics and Related Research*, Vol. S329, 1996, pp. S148-S159.

44. Medley, J. B., Dowling, J. M., Poggie, R. A., Krygier, J. J., and Bobyn, J. D., "Simulator Wear of Some Commercially Available Metal-on-Metal Hip Implants", Alternative Bearing Surfaces in Total Joint Replacement, ASTM STP 1346, J. J. Jacobs and T. L. Craig, Eds., American Society for Testing and Materials, 1998, pp. 92-110.

45. Medley, J. B., Krygier, J. J., Bobyn, J. D., Chan, F. W., Lippincott, A., and Tanzer, M., "Kinematics of the MATCO Hip Simulator and Issues Related to Wear Testing of Metal-Metal Implants", *Proceedings of the Institution of Mechanical Engineers*, Vol. 211, Part H, 1997, pp. 89-100.

46. Medley, J. B., Krygier, J. J., Bobyn, J. D., Chan, F. W., and Tanzer, M., "Metal-Metal Bearing Surfaces in the Hip. Investigation of Factors Influencing Wear", *Transactions of the Orthopaedic Research Society*, Vol. 20, 1995, p. 765.

47. Merritt, K., and Brown, S. A., "Distribution of Cobalt Chromium Wear and Corrosion Products and Biologic Reactions", *Clinical Orthopaedics and Reated Research*, No. S329, 1996, pp. S233-S243.

48. Oberländer, C., Franck, M., Campbell, P. A., Celis, J. P., and Roos, J., "Comparative Investigation by Laser Profilometry, Scanning Electron Microscopy and Atomic Force Microscopy of Wear on Solar-Beam-Irradiated Partially Oxidized TiN Coatings", *Thin Solid Films*, Vol. 241, 1993, pp. 222-229.

49. Park, S. H., McKellop, H., Lu, B., and Chan, F. W., "Wear Patterns Produced in Hip Simulator Tests of Metal-Metal Implants", *Transactions of the 23rd Annual Meeting of the Society for Biomaterials*, in press, (May 1997), p. 191.

50. Park, S.-H., McKellop, H., Lu, B., Chan, F. W., and Chiesa, R., "Wear Morphology of Metal-Metal Implants: Hip Simulator Tests Compared with Clinical Retrievals", Alternative Bearing Surfaces in Total Joint Replacement, ASTM STP 1346, J. J. Jacobs and T. L. Craig, Eds., American Society for Testing and Materials, 1998, pp. 129-143.

51. Paul, J. P., "Forces Transmitted by Joints in the Human Body", *Proceedings of the Institution of Mechanical Engineers*, Vol. 181-F, 1967, pp. 8-15.

52. Phillips, H., and Tucker, J. K., "Cementless Total Hip Replacement", Post graduate Textbook of Clinical Orthopaedics, N. H. Harris, Ed., Bristal, Boston, 1983, pp. 687-695.

53. Poggie, R. A., "A Review of the Effects of Design, Contact Stress, and Materials on the Wear of Metal-on-Metal Hip Prostheses", Alternative Bearing Surfaces in Total Joint Replacement, ASTM STP 1346, J. J. Jacobs and T. L. Craig, Eds., American Society for Testing and Materials, 1998, pp. 47-54.

54. Prutton, M., Introduction to Surface Physics, Oxford University, NY, 1994.

55. Raman, R. V., and Rele, S. V., "A Novel Rapid Consolidation Powder Metallurgy Approach to Fabricate High Fatigue Strength and Corrosion Resistant Co-Cr-Mo-C Alloys for Demanding Applications", Powder Metallurgy in Aerospace, Defence and Demanding Applications, Metal Powder Industries Federation, Princeton, USA, 1993, pp. 317-324.

56. Rieker, C. B., Köttig, P., Schön, R., Windler, M. and Wyss, U. P., "Clinical Wear Performance of Metal-on-Metal Hip Arthroplasties", Alternative Bearing Surfaces in Total Joint Replacement, ASTM STP 1346, J. J. Jacobs and T. L Craig, Eds., American Society for Testing and Materials, 1998, pp. 144-156.

57. Saikko, V. O., "A Three-Axis Hip Joint Simulator for Wear and Friction Studies on Total Hip Prostheses", *Proceedings of the Institution of Mechani-*

cal Engineers, Vol. 210, 1996, pp. 175-185.

58. Saikko, V. O., Nevalainen, J., Revitzer, H., and Ylinen, P., "Metal Release from Total Hip Articulations in Vitro – Substantial from Co-Cr/Co-Cr, Negligible from CoCr/PE and Alumina/PE", *Acta Orthopidica Scandinavia*, Vol. 69, No. 5, 1998, pp. 449-454.

59. Sarkar, A. D., Friction and Wear, Academic Press, London, 1980.

60. Scales, J. T., "Arthroplasty of the Hip Using Foreign Materials: A History", *Proceeding of the Institution of Mechanical Engineers*, Vol. 181, Part 3-F, 1966-67, pp. 63-84.

61. Schey, J. A., "A Systems View of Optimizing Metal on Metal Bearings", *Clinical Orthopaedics and Related Research*, Vol. S329, 1996, pp. S115-S127.

62. Schmalzried, T. P., Guttmann, D., Grecula, M., and Amstutz, H. C., "The Relationship Between the Design, Position, and Articular Wear of Acetabular Components Inserted without Cement and the Development of Pelvic Osteolysis", *Journal of Bone and Joint Surgery*, Vol. 76-A, No. 5, 1994, pp. 677-688.

63. Schmalzried, T. P., Szuszczewicz, E. S., Akizuki, K. H., Petersen, T. D., and Amstutz, H. C., "Factors Correlating with Long Term Survival of McKee-Farrar Total Hip Prostheses", *Clinical Orthopaedics and Related Research*, No. S329, 1996, pp. S48-S59.

64. Schmidt, M. B., and Lunn, M. E., "Comparison of Metal-on-Polyethylene and Metal-on-Metal Hip Component Wear Using Two Different Joint Simulators", *Transactions of the Orthopaedic Research Society*, Vol. 23, 1998, p. 421.

65. Schmidt, M. B., Weber, H., and Schön, R., "Cobalt Chromium Molybdenum Metal Combination for Modular Hip Prostheses", *Clinical Orthopaedics and Related Research*, No. S329, 1996, pp. S35-S47.

66. Semlitsch, M., and Willert H.-G., "Implant Materials for Hip Endoprostheses: Old Proofs and New Trends", *Archives of Orthopaedic & Trauma Surgery*, Vol. 114, 1995, pp. 61-67.

67. Sherman, J., "A Comparison of Gold & Chromium-Cobalt Casting Alloys", McGill University, Faculty of Dentistry, Prosthetic seminars, Vol. 2, 1965-66, paper #28.

68. Sims, C T., "A Contemporary View of Cobalt-Base Alloys", *Journal of Metals*, Dec. 1996, pp. 27-42.

69. Sotereanos, N G., Engh, C. A., Glassman, A. H., Macalino, G. E., and Engh, C. A. Jr., "Cementless Femoral Components Should Be Made from Cobalt Chrome", *Clinical Orthopaedics and Related Research*, No. 313, 1995, pp. 146-153.

70. St. John, K. R., Poggie, R. A., Zardiackas, L. D., and Afflitto, R. M., "Comparison of Two Cobalt-Based Alloys for Use in Metal-on-Metal Hip Prostheses: Evaluation of the Wear Properties in a Simulator", Cobalt-Base Alloys for Biomedical Applications, ASTM STP 1365, J. A. Disegi, R. L. Kennedy, and R. Pilliar, Eds., American Society for Testing and Materials, West Conshohocken, PA, 1999, pp. 145-155.

71. Streicher, R. M., "Dr. Streicher's Response to Drs. Walker and Blunn", *Journal of Arthroplasty*, Vol. 13, No. 3, 1998, pp. 346-347.

72. Streicher, R. M., "The Case for Using Metal-on-Metal", *Journal of Arthroplasty*, Vol. 13, No. 3, 1998, pp. 343-345.

73. Streicher, R. M., Schön, R., and Semlitsch, M., "Investigation of the Tribological Behaviour of Metal-on-Metal Combinations for Artificial Hip Joints", *Biomedizinische Technik*, Vol. 35, No. 5, 1990, pp. 107-111..

74. Streicher, R. M., Semlitsch, M., Schön, R., Weber, H., and Rieker, C., "Metal-on-Metal Articulation for Artificial Hip Joints: Laboratory Study and Clinical Results", *Proceedings of the Institution of Mechanical Engineers*, Vol. 210, 1996, pp. 223-232.

75. Unsworth, A., Hall, R. M., burgess, I. C., Wroblewski, B. M., Streicher, R. M., and Semlitsch, M., "Frictional Resistance of New and Explanted Artificial Hip Joints", *Wear*, Vol. 190, 1995, pp. 226-231.

76. Varano, R., Yue, S., Bobyn, J. D., and Medley, J. B., "Co-Cr-Mo Alloys Used in Metal-Metal Bearing Surfaces", Alternative Bearing Surfaces in Total Joint Replacement, ASTM STP 1346, J. J. Jacobs and T. L. Craig, Eds., American Society for Testing and Materials, 1998, pp. 55-68.

77. Wagner, M., and Wagner H., "Preliminary Results of Uncemented Metal on Metal Stemmed and Resurfacing Hip Replacement Arthroplasty", *Clinical Orthopaedics and Related Research*, No. S329, 1996, pp. S78-S88.

78. Waitz, T., and Karnthaler, H. P., "The f.c.c. to h.c.p. Martensitic Phase Transformation in CoNi Studied by TEM and AFM Methods", *Acta Materialia*, Vol. 45, No. 2, 1997, pp. 837-847.

79. Walker, P. S., and Gold, B. L., "The Tribology (Friction, Lubrication and Wear) of All-Metal Artificial Hip Joints", *Wear* Vol. 17, 1971, 285-299.

80. Wang, A., Yue, S., Bobyn, J. D., Chan, F. W., and Medley, J. B., "Surface Characterization of Metal-on-Metal Hip Implants Tested in a Hip Simulator", *Wear*, Vol. 225-229, 1999, pp. 708-715.

81. Wang, A., Bobyn J. D., Yue, S., Medley, J. B., and Chan, F. W., "Residual Abrasive Material from Surface Grinding of metal-Metal Hip Implants: A Source of Third-Body Wear?", Cobalt-Base Alloys for Biomedical Applications, ASTM STP 1365, J. A. Disegi, R. L. Kennedy, and R. Pilliar, Eds., American Society for Testing and Materials, West Conshohocken, PA, 1999, pp. 125-134.

82. Wang, Z. G., and Xu, Y. B., "Dislocation Structures in Single Crystal Nickel– and Cobalt-Based Superalloys Under Tensile and Fatigue Loading", *Defect and Diffusion Forum*, Vol. 152, 1997, pp. 1-18.

83. Weber, B. G., "Experience with the Metasul Total Hip Bearing System", *Clinical Orthopaedics and Related Research*, No. S329, 1996, pp. S69-S77.

84. Willert, H. G., Buchhorn, G. H. H., Göbel, D., Köster, G., Schaffner, S., Schenk, R., and semlitsch, M., "Wear Behavior and Histopathology of Classic Cemented Metal on Metal Hip Endoprostheses", *Clinical Orthopaedics and Related Research*, No. S329, 1996, pp. S160-S186.

85. Williams, J. A., Engineering Triboloby, Oxford Press, NY, 1994.

86. Zhang, L., and Mahdi, M., "Applied Mechanics in Grinding – IV. The Mechanism of Grinding Induced Phase Transformation", *International Journal of Machine Tools & Manufacture*, Vol. 35, No. 10, 1995, pp. 1397-1409.